The Function of $Na_V1.8$ Clusters in Lipid Rafts

Amber Finn

Department of Life Sciences

Imperial College London

PhD Thesis

Abstract

$Na_V1.8$ is a voltage gated sodium channel mainly expressed on the membrane of thin diameter c-fibre neurons involved in the transmission of pain signals. In these neurons $Na_V1.8$ is essential for the propagation of action potentials. $Na_V1.8$ is located in lipid rafts along the axons of sensory neurons and disruption of these lipid rafts leads to $Na_V1.8$ dependant conduction failure.

Using computational modelling, I show that the clustering of $Na_V1.8$ channels in lipid rafts along the axon of thin diameter neurons is energetically advantageous and requires fewer channels to conduct action potentials. During an action potential $Na_V1.8$ currents across the membrane in these thin axons are large enough to dramatically change the sodium ion concentration gradient and thereby void the assumptions upon which the cable equation is based. Using scanning electron microscopy $Na_V1.8$ is seen to be clustered, as are lipid raft marker proteins, on neurites at scales below 200nm. FRET signals show that the lipid raft marker protein Flotillin is densely packed on the membrane however disruption of rafts does not reduce the FRET signal from dense protein packing. Using mass spectrometry I investigated the population of proteins found in the lipid rafts of sensory neurons. I found that the membrane pump NaK-ATPase, which restores the ion concentrations across the membrane, is also contained in lipid rafts. NaK-ATPase may help to offset concentration changes due to $Na_V1.8$ currents enabling the repeated firing of c-fibres, which is associated with spontaneous pain in chronic pain disorders.

Table of Contents

Declaration of Originality

The work contained in this document is solely that of the author. Any contribution made by others is clearly acknowledged and works appropriately referenced.

Abbreviations

BDNF	Brain Derived Neurotrophic Factor
CDF	Cumulative Distance Function
CNS	Central Nervous System
CTB	Cholera Toxin Beta subunit
DMEM	Dulbecco's Modified Eagle Medium
DRG	Dorsal Root Ganglion
DRM	Detergent Resistant Membrane
FBS	Foetal Bovine Serum
FRET	Förster Resonance Energy Transfer
GFP	Green Fluorescent Protein
GM1	monosialotetrahexosylganglioside
GO	Gene Ontology
HEK	Human Embryonic Kidney
MBCD	Methyl-Beta-Cyclodextrin
NaK-ATPase	Sodium Potassium Transporting ATPase pump
ND7	Mouse Neuroblastoma and Rat Neuron Hybrid Cell Line
NGF	Neuron Growth Factor
PBS	Phosphate Buffered Saline
PC12	Rat adrenal gland phaeochromocytoma derived cell line
PFA	Paraformaldehyde
PNS	Peripheral Nervous System
SEM	Scanning Electron Microscope/y
Thy1	Thy 1membrane glycoprotein

Acknowledgments

I would like to thank:

My supervisor Dr Kenji Okuse for help and guidance

Dr Alessandro Pristera for help with laboratory techniques, particularly the expression of cloned constructs, and previous work which inspired my PhD research.

Dr Richard Swanwick, Dr Kersti Karu, Dr Ko Hasebe and the rest of the Okuse lab for help with laboratory techniques and support.

Dr Bill Wisden, Dr Nick Franks FRS, and Dr Stephen Brickley, for helpful suggestions and feedback.

Dr Aldo Faisal and Mohammad Neishabouri for collaborative work on computational modelling.

My husband Alistair Finn for limitless support and understanding.

My daughter Iona for helping me stay positive and grounded.

My mother for helping me to have time to work and encouraging me.

1 Introduction

1.1 Pain

1.1.1 Definition and Categorisation

Pain is defined as “An unpleasant sensory and emotional experience associated with actual or potential tissue damage, or described in terms of such damage”(IASP 2011). Pain is a very important protective mechanism against potential damage to an organism, and even some of the most primitive organisms have mechanisms to remove themselves from noxious stimuli. Nociception is the detection of noxious stimuli. However, the actual sensation of pain only occurs in the brain and therefore to be considered pain, rather than just nociception, there must be an unpleasant affective aspect. As such pain in non-verbal organisms can only be inferred from behaviour rather than directly recorded by self report. Facial expression can be used in mice (Langford et al. 2010) and infants (Prkachin 2009) as a indicator of pain and responses to noxious stimuli in animals, such as paw withdrawal, can be used to infer pain intensity. As pain is a sensation that occurs in the brain it is inherently subjective. Even in humans it is difficult to compare painful experience between individuals due to differences in perception and reporting. Pain is frequently measured as a self reported score on a scale of 1 to 10.

Pain can be broadly categorised depending on the cause and to some extent the mechanisms involved. Acute pain arises from a direct insult and resolves once the stimulus is removed. Inflammatory pain arises from the body’s own response to injury. Tissue damage at the site of the stimulus leads to an inflammatory response and hyper-sensitivity to further stimulus. This damage often follows after acute pain which accompanies the stimulus. Both these forms of pain are clearly biologically useful to protect our bodies from injury and promote recovery. Chronic pain is pain that persists over a long period of time. Chronic pain can either be due to an ongoing physiological problem, such as back injury or arthritis, or can be defined as neuropathic pain, which arises from damage directly to the nervous system itself. Unlike pain due to other causes neuropathic pain has no biologically protective role. Some chronic pain, which

started out with a physiological cause, can cause irreversible changes to the nervous system and therefore chronic pain can possibly be considered a disease state in itself (Tracey & Bushnell 2009).

Neuropathic pain is defined as “pain initiated or caused by a primary lesion or disease in the peripheral or central nervous system”(IASP n.d.) It has many varied causes that range from trauma to disease and drug treatments. Trauma caused by accidents or surgery can sever or compress nerves. Metabolic disorders such as diabetes and diseases such as herpes zoster lead to the damage of nerve fibres innervating the skin. Many drug treatments, including anti-HIV and chemotherapy drugs, can also lead to nerve damage and neuropathic pain. Inherited syndromes in which neuropathic pain is a symptom have been shown to be caused by a mutation to sodium channels (Fischer & Waxman 2010; Faber et al. 2012). Neuropathic pain is characterised by a variety of painful symptoms; these include spontaneous pain, hyperalgesia and allodynia. Spontaneous pain, which can also occur in inflammatory states, arises with no apparent painful stimulus (Djouhri et al. 2006). Hyperalgsia occurs when normally mildly painful stimulus is experienced as intensely painful. Allodynia is a painful sensation arising from a normally non-painful stimulus such as light touch, warmth or mild cold. Sensory loss is also a common symptom in patients with neuropathic pain. Loses can include regions of numbness and increased thresholds of response to mechanical and thermal stimulation, this arises from lost innervation of the skin due to nerve damage.

Neuropathic pain affects approximately 10% of the adult population (Yawn et al. 2009) across different countries and together with other forms of chronic pain is estimated to affect 20-30% of the population (Breivik et al. 2006; Johannes et al. 2010). Chronic pain is often associated with depression, anxiety and insomnia. Therefore the treatment of pain is the focus of many researchers from clinicians to molecular biologists. Although effective and easily available treatments exist for the control of acute and inflammatory pain, such as non-steroidal anti-inflammatory drugs (NSAIDS), these are generally ineffective for the treatment of neuropathic pain. Even drugs

targeted at neuropathic pain work in relatively few, less than 50%, of patients and often have little effect on reducing pain scores. This has lead to drugs originally for other uses, such as anti-depressants, being used for treatment of neuropathic pain. These can be quite effective and their mode of action is thought to involve regulation of serotonin (5HT), but remains uncertain (Sindrup et al. 2005). New treatments for chronic pain, and specifically neuropathic pain, could have the ability to changes peoples' lives and save the health care system large sums of money. Often the limiting effect on peoples' lives of chronic pain leads to further ill health (Crombez et al. 1999).

1.1.2 Nociceptors – Classification, Anatomy and Connectivity

Sensory neurons which innervate the skin have their cell bodies in the dorsal root ganglions (DRG). The distal axonal branches of the lower limb DRG neurons, along with motor neurons, form the sciatic nerve and their proximal axonal branches connect with the central nervous system (CNS) in the dorsal horn of the spinal cord. Primary sensory afferents fall into two groups; those which respond to low threshold stimuli and those that respond to high threshold stimuli. DRG neurons are classified into 3 sub-groups by their sensory modality and morphological features (Table 1-1). Aβ neurons have large diameter cell bodies and axons, which are myelinated. Aδ have thinly myelinated, medium diameter axons and c have small diameter axons and are unmyelinated (Lawson 2002). Nociceptors, which are neurons activated by high threshold possibly harmful stimuli, are present in all of the sub-types, as are neurons detecting low intensity stimulus. However, nociceptors seem to be mostly made up of neurons with Aδ and c-fibre afferents, whereas Aβ are mainly activated by non-noxious stimuli. Aδ nociceptors respond to painful stimulus by generating fast travelling signals, giving rise to a sensation of acute pain. C-type nociceptors have a slower speed of conduction than Aδ neurons, less than 2 m/s compared with 14-30 m/s, due to their lack of myelination and small diameter. The pain following c-fibre stimulation is often described as a burning pain and it is noticeably delayed from the time of insult. C-type nociceptors are involved in the sensation of inflammatory and neuropathic pain.

Cell Type	Aβ	Aδ	C
Soma Diameter (μm)	30+	10-30	10
Axonal Diameter (μm)	6-12	1-5	0.1-2.0
Myelination	Thickly myelinated	Thinly myelinated	Remak bundles
Conduction speed (m/s)	5-75	5-35	0.4 -2
Dominant Sensory modality	Low threshold mechano-reseptors	First Pain	Pain, heat and cold

Table 1-1 DRG cell types. Properties of the different classes of DRG neuron and nerve fibres.

Some c-type sensory neurons respond to low intensity stimulus, such as slowly moving light touch, instead of high intensity stimulus. However, these neurons produce very little substance P from their subcutaneous terminals upon activation, unlike nociceptive c-type neurons, which act to induce inflammation. Mechano-sensitive (non-nociceptive) c-fibre neurons conduct faster that nociceptive ones and slowed much more quickly in response to sustained firing (Weidner et al. 1999).

DRG neurons can also be classified by differential expression of marker proteins. Aδ neurons express Transient Receptor Kinase B (TrkB) and are trophic for brain derived neurotrophic factor (BDNF). C-type neurons can be split into two sub groups, those that express Transient Receptor Kinase A (TrkA) and those that can be labelled by lectin IB4.

Peripheral nerve injury frequently leads to the development of neuropathic pain, and therefore is widely used in animal models of neuropathic pain. These forms of injury, which include sciatic nerve ligation or transaction, lead to increased activity in both the injured nociceptor fibres and nearby undamaged fibres (Djouhri et al. 2006). Injury also leads to changes, such as in the expression and distribution of proteins, in the damaged neurons as well as surrounding neurons and glial cells.

1.1.3 Anatomy of the Pain Pathway

Pain signals progress through the nervous system from the periphery to the brain. Nociceptors are the first step in pain pathways. In the dorsal horn of the spinal cord

nociceptors synapse in lamina I, II and V. In the superficial laminar, I and the outer part of II, the spinal cord neurons with which they connect form direct connections with the brain as part of the ascending pathway. In laminar V nociceptors synapse with wide dynamic range neurons which also connect with other sensory neurons and neurons of the descending pathway and perform a degree of processing before information is transmitted to the brain.

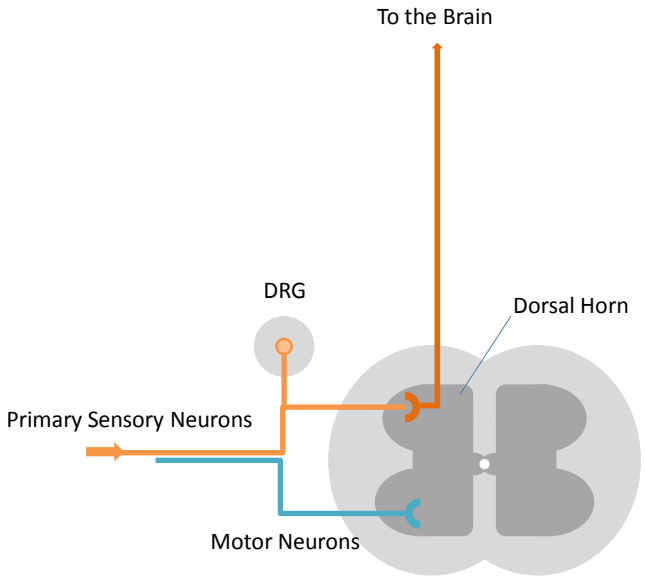

Figure 1-1 Pain pathway from the periphery to the brain. Painful stimulus elicits a response in the afferent nerve fibres of DRG neurons. These signals are relayed to the central nervous system (CNS) when DRG neurons synapse in the dorsal horn of the spinal cord.

The spinal cord also contains many glial cells, such as microglia and astrocytes which can modify the properties of the neurons. Following nerve injury endogenous spinal microglia proliferate in the dorsal horn and transition from a resting to activated state, (Rothman et al. 2009). They also move via chemotaxis and produce cytokines and chemokines. Descending pathways from the brain modify the input from the periphery at the level of the spinal cord, (Seal et al. 2009), the modulation can be both inhibitory and excitatory. Together these factors, at the level of the spinal cord, can enhance the sensation due to a pain state and are termed central sensitisation.

Ascending pathways from lamina I of the dorsal horn connect to the parabrachial and limbic system in the brain, whereas the ascending pathway from laminar V connects to the thalamus and cortex. The input to the cortex and thalamus gives rise to the sensation of the location and intensity of the stimulus and the limbic system gives rise to the negative affective aspects of painful sensation.

Neuropathic pain involves all levels of the nervous system. Specific areas of the brain are involved in pain processing; these are collectively referred to as the pain matrix (Tracey 2008). It includes the somatosensory, cingulate, and insular cortices and also areas associated with affective aspects such as the amygdala. The brain can modulate painful inputs in the dorsal horn via the descending pathway, which originates in the rostroventral medulla (RVM).

1.2 Sodium Channels

1.2.1 Ion Channels and Signal Transduction

Ion channels are proteins which create and control pores in the membranes of cells to help regulate the concentration of ions within the cell. At equilibrium ion channels, in conjunction with ion pumps, maintain osmotic pressure of the cells and ensure the availability of elements the cell needs to function.

Neurons have made use of adapted ion channels to produce and transmit electronic signal based on the movement of ions instead of electrons. Heart and muscle tissues also use ion channels to produce ionic currents. Sodium, potassium and calcium channels share a common ancestor. Voltage gated sodium channels are essential for the initiation and transmission of action potentials (AP) in the nervous system. Sodium channels change state depending on the voltage difference across the membrane, they can be open, closed or in a state of inactivation. When in the open state sodium ions can pass through them freely, so that a currently is produced across the membrane in proportion to the voltage across it. Voltage gated potassium channels are also involved in the transmission of AP.

1.2.2 Voltage Gated Sodium Channels

Voltage gated sodium channels consist of a large alpha subunit and a smaller partner beta subunit. The alpha sub unit contains the pore of the channel through which sodium ions pass.

The beta subunit modifies the properties of the channel and can increase the density of the channels on the plasma membrane, but they are not necessary in order for the channel to be functional. There are 4 different beta subunits, all of which are found in both the central and peripheral nervous system.

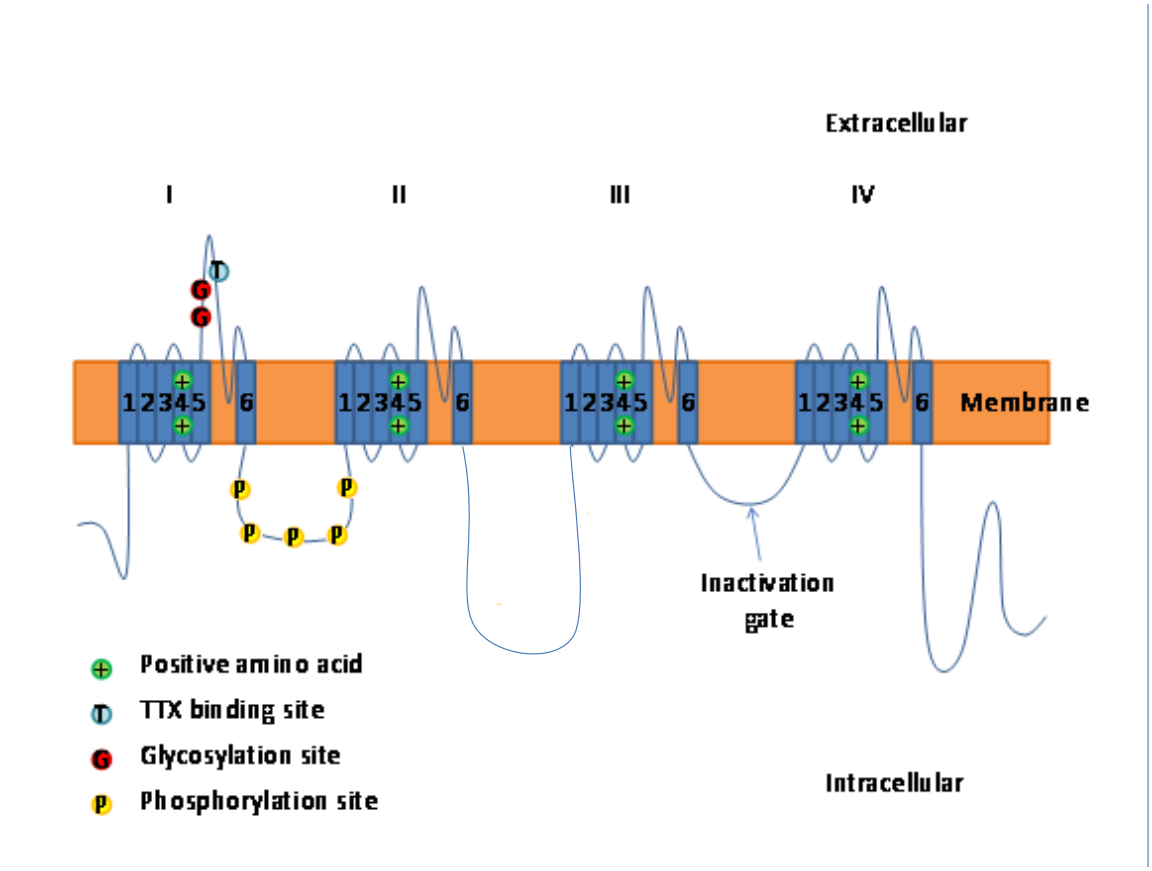

Figure 1-2 Schematic representation of a generalised voltage gated sodium channel. Diagram of the amino acid chain of a VGSC showing trans-membrane segments and sites of interest.

All alpha sub units share a common structure, with 4 homologous repeat domains each containing 6 trans-membrane segments. The fourth segment of each repeat acts as a

voltage sensor due to positively charged amino acids in the trans-membrane region. These cause the segment to shift in response to changes in the membrane voltage and changing the conformation of the channel. Segments 5 and 6 of each repeat face the pore region of the channel and part of the loop between them enters the pore of the channel.

There are 10 mammalian voltage gated sodium channels. Nine have been well described and play a role in the conduction of electrical signals. Sodium channels are named according to the system based on potassium channels, starting Na of the ion they are selective for, then subscript V for voltage gated, then the number of the family, currently only 1, and then a decimal point and number for each unique channel, 1 through 9 (Goldin 2000). $Na_V1.1$, $Na_V1.2$, $Na_V1.3$ and $Na_V1.7$ are closely related to each other, and $Na_V1.5$, $Na_V1.8$ and $Na_V1.9$ form another related group. $Na_V1.4$ and $Na_V1.6$ stand apart from these sub-groupings. The tenth channel Na_X has not been well characterised and it is thought it is not involved with the conduction of action potentials. It is sensitive to sodium levels in the extra cellular medium and has been shown to be integral to sodium homeostasis (Shimizu et al. 2007). It is also thought to have a role in the setting of the resting membrane potential of the cells in which it is found (Ke et al. 2012). Sodium channels are also located separately anatomically, with $Na_V1.1$, $Na_V1.2$, $Na_V1.3$, $Na_V1.6$ and $Na_V1.7$ located in the nervous system, $Na_V1.8$ and $Na_V1.9$ located mainly in DRG neurons, $Na_V1.5$ in the cardio myocytes of the heart and $Na_V1.4$ at the skeletal muscular junctions. Sodium channels are also classified based on their sensitivity to Tetrodotoxin (TTX), a potent neuro-toxin produced by bacteria resident in the puffer fish. TTX sensitive channels are blocked by the toxin, stopping the passage of ions through the pore. Only the sub-grouping of $Na_V1.5$, $Na_V.18$ and $Na_V1.9$ are known to be TTX resistant.

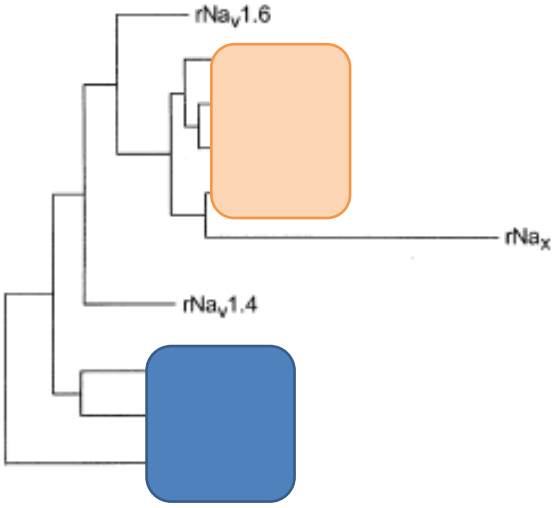

Figure 1-3 Phylogenetic relationships between VGSC sub units. Na$_V$ 1.2, 1.1, 1.3 and 1.7 form one sub group and Na$_V$ 1.5, 1.8 and 1.9 another. Na$_V$1.6 and Na$_V$1.4 are not part of any closely related group. Na$_X$ is more distantly related and may only regulate resting potentials. Adapted from (Goldin 2000).

1.3 Na$_V$1.8

1.3.1 Characteristics, Structure, Location

Na$_V$1.8 is a tetrodotoxin (TTX) resistant voltage gated sodium channel. In common with the other voltage gated sodium channels it contains 4 domain repeats each with 6 trans-membrane alpha-helix segments. In rats its 1957 amino acid sequence is encoded by the 97 kbp gene SCN10A, which in humans is located on chromosome 3. There are two other known splice variants.

Na$_V$1.8 contains the modification of a single amino acid, in common with Na$_V$1.9 and Na$_V$1.5, which confers TTX resistance. The site of the mutation is in the outer pore of the folded functional channel (Fozzard & Lipkind 2010).This inhibits the binding of TTX such that the channel functions up to concentrations of 75 µM, whereas TTX sensitive channels cannot function in concentrations above 100 nM (Elliott & Elliott 1993).

The C-terminus of $Na_V1.8$ regulates membrane channel density, via influences on trafficking of the protein, and inactivation properties of the channel (Choi et al. 2004). This might be due to the amino acid motif PXY, which has been shown in other channels to mediate the removal of the channels from the membrane (Abriel et al. 2000).

$Na_V1.8$ expression is mainly restricted to primary sensory neurons that produce c-fibres (Benn et al. 2001). These cells are found in the dorsal root ganglion (DRG) and their axons in the sciatic nerve (Nassar et al. 2005). It is also expressed in neurons of the nodose and cranial sensory ganglion and in heart tissue. In rats the expression of $Na_V1.8$ begins on embryonic day 15 and increases with age until it reaches adult levels on postnatal day 7.

1.3.2 Role in Conduction

In small diameter c-type neurons of the DRG $Na_V1.8$ is crucial for the transmission of action potentials, being responsible for at least 80 % of the current in the rising phase (Renganathan et al. 2001). Small diameter DRG neuron cells with $Na_V1.8$ absent produce only small graded responses instead of APs, despite having the same resting potential, and current and voltage thresholds. The presence of $Na_V1.8$ doesn't affect the resting potential. As $Na_V1.8$ is responsible for the majority of the current in small diameter DRG neurons it has been recognised that this is the channel responsible for the TTX-R current that has been recorded in these cells. In fact the only other TTX resistant sodium channel present in DRG neurons, $Na_V1.9$, has been shown to be insufficient to produce AP, but instead affects resting potential by producing a persistent current. DRG neurons also express $Na_V1.7$ along their entire length (Black et al. 2012). As such the exact relative contributions have not been distinguished.

The $Na_V1.8$ mediated TTX-R current has different properties to the TTX-S current, associated with $Na_V1.7$, in DRG neurons. The TTX-R current has slower time to peak and a longer over shoot and is therefore sometimes referred to as the slow current. However, the recovery from inactivation is much faster for the TTX-R compared to the TTX-S, this means that the channels are re-primed quickly and able to fire repeated AP

in quick succession. These differences are due to differences in the voltage dependence of inactivation. As cells with a large proportion of $Na_V1.8$ sodium channels are able to fire long trains of AP in response to a stimulus (i.e. their response continues to be the same) they are slowly adapting. C-fibres containing $Na_V1.8$ can conduct spike trains at a frequency of up to 50 Hz (Olausson 1998).

1.3.3 Pain

As the crucial element in the transmission of pain signals, VGSC are intimately linked to pain states. Pain states are also associated with changes in VGSC expression, especially in peripheral neurons. In neuropathic pain states changes in the expression of VGSC have been linked to the development of hypersensitivity and allodynia.

As the predominant VGSC in c-type neurons, $Na_V1.8$ is essential for the detection of nociceptive stimulus. Their involvement in the development and maintenance of neuropathic pain has been less clear. There is evidence both supporting their role in neuropathic pain and evidence to the contrary. A reduction in $Na_V1.8$ currents has been shown after injury to peripheral nerves that leads to neuropathic pain behaviours in animal models (Cummins & Waxman 1997). A reduction in expression in human neuropathic pain patients has also been observed. A corresponding reduction in TTXr currents was also observed. $Na_V1.8$ knock out (KO) animals show significant deficit in their ability to sense noxious mechanical stimuli, and some deficit in noxious thermo-reception. These KO animals otherwise appear normal and there is an up regulation of other TTXs VGSC to compensate for their lack of $Na_V1.8$. KO animals still develop neuropathic pain behaviours normally in pain models (Matthews et al. 2006).

Antisense knock down of $Na_V1.8$ after spinal nerve ligation (SNL) reverses neuropathic pain behaviour in rats (Gold et al. 2003). The contribution $Na_V1.8$ plays in the development of pain behaviours in this model of neuropathic pain is attributed to its redistribution to the axons of uninjured c-type DRG neurons as seen via immunoreactivity. This increase in channels in the unmyelinated axons is not clearly linked to an increase in transcription in the cells bodies in the DRG. Specific blocking of $Na_V1.8$ has an analgesic affect, leading to the reduction of pain behaviour in response

to usually painful stimulus and a reduction in the symptoms associated with pain models (Gaida et al. 2005). Of particular interest is the case of a scorpion toxin, which in most mammals leads to an intense sensation of pain by activating the $Na_V1.7$ channel, but which in the grasshopper mouse is a specific blocker to its mutated version of $Na_V1.8$, thereby acting as a powerful analgesic (Rowe et al. 2013).

Other VGSC are involved in the transmission of pain signals. $Na_V1.7$ in particular has been shown to be crucial to the detection of normal acutely painful stimulus. Where individuals have certain mutations to the gene encoding $Na_V1.7$, such that it is not fully functional, they are unable to sense pain (Cox et al. 2010). This deficit can easily lead to bodily injury due to the persons normal protection mechanisms not functioning. $Na_V1.7$ is also expressed in the c-type neurons that express $Na_V1.8$. Again its role in neuropathic pain is uncertain as neuropathic pain still develops normally in $Na_V1.7$ knock out mice, even if $Na_V1.8$ is also knocked down, (Nassar et al. 2005).

There are multiple ways that VGSC can affect the signals transmitted by neurons. Their electrophysiological properties can change, leading to changes in current passed through them. Their distribution can change to allow for easier AP generation or transmission. The functional expression of channels can change, either through translocation to and from the membrane or by the production of more channels.

1.3.4 Interactions

Like other VGSCs $Na_V1.8$ is associated with sodium channel β sub units in order to exhibit its full electrophysiological properties. The β3 subunit can enhance the current amplitude from $Na_V1.8$ by promoting its expression on the plasma membrane. The c-terminus of β3 masks the endoplasmic reticulum retention motif on the first intracellular loop of $Na_V1.8$ and therefore promotes trafficking to the surface (Zhang et al. 2008). Association with a single β1 subunit increases $Na_V1.8$ functional expression by six times (Vijayaragavan et al. 2001).

$Na_V1.8$ also associates with other proteins. Yeast two hybrid screening has shown at least 28 potential interacting protein partners (Malik-Hall et al. 2003), of which only one, p11, has been investigated in detail.

$Na_V1.8$ has also been shown to associate with Aquaporin 1 (AQP1), a water channel which regulates cell osmotic water permeability. The function of $Na_V1.8$ is impaired in the absence of AQP1. This leads to reduced thermal inflammatory pain perception in AQP1 knockout mice, due to reduced $Na_V1.8$ dependant sodium current in DRG neurons (Zhang & Verkman 2010).

p38 mitogen-activated protein kinase is activated in DRG neurons following nerve injury and peripheral inflammation. p38 co-localises and regulates the function of $Na_V1.8$ by direct phosphorylation (Hudmon et al. 2008).

Various molecules $Na_V1.8$ interacts with have been shown to be necessary for cell surface functional expression of the channel in cell lines. Sodium channel β1 sub unit, p11 and lidocaine, a local anaesthetic, have all been shown by various studies to improve functional expression (Zhao et al. 2007).

1.4 Lipid rafts

1.4.1 Structure

The plasma membrane of cells is called a lipid bi-layer, this describes how it is made up of two opposing layers of lipid molecules. The lipids are mainly phospholipids which have a polar head group and hydrophobic tail groups (usually two). These lipids are amphiphiles as these have a hydrophobic and a hydrophilic region which oppose each other. This causes the hydrophobic tails to face into the middle of the membrane and the hydrophilic heads to face the outer plasma. The membrane also contains many other molecules including proteins. The configuration of the constituents of the membrane has traditionally been described with the fluid mosaic model. This model states that the lipids and other molecules in the membrane form a two dimensional liquid in which the constituents can diffuse freely leading to a homogenous mix (Singer & Nicolson 1972).

However, it has since been shown that some molecules are enriched in the inner or outer leaflet of the membrane (Brown & London 1998; Simons & Van Meer 1988) and

that some areas of the membrane are more resistant to solubilisation with ionic detergents. These areas are referred to as detergent resistant membrane (DRM), and they have been found to be enriched in cholesterol and sphingolipids. These areas of the membrane have been described as lipid rafts due to their higher stability than the surrounding membrane (Simons & Ikonen 1997). Cholesterol packs densely with saturated lipids of the membrane due to its relatively small hydrophilic head group, this leads to lipid rafts being more rigid than the rest of the membrane, and less accessible to detergents. The saturated fatty acid side chains of the phospholipids contained in lipid rafts are not kinked like their unsaturated counterparts, therefore they are able to pack more closely with cholesterol.

1.4.2 Constituents

Lipid rafts contain higher levels of sphingolipids and cholesterol as well as phosopholipids with saturated fatty acid side chains, such as phosphatidylinositol phosphates, than the surrounding membrane. The surrounding non-raft membrane has high levels of glycerophospholipids, such as phosphatidylcholine, which is depleted in lipid rafts. Lipid rafts also contain more glycosphingolipids, such as gangliosides. Cholesterol has a small hydrophilic hydroxyl group in the outer polar region of the membrane and a large rigid hydrophobic planar structure into the membrane. It takes up more space internally in the membrane than externally unlike phospholipids.

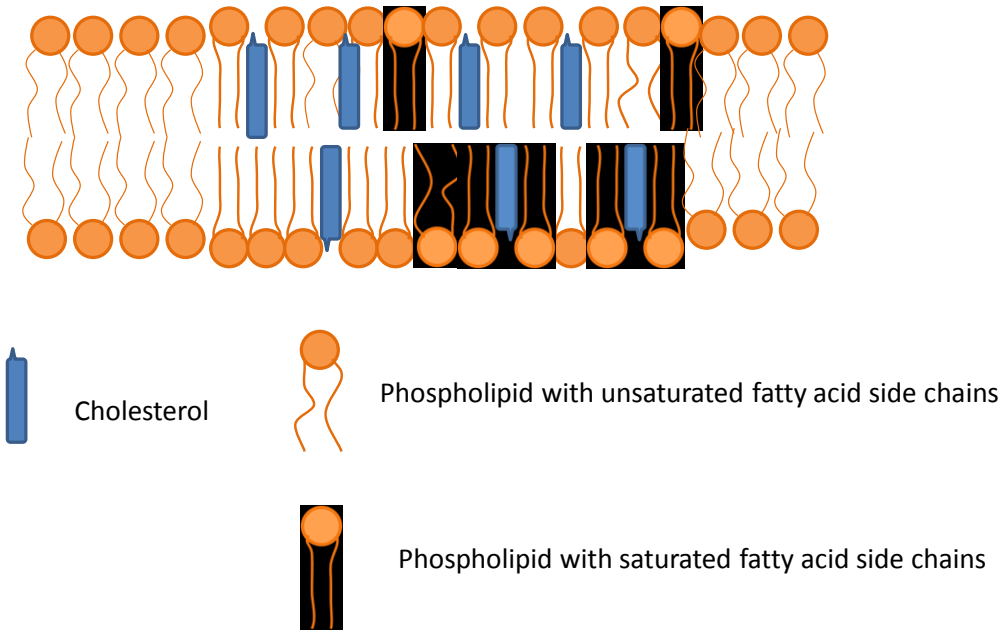

Figure 1-4 Diagram of the arrangement of lipids in planar raft membrane. The surrounding membrane is made up of primarily lipids with unsaturated side chains, which are kinked. The raft portion in the centre has higher proportions of cholesterol and saturated phosopholipids. These components cause it to be slightly thicker than the surrounding membrane.

1.4.3 Properties

The unique composition of lipid rafts gives them different properties to the surrounding membrane. Lipid rafts are thicker and stiffer. Their components diffuse slower within them and are more resistant to micelle forming amphiphiles. Lipid rafts are thicker than the surrounding membrane, this has been observed using electron microscopy and atomic force microscopy (Yuan et al. 2002).

Membrane lipids can form different phases of organisation. The phase depends on the composition and temperature of the membrane. At low temperatures membranes can form into the gel phase, where lipids form a crystal structure which lacks lateral diffusion, this is the least fluid phase and generally known as the gel phase. Lipid membranes at biological temperatures generally form more fluid phases, known as the

liquid ordered (L_O) phase, and the liquid disordered (L_D) phase. The L_D phase is the most fluid and molecules can diffuse laterally freely. This is the phase which most resembles the classic Singer-Nicholson fluid mosaic model. Lipid rafts are thought to exist in the L_O phase. In this phase molecules are tightly packed together, but unlike the gel phase they are still able to move laterally, although with less freedom than in the L_D phase.

1.4.4 Protein Organisation

As well as differences in lipid composition between rafts and the surrounding membrane there are also differences in the protein populations residing in them. Some proteins are so highly enriched in the rafts of the membrane, that they can be used as markers for these regions, such as Flotillin, which is used as a marker for planar lipid rafts. Lipid rafts can also form invaginations called caveolae due to the inclusion, in the inner leaflet of the membrane, of the protein Caveolin. Caveolin forms a hairpin shape homo-dimer, which, when inserted, causes positive curvature of the membrane, and so helps form the invagination. Types of protein that tend to be included in rafts, are glycosylphos-phatidylinositol (GPI) anchored and transmembrane proteins. For transmembrane proteins the sequence of amino acids in the transmembrane region influences the degree of affinity for raft membrane.

Lipid rafts have been shown to be the location of signalling proteins, such that, clustering of lipid rafts can then lead to signal transduction by the interaction of proteins from separate rafts being brought into close proximity (Simons & Toomre 2000).

The membrane associated protein Annexin A2 has been shown to be associated with lipid rafts. Two units of Annexin A2 form a hetrotetramer with two Annexin 2 light chain proteins, usually known as p11. It has been shown to bind to acidic phospholipids of the inner leaflet in a Calcium (Ca2+) dependant manor, but bind to phosphatidylinositol (4,5)-bisphosphate, which is enriched in rafts, in a calcium independent manor, Figure 1-5. This calcium independent binding uses the linker region of the Annexin A2 – p11 complex which leaves the Annexin A2 able to bind

laterally with other Annexin A2 – p11 complexes. This lateral binding could stabilise smaller rafts so they can coalesce into large raft platforms. Therefore this is a possible method of raft clustering. $Na_V1.8$ also binds to p11 and as the p11 binding sites are different for Annexin A2, residues 85-91 (Kube et al. 1992), and $Na_V1.8$, residues 33-78 (Poon et al. 2004), it might be possible that a complex with $Na_V1.8$ and Annexin A2 could be formed.

.

Model of membrane domain stabilization mediated by annexin A2.

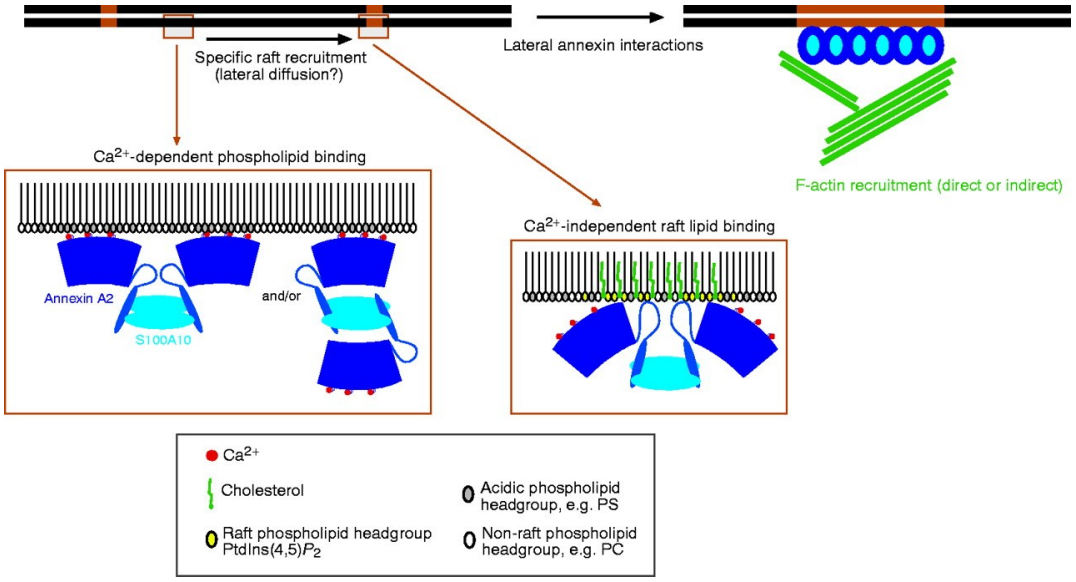

Rescher U , and Gerke V J Cell Sci 2004;117:2631-2639

Figure 1-5 Annexin A2 can facilitate lipid raft clustering. Annexin A2 can bind to the lipid raft portion of the membrane in a calcium independent manner, which enables additional interactions between Annexin A2 assemblies and encourages clustering of the membrane rafts. Adapted from (Rescher & Gerke 2004).

1.4.5 Protein Functional Modification

Trans-membrane protein structure is often postulated based on the amino acid sequence. This can be done as trans-membrane regions often follow set patterns, such as the alpha helix, and the amino acids match the properties of the membrane in terms of their hydrophobicity. Certain amino acids are more hydrophobic and are therefore more likely to reside inside the membrane. Sometimes hydrophilic polar amino acids are trans-membrane, but this can be interpreted, such as in the case of sodium channels, as being a pore forming region, which will therefore be in contact with an aqueous environment. The different properties of lipid rafts can affect the proteins within them. Their increased thickness may increase the partitioning of proteins within them that have a closer match in the length of their hydrophobic region (McIntosh et al. 2003). They are also stiffer than the surrounding membrane. Some transmembrane proteins undergo conformational changes as part of their function. The stiffness of the surrounding membrane and the strength of hydrophobic coupling with it can regulate conformational change and therefore protein function. A well known example is the gramicidin channel (Lundbaek et al. 2004). In the case of gramicidin a single protein is not functional, being inserted only halfway through the membrane. When two proteins meet each other (one in either leaflet of the membrane) they can form a pore in the membrane, but only if the membrane is flexible enough to allow it to be deformed to a narrower thickness. A more complex example is the sodium channel $Na_V1.4$, whose electrophysiological properties can be regulated by the stiffness of the membrane in which it is inserted. The channel's inactivation properties can be changed by removal of cholesterol from the membrane, which causes the membrane to become less rigid. Cholesterol depletion is also used as a method of lipid raft disruption. The cholesterol in the membrane inhibits the sodium channel inactivation.

1.5 $Na_V1.8$ Clustering and Lipid Raft Localisation

1.5.1 Channel Clustering

Many types of voltage gated sodium channels (and other ion channels) are not distributed homogeneously on the membranes of nerve cells. Most notably in myelinated neurons sodium channels are clustered at the nodes of Ranvier, where there are gaps in the myelination, allowing access to the extracellular medium. This clustering is essential for salutatory conduction, which enables the fast and efficient propagation of signals in myelinated neurons. The development of clustering at nodes has been shown in some cases to be dependent on contact of the cell membrane with myelinating Schwann cells (Vabnick et al. 1996). Although in other cases treatment with Oligodendrocyte conditioned media has been shown to be sufficient to induce clustering of the channel $Na_V1.2$ (Kaplan et al. 2001). This myelin independent clustering is set by electrical activity in the neuron, such that an increase in sodium currents leads to a decrease in clustering. In bipolar neurons there are also dense clusters at the axon initial segment (AIS), which is where the axon emerges from the soma. These clusters contain a higher density of sodium channels than elsewhere in the neuron and can be essential for the initiation and propagation of AP in neurons (Kole et al. 2008). The mechanism underlying the clustering of channels in the AIS is dependent on the formation of complexes linked to the cytoskeleton via the scaffold protein ankyrin G (AnkG). Initially AnkG is the first protein clustered in the AIS, where it binds to the plasma membrane via it membrane binding domain. VGSC bind directly to AnkG through its membrane binding domain (MBD), which is an ankyrin repeat domain. The region of the VGSC which binds AnkG is a highly conserved region in the loop between domain II and III.

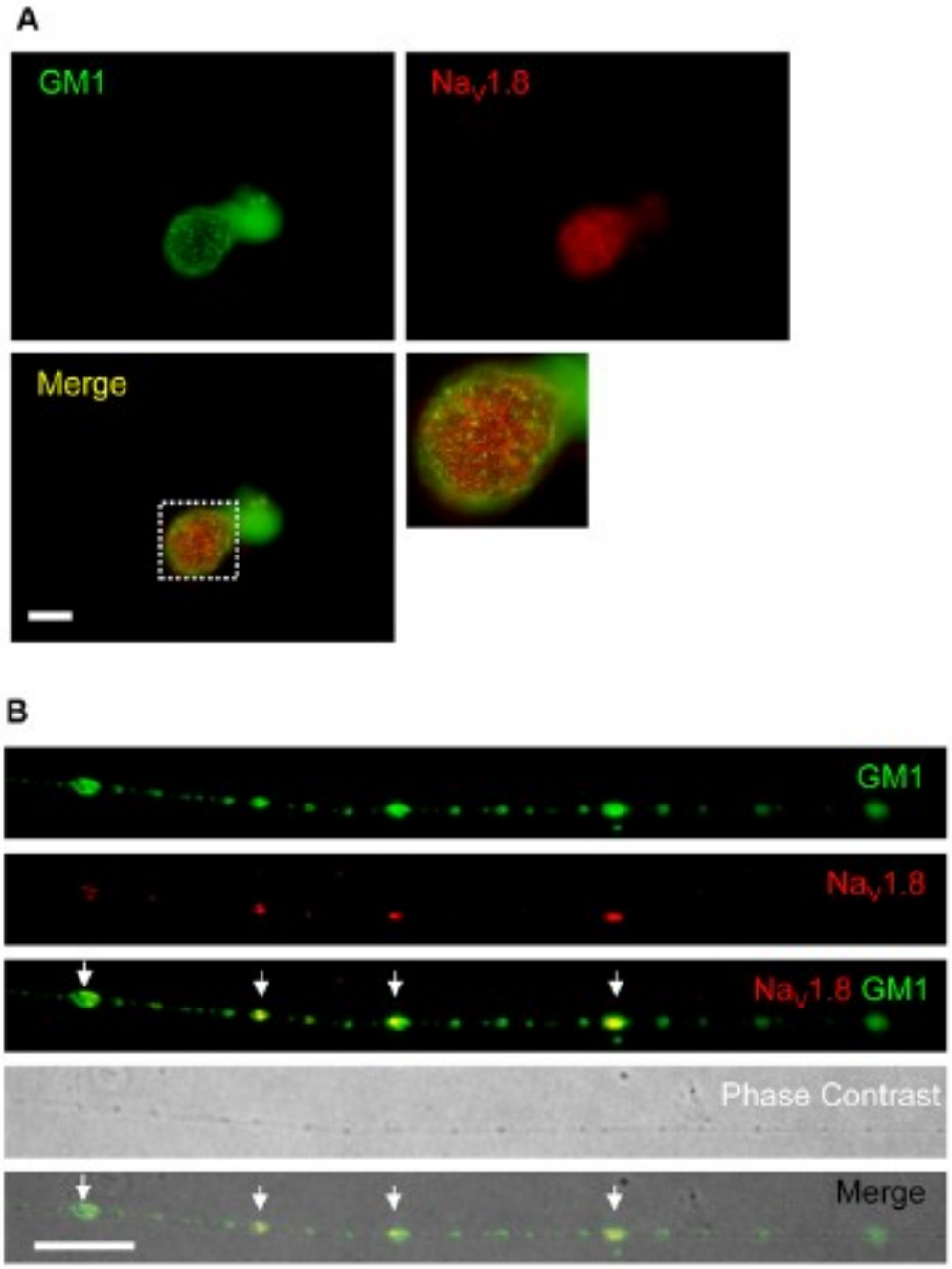

Figure 1-6 Na$_V$1.8 shown to co-localise with lipid raft maker GM1 on neurites but not in the cell body. Using immunofluorescence Na$_V$1.8 is shown to be distributed in clusters along the length of neurites, which also contain GM1. Cells shown are from cultured rat DRG neurons two days after plating. Scale bars show 20 µm. A. In the cell body Na$_V$1.8 does not co-localise with GM1 and expression in mainly intracellular. B. Along the neurites Na$_V$1.8 and GM1 are discretely clustered. Na$_V$1.8 colocalises with GM1 but not all GM1 clusters immunofluorescent labelling of Na$_V$1.8. From (Pristerà et al. 2012)

1.5.2 $Na_V1.8$ Clustering and Lipid Raft Association

DRG neurons are pseudo-unipolar. Their axons run directly from the periphery to the spinal cord, forming the sciatic nerve. Their cell bodies are on a side branch, located in the dorsal root ganglion. As their axon does not emerge from the soma, they have no AIS.

As c-type neurons have no myelination or AIS, it was assumed that, in the absence of known clustering mechanisms, VGSC would be evenly distributed along the axons. However, $Na_V1.8$ has been observed to be discretely clustered along the length of DRG axons despite the absence of myelination (Pristerà et al. 2012). This has been observed in both ex vivo, in axons of the sciatic nerve, and along the neurites of cultured cells, shown in Figure 1-6. Moreover these clusters are co-localised with lipid raft marker proteins. These include ganglioside GM1, Thy1, Flotillin and Caveolin. The clustering with lipid raft makers is not observed in the cell bodies of DRG neurons.

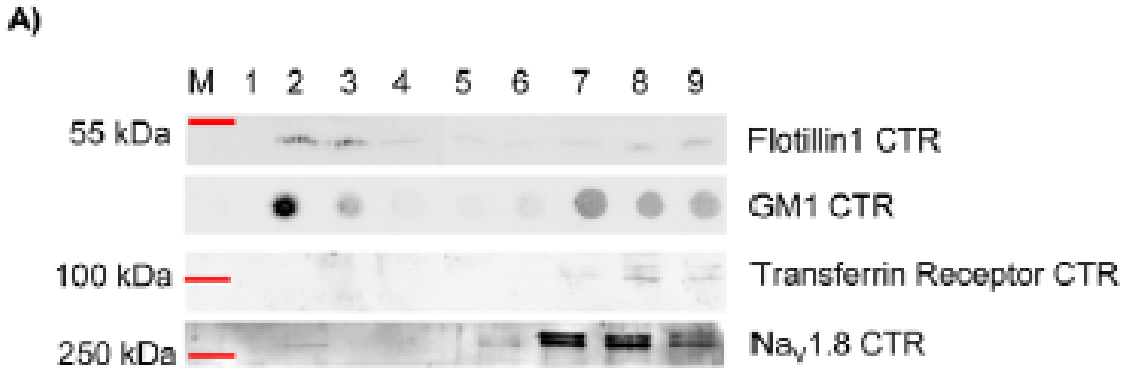

Figure 1-7 $Na_V1.8$ is co-localised with lipid raft marker proteins in the DRM extracted from cultured DRG neurons. From (Pristerà et al. 2012).

This co-localisation is also observed after sub-cellular fractionation to extract the lipid raft membrane from cell or tissue homogenate. The clustering of $Na_V1.8$ in DRG neurons is thought to be functionally important, as disruption of the lipid rafts in cultured DRG neurons leads to a failure to transmit signals along their neurites. This effect has been shown to be dependant specifically on TTX resistant sodium channels, of which, $Na_V1.8$ is known to be the most critical for AP propagation.

1.6 Aims

There is evidence for an association of $Na_V1.8$ with lipid rafts in the axons of DRG neurons. The inclusion of $Na_V1.8$ in lipid rafts may lead to a unique localisation and environment in which it functions. The nature of an association and its functional significance require further detailed investigation.

Clustering of $Na_V1.8$ in itself, regardless of the lipid environment, may be key to it fulfilling its role in the propagation of action potentials. The clustering of $Na_V1.8$ observed is reminiscent of nodes of Ranvier, which increase efficiency and signal velocity in myelinated neurons. Although the myelin upon which this action depends is absent, clustering may still have an advantageous effect on conduction in these small diameter fibres. Clustering of $Na_V1.8$ may change the electrical properties of the axon. The degree and distribution of clustering may well influence conduction properties. Effects may be dependant on specific gating properties, such as those of $Na_V1.8$ or other channels may also benefit from clustering. The axons of c-type DRG neurons are also known to have very thin axons and this may influence whether clustering is functionally useful.

The precise distribution of $Na_V1.8$ along the axons of DRG neurons and how this is associated with the distribution of lipid rafts is not clear as lipid rafts frequently exist below the limit of conventional light microscopy. $Na_V1.8$ may be contained in lipid rafts when observed below the light microscopy limit. The distribution of $Na_V1.8$ at this scale and how that relates to the distribution of lipid rafts will further define their relationship to each other. Observing how densely packed channels within clusters are and if this is reflected by other proteins residing within lipid raft will help develop models in the future. Observing any changes in distribution when rafts are disrupted will show an association and support it functional role in signal propagation.

Lipid rafts are known to acts as micro-domains that bring together proteins in order to increase their levels of interaction. Finding the population of proteins contained within the rafts of $Na_V1.8$ expressing neurons will help identify whether the inclusion of

$Na_V1.8$ in lipid rafts enables its interaction with other proteins that it requires to be functional.

The functional role of an association of $Na_V1.8$ with lipid rafts may be due to one or possibly multiple factors. It may be the distribution of the channels, the lipid or the protein environment.

1.6.1 Hypothesis

The inclusion of $Na_V1.8$ in lipid rafts along the axons of DRG neurons is important for its function of transmitting signals along the axons of DRG neurons.

1.6.2 Investigations

The study aims to test the hypothesis by investigating:

- The effect of $Na_V1.8$ clustering in by computational modelling. The main outcomes to be assessed are the minimum number of channels required to prevent conduction failure, the difference in conduction velocity and the efficiency of action potential propagation.
- The distribution of $Na_V1.8$ at the scale of lipid rafts and the effect on this distribution of the disruption of lipid rafts.
- The population of proteins also residing in the lipid rafts of DRG neurons, which may be potential functional partners of $Na_V1.8$. The signally networks which the lipid raft proteins may be involved in.

2 Computational Modelling of Clustered $Na_V1.8$

2.1 Introduction

2.1.1 Signal Transduction in Neurons

The nervous system carries information by means of action potentials (APs) along its constituent neurons. Action potentials are electrochemical signals that propagate along the axon of a neuron. AP are actively propagated as passive signals would decay over the length of the axon. The AP is sustained by current passed across the membrane. This is only possible due to chemical gradients across the membrane produced by the cell using pumps, which requires energy.

2.1.1.1 Cable Theory

In the absence of specific voltage gated ion channels signals propagate passively along axons according to cable theory. In this case the signal decays along the length of the axon and the rate of this decay is dependent on the electronic insulation of the membrane and the resistance of the cytoplasm of the axon (Jack et al. 1975). The signal decays according to the cable equation:

Equation 2.1

$$\frac{d}{4R_i}\frac{\partial^2 V}{\partial z^2} = C_m\frac{\partial V}{\partial t} + \frac{V}{R_m}$$

Where $\boldsymbol{d}$ is the diameter of the axon, $\boldsymbol{R_i}$(Ωcm) is the cytoplasmic resistivity of the axon, $\boldsymbol{C_m}$(μF/cm^2) is the membrane capacitance per unit area, $\boldsymbol{R_m}$ is the membrane resistance and $\boldsymbol{V}$ the membrane potential at distance $\boldsymbol{z}$ and time $\boldsymbol{t}$ along the axon. Solutions to this equation in a steady state are:

Equation 2.2

$$V_z = V_0 e^{-z/\lambda}$$

Equation 2.3

$$V_t = V_0 e^{-t/\tau}$$

This shows that along the length of the axon, with a steady voltage at V_0 at one point, the voltage decays exponentially away from that point according to the length constant λ, which is given by:

Equation 2.4

$$\lambda = \sqrt[2]{\frac{dR_m}{4R_i}}$$

So that voltage will decay faster with higher cytoplasmic resistivity, reducing the current flow along the axon, and slower with higher membrane resistance as current is prevented from leaking out of the axon. Similarly voltage in one location decays exponentially with time according to the time constant τ, which is given by:

Equation 2.5

$$\tau = R_m C_m$$

So that the voltage will decay slower the higher the membrane resistance is, as the charge is impeded from leaking out. The voltage will decay slower the higher the membrane capacitance is, as it takes longer to charge the membrane. These identities (equations 3.4 and 3.5) make it possible to rewrite the cable equation 3.1 as:

Equation 2.6

$$\lambda^2 \frac{\partial^2 V}{\partial z^2} = \tau \frac{\partial V}{\partial t} + V$$

The voltage V in this case is measured compared with the resting membrane voltage. At rest neuronal membrane typically has a potential difference across the membrane of -60 to -70 mV. This potential difference is due to differences in ion concentrations either side of the membrane, which can be likened to a capacitor. Given the ion concentrations and their individual charges the potential is given by the Nernst equation:

Equation 2.7

$$V_{Rest} = \frac{RT}{F} \ln\left(\frac{P_K[K]_o + P_{Na}[Na]_o}{P_K[K]_i + P_K[Na]_i}\right)$$

Where $R$and F are the ideal gas and Faraday's constant respectively. T is temperature. The $P_I[I]_o$terms are the product of the permeability and concentration of ionic species I, with the subscript *o* for extracellular and *i* for intracellular. The Equation 2.7 shown only considers potassium and sodium ions, but the more generalised Goldman-Hodgkin-Katz equation can be used to include all ionic species. The voltage given by this equation, V_{Rest}, is the membrane potential when there a no perturbations and is the point from which changes to the potential are measured. In most systems it is considered to be a constant value and this assumes the ionic concentrations remain approximately constant.

2.1.1.2 Active signal Transduction

Passive conduction will not adequately transmit signals along the entire length of axons in most neurons due to signal decay. Instead signals are actively propagated along axons as action potentials (AP) using currents from voltage gated sodium and potassium channels. The currents required to generate an AP can be obtained by the opening of these channels, such that, due to concentration gradients, the ions flow across the axonal membrane. The ion concentration gradients are produced and maintained by continual pumping of ions across the axonal membrane. The Nernst-Planck model uses the known gradients to determine the resting membrane potential and the reversal potential for each individual ionic species. An ion's reversal potential is reached when the membrane potential is balanced with its concentration gradient so there would be no movement of that specific ion across the membrane with open channels. An AP is propagated by the opening and closing of channels along the membrane, which happens in response to changes in the membrane voltage.

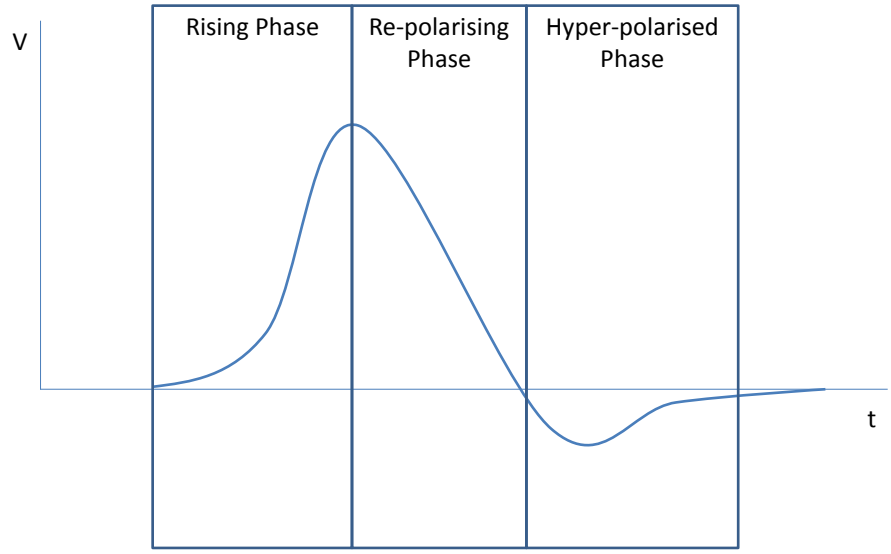

Figure 2-1 A characteristic action potential. Shown are the three temporal phases, rising phase, re-polarising phase and hyper-polarised phase at one point along the length of the axon.

An AP has a characteristic shape which can be broken down into at least three distinct phases. The first is the rising phase of the AP, in which the membrane rapidly depolarises due to the arrival of the AP. This triggers VGSC to open and pass current which in turn further depolarises the membrane. The repolarising phase occurs next as voltage gated potassium channels open and sodium channels close. Finally there is the hyperpolarised phase, where the membrane potential is lower than the resting potential and sodium channels are inactivated, so that they cannot be reopened. The inactivation of sodium channels gives rise to the refractory period during which is it not possible to trigger another AP and this prevents AP being back propagated. AP are propagated along the axon by an axial current, the charge carriers of which are the ions in the axoplasm, mainly potassium. The axial current partly depolarises membrane further ahead. This depolarisation triggers sodium channels to open thereby regenerating the AP in the new patch of membrane. The degree of depolarisation required to trigger the regeneration of the AP is known as the threshold potential.

2.1.2 Electrophysiological Properties of C-type $Na_V1.8$ Expressing Neurons

The axons of c-type neurons are very thin, between 0.1 µm and 2 µm thick (Waxman 1995). The thinner an axon is, the more important channel noise and the distribution of open channels becomes, as individual channels have more effect on the propagation of each action potential (Faisal & Laughlin 2007). Axons appear to have a natural lower limit of around 0.1 um thick, as they are not normally found below this diameter. This limit appears to be due spontaneous firing of AP in the axons below this diameter. In thin axons the signal to noise ratio become large enough to disrupt the accurate transfer of information through the neuron. This thinness, which is characteristic of c-type neurons, has made studying them difficult. They are so delicate that patch clamp recordings are difficult to make and conventional microscopy cannot spatially resolve features of interest well.

In c-type neurons $Na_V1.8$ conducts at least 80% of the rising phase trans-membrane current of an action potential. Recent data shows $Na_V1.8$ clustering along the length of these fibres despite lack of myelination.

Clusters of $Na_V1.8$ are observed to be between 50 nm and 200 nm wide, although they could be smaller due to the limiting resolution of light microscopy used. Using light microscopy these clusters are estimated to contain around 50 channels, based on known current density and single channel conductance. Although this could be an underestimate as not all channels may be open even when the peak current passes the membrane. $Na_V1.8$ channels have so far only been recorded from in the soma of cultured DRG neurons and cell lines, but not directly from the axons of c-type neurons. Some c-type neurons have axons over a meter long in humans. Therefore the reliability with which they transmit AP is crucial as even a small probability of conduction failure would be problematic over such long distances.

2.1.3 NEURON – a simulator of neurons

Conventionally neurons are computationally modelled using a compartmental model. A compartmental model is one in which the length of the neuron is split up into small units, each of which is considered to be iso-potential at any given point in time. The

length of the compartments must be small enough for the assumption of iso-potentiallity to be a valid one for the model. As the length constant determines the spread of potential along the axon, the compartments need to be significantly shorter than the length constant, λ, for the model to be considered valid. Similarly the size of the time step through which the model iterates must be small compared to the time constant of the axon, τ.

NEURON is a simulation environment which allows compartmental models of single neurons or networks of neurons to be easily specified (Hines & Carnevale 2001). All the electrophysiological properties, as well as the morphological features can be specified and then the computational aspects, such as compartment length and time step, defined. The different ion channels used in the model membrane can either be selected from a predefined selection, such as Hodgkin Huxley squid giant axon channels, or the user can create a channel by inputting the properties they require.

2.1.4 Stochastic models

Classically models of neurons have simulated a large number of channels, such as all those in a specified area of membrane, as a single population. Using this method the gating of the channels, which is dependent on the membrane voltage, is used to determine the probability of any one channel being in an open state. This probability is then used to give the proportion of open channels in the whole population and therefore the fractional conductance in a given compartment. These models are termed deterministic models. This is because the channel conductance can be given as a function of purely voltage and time, therefore given the same conditions a simulation will always produce the same output. The number of open channels will always be the same at a certain point in time and so whether or not an AP is conducted is determined.

In real neurons there are fluctuations in the number of open channels, which leads to noise. When there are a large number of channels, noise has very little impact on the propagation of AP, as individual channel noise is averaged out over the population. However, as the gating rate formulae only give the proportion of channels in each

possible state, when there are a small number of channels the proportion in each state may differ substantially from the proportion predicted by the model.

Stochastic modelling instead accurately models the probabilistic nature of the ion channels. Random number generators are used with the gating kinetics to model the states of the channels and their transitions based on probabilities.

Thin axons have relatively few channels per unit length, therefore few per iso-potential compartment when modelling them. This makes stochastic modelling useful for accurately modelling thin axons.

In thin axons the current from only a few channels can have large effects on the propagation of AP. Small groups of channels which are spontaneously open can cause AP to jump forward. Relatively few channels are crucial for the start of the chain reaction which is the AP early rising phase, as the current from one channel can depolarise the membrane enough to trigger many more to open.

Stochastic models of voltage gated channels make use of Markov models. The transitions between states are probabilistic. The 8 state Markov model is analogous to the classical Hodgkin-Huxley sodium channel gating particles. Classically there are three activation, m, and one inactivation, h, gating particles. Each takes a value from 0 to 1 and the resulting product gives the proportion of open channels, such that the conductance g is given by:

Equation 2.8

$$g = g_{max} m^3 h$$

Where $g_{max}$is the maximum conductance and the product $m^3 h$ has a value between 0 and 1. This represents each individual channel having four gating particles which can be in either of two positions, represented by 0 or 1. The channel can have any combination of arrangements of these gating particles, leading to 16 possible arrangements, such as 0000, 1010 or 1111. However as the 3 m particles all have the same gating kinetics they are indistinguishable leading to only 8 unique states, such that 0, 1, 2 or 3 m gates are open and the h gate is open or closed.

The transitions between states are given by the gating rates which are functions of voltage and time. The gating rates are denoted by α and β for the forward and reverse rates respectively, with a sub script denoting which gating particle they refer to.

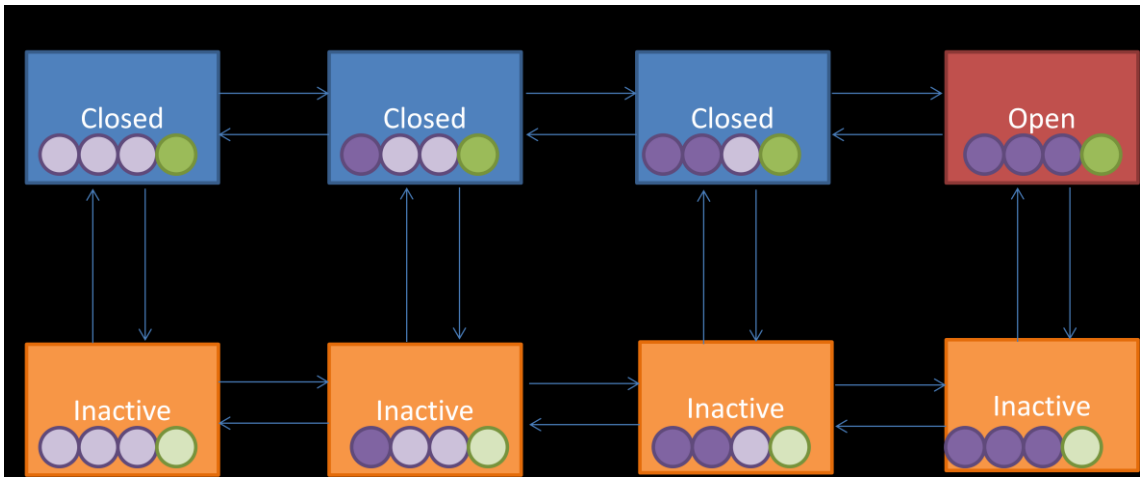

Figure 2-2 Diagram of the 8 state Markov model used for stochastic channels that is equivalent to the deterministic Hodgkin Huxley gating schema. Of 8 possible states, nly 1, the open state, allows the passage of ion through the channel. The three closed states are equivalent to each other as are the 4 inactive states. None of these 7 states allow the passage of ions through the channel to cross the membrane. The states of the individual gating particles are represented by the circles within each state. The three purple circles represent the three interchangeable m particles, with dark fill showing the particles are in the configuration required for the open state. The green circle represents the inactivation gating particle, and again the dark fill shows the particle is in the state require for the channel to be open. Gating between stated is represented by arrows between them, which are labelled with the rates of transition between states. The alpha and beta rates are multiplied by the number of gating particles currently residing in that state that are available for transition.

Markov models of Sodium channels have traditionally had 8 states corresponding to all the possible configurations of the Hodgkin-Huxley (HH) gating particles, Figure 2-2. More recently the possible configurations of states has become diverse as additional gating particles, such as slow inactivation have been added to models (Fink & Noble 2009). Using the 8 state model allows the same gating rates to be used in both stochastic and HH like models and therefore direct comparisons can be made.

2.1.5 Modelling Clustered Channels

Little work has been conducted on the effects of sodium channel clustering in un-myelinated fibres. One known study found few effects (Zeng & Tang 2009), however the model mainly simulated axons with diameters of 10 µm, much larger than for c-fibres. In one case they looked at the effect of axon diameter, comparing deterministic and stochastic models from 1 µm to 10 µm. They found little difference according to either axon diameter or between deterministic and stochastic simulations. At the lowest axon diameter, of 1 µm, deterministic simulations gave higher efficiency due to clustering that stochastic simulations. The degree of clustering they examined was much greater than we have observed for $Na_V1.8$, with clusters every 20 µm rather than every 2-5 µm. They also investigated the effect of the clustering of Potassium channels. They find that increasing the Potassium conductance of the axon reduces the required Sodium conductance when the channels are clustered. They found potassium channels clustering lead to faster AP conduction.

2.2 Aim

I aim to distinguish whether and under what conditions the clustering of the channel $Na_V1.8$ is advantageous to the conduction of AP along the length of an axon. In myelinated axons where the channels are clustered, few channels overall are required than if there was no myelination. Is it the case that clustered channels in unmyelinated axons also enable fewer channels to be able to conduct an AP? If fewer channels are required this would reduce the workload for the cells in producing, transporting and dismantling the channel proteins. The fewer channels required it is likely the lower the metabolic load associated with the conduction of an AP, due to less total current passing the membrane. Does channel clustering lead to increased energy efficiency? Myelinated axons conduct faster and require less current, although this is due in large part to the insulating properties of the myelin, clustering itself may lead to some improvements. Finally, how much of a role does the gating properties of $Na_V1.8$ and the morphology of C-type neurons play in difference seen when channels are clustered.

2.3 Methods

2.3.1 Neuron Simulations

Simulations were run using the NEURON (Hines & Carnevale 2001) development environment. Models were defined using hoc code, which was then executed by NEURON. Hoc code was written in a text editor. An example of the hoc code for the simulations is in appendix A. For most simulations there was a code for the model with evenly distributed channels and one for channels clustered in rafts, but with all other parameters the same. The gating parameters for channels specifically required for these models were entered using the channel builder section of the NEURON user interface. For deterministically gated channels, the required density of channels was added to each compartment for modelling and treated as a population of channels during the simulation. For stochastic simulations each individual channel was inserted and modelled separately using the hoc code. The location for each stochastic channel was defined by taking the total number of channels per section and dividing the distance over which they were distributed by it, then iterating through the segment inserting the channels.

Variables required to contain the properties of the neuron were defined and populated at the start of the code. The custom defined channels created using the NEURON user interface were saved as session files. These session files were then called by the hoc files when the mechanism was required for insertion into compartments of the model. Result variables were output to Excel where they were also analysed. The gating kinetics and conductances of these channels are in Table 2-1.

Properties	$Na_V1.8$	NaHH	KFast
α_m	$\frac{3.83}{1+e^{0.087(-2.58-V)}}$	$\frac{0.1(V+35)}{1-e^{-.01(V+35)}}$	
β_m	$\frac{6.894}{1+e^{-0.05(-61.2-V)}}$	$4e^{-0.056(V+60)}$	
α_h	$0.013536e^{-0.0216(V+105)}$	$0.07e^{-0.05(V+60)}$	
β_h	$\frac{0.61714}{1+e^{0.083(21.8-V)}}$	$\frac{1}{1+e^{-0.1(-30-V)}}$	
α_n			$\frac{0.00799(V+72.2)}{1-e^{-0.91(V+72.2)}}$
β_n			$\frac{-0.0142(V+55)}{1-e^{0.095(V+55)}}$
Conductance	20 pS per channel	20 pS per channel	0.017 S/cm^2

Table 2-1 Gating rate parameters. For Sodium channels the m and h gating particle rates are shown and the n gating particle rates are shown for the Potassium channel.

The morphology and properties of the simulated neuron were chosen to closely match those of c-type neurons. The default diameter chosen was at the lower end of the known range for c fibres of 0.1 µm. This was chosen as the reliability of conduction is lowest at these diameters and the effect due to individual channels is the greatest. Long axons of 10 mm were simulated as c-fibres are often long as they connect the periphery with the central nervous system, although their length can far exceed this length. A long model length also helped to minimise effects from the ends of the axon and demonstrate reliable conduction. The potassium channel included in the model is responsible for the fast potassium current and has been used in previous models of c type neurons that express $Na_V1.8$ (Baker 2005).

Parameters were varied in order to help investigate differences in AP propagation with clustered channels. As only transmission rather than initiation of AP was of interest, the start of the axon, where the AP was triggered, was modelled using classical Hodgkin Huxley channels at a high enough density to guarantee an AP was generated. It was checked that the AP generated in this initial section would not propagate very far down the axon without additional channels further along its length. In NEURON the iso-potential compartments are called segments, there can be many of these in a section of the neuron with the same properties. As previously discussed these need to

be small compared to the length constant of the axon in order to accurately model the propagation of charge along the axon. In this case we used segments 100 nm long.

$Na_V1.8$ channels were defined for the model. Deterministic channels were based on the Hodgkin Huxley gating schema but with custom defined gating kinetics. Therefore, they had 4 gating particles; 3 open/closed particles, m, and 1 inactivation particle, h. Each gating particle takes a value from 0 to 1 and the product of all 4 gives the total probability of the channel being open. Stochastically gated $Na_V1.8$ channels use the same gating kinetics but applied to an 8 state Markov model. The 8 states are all the possible combinations of the three m and one h particles taking either the value of 0 or 1. Only one of the 8 states is open and allows current to pass through the channel. The deterministic channel model is appropriately used to model populations of channels rather than single channels, whereas the stochastic model can be used to model individual channels. If stochastic gating is used to model populations, the number of channels in each state can be tracked instead of the state of each channel individually.

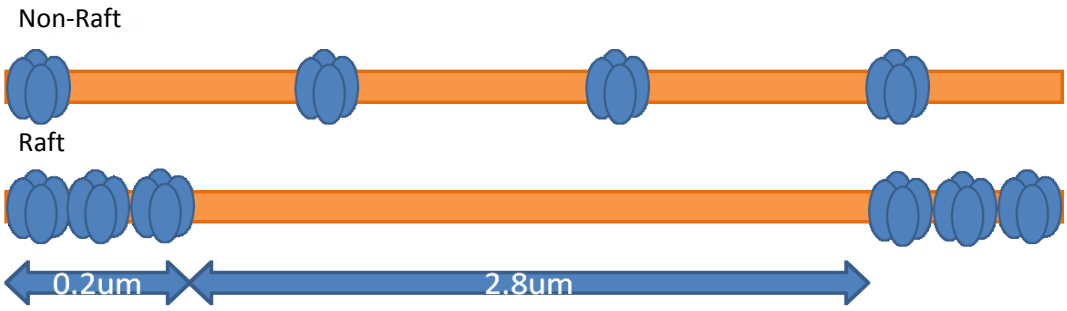

Figure 2-3 Diagram of the distribution of ion channels in raft and non-raft models. In raft models channels were evenly distributed within the confined area of the raft, where as in non-raft models the channels were evenly distributed along the entire length of the axon. The same over all density of channels was considered when comparisons were made.

The number of channels to use in the model was estimated from known current densities, using the single channel conductance, and agreed well with estimates from confocal microscopy. The default model used rafts 0.2 µm long distributed regularly every 3 µm, each containing 54 channels with the single channel conductance of 20 pS.

Property	**Value**
Raft separation	2.8 µm
Raft length	0.2 µm
Number of channels per raft	54
Axon diameter,d	0.1 µm
Axial resistance (of cytoplasm), R_i	70 Ωcm
Membrane Capacitance, C_m	0.81 µF/cm^2
Passive membrane conductance	0.00017 S/cm^2
Membrane resistance, R_m	7100 Ωcm^2
Approximate length constant, λ	160 µm
Approximate time constant, τ	5.8 ms

Table 2-2 Default NEURON model parameters. Some parameters were varied, in which case the default value is shown.

Potassium channels were excluded from the raft portions of the axon. Potassium channels used were based on fast potassium channels, which have been previously used when modelling neurons expressing $Na_V1.8$ (Baker 2005b).

2.3.2 Modigliani Stochastic Simulations

The Modigliani simulator (http://www.doc.ic.ac.uk/~afaisal/FaisalLab/Modigliani/) was used to model stochastic $Na_V1.8$ channels in c-type neurons. It has previously been used to model small diameter neurons with stochastic channels. Modelled neurons had the same properties as used for NEURON models, shown in Table 2-2. $Na_V1.8$ channels used the gating schema shown in Table 2-1, although the potassium channels

used were based on Hodgkin Huxley channels. Potassium channels were excluded from rafts.

2.4 Results

Models where $Na_V1.8$ channels were clustered in rafts were compared with models where $Na_V1.8$ was evenly distributed along the axon. The number of channels in the rafts was varied in order to investigate the minimum number of channels required to conduct AP along the axon and the effect of channel number on the properties of propagation. The estimated number of channels per cluster was 54, this was modelled with clusters every 3 µm. The number of channels was reduced in order to find the minimum that would support conduction. Both raft and non-raft models were simulated with stochastic and deterministic $Na_V1.8$ channels as well as classical Hodgkin-Huxley channels.

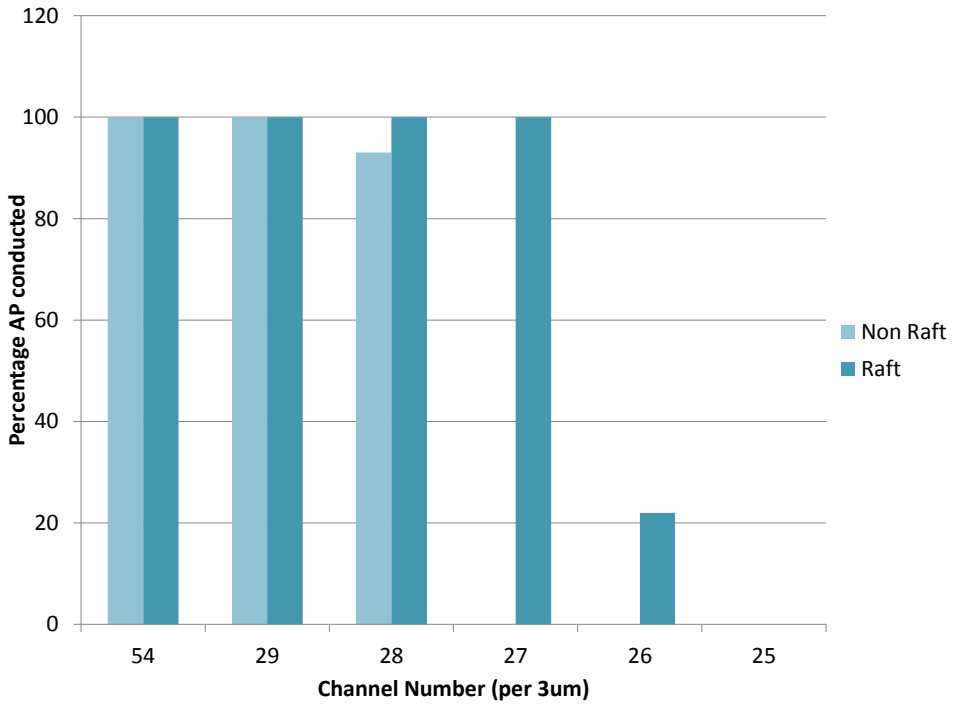

Figure 2-4 Percentage of AP conducted for a given number of stochastic $Na_V1.8$ channels per cluster. For non raft models the given number of channels were evenly spaced over 3 µm of the length of the axon, and this density was consistent along the length of the axon. For raft models the given number of channels were evenly

distributed along 0.2 µm of axon, and these clusters were space every 3 µm, such that the total number of channels were the same in both models. 100 runs of each model were simulated. Non raft models failed to conduct any AP with less than 28 channels.

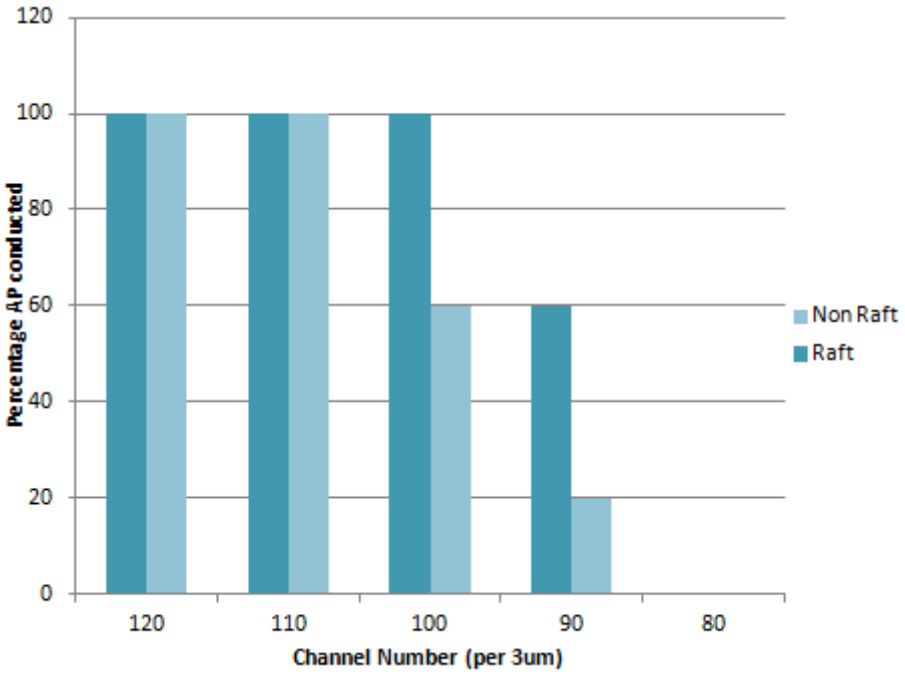

Figure 2-5 Percentage of AP conducted for a given number of stochastic Hodgkin-Huxley channels per cluster. 10 Repeat simulations of the each model was run for each given number of channels. Models with channels clustered into rafts conducted AP reliably with 100 channels, some AP with 90 channels and none with 80 channels per cluster. With the same overall number of channels non-raft models were less reliable, only conducting 100 % of AP with 110 channels per cluster.

2.4.1 Fewer Channels Required when Clustered into Rafts

The number of channels per cluster in all Neuron models was varied to find the minimum number required for action potentials to be transmitted. For deterministically modelled $Na_V1.8$ channels there was a small difference between raft and non-raft models with 25 channels per cluster being the minimum required in the non-raft model and 24 in the raft model. As channel noise effects have been shown to be important in thin axons, models were also simulated with stochastically gated $Na_V1.8$ channels, such that separate runs lead to unique outcomes. When the numbers of channels is near the approximate minimum, an action potential may or may not be conducted the full length of the axon. As there was no absolute cut off in

the stochastic models the percentage of action potentials propagated over multiple runs is shown in Figure 2-4 and Figure 2-5.

One hundred runs of each condition where simulated for stochastic $Na_V1.8$ models, Figure 2-4. When both clustered and evenly distributed $Na_V1.8$ models had 29 or more channels per section they propagated 100 % of AP the entire length of their axons. The evenly distributed model still conducted over 90 % of AP with 28 channels per cluster but no AP were conducted the full length of 10 mm with less than 28 channels. The raft models still conducted 100 % of AP with 28 and 27 channels, but with 26 channels only 22 % of AP were conducted and with less than 26 channels none were conducted at all. Stochastically gated channels required higher minimum numbers of channels than the models with deterministically gated channels.

Minimum no. of Channels to Conduct all AP	**Stochastic Clustered**	**Stochastic Even**	**Deterministic Clustered**	**Deterministic Even**
$Na_V1.8$	27	29	24	25
Hodgkin Huxley	100	110	Not Modelled	Not Modelled

Table 2-3 Minimum number of channels required to conduct all AP that were simulated the entire length of the axon.

The minimum number of channels required to conduct AP did not vary considerably between clustered and evenly distributed models or depending on whether they are simulated deterministically o r stochastically, Table 2-3. For both deterministic and stochastic simulations the number require by clustered models was lower, which could be advantageous for a neuron. The minimum numbers were found to be much lower than the estimated number of channels from other observation of 54. Although there is a still much uncertainty about the number of $Na_V1.8$ channels existing in small diameter c-type neurons and their single channel conductance. Using stochastic simulations for models with Hodgkin-Huxley sodium channels also showed fewer channels required when they were grouped in clusters. This leads to the possibility that channel clustering in thin axons generally requires fewer channels overall rather than being dependant on a specific channel type.

2.4.2 Clustered Channels Conduct AP Faster

Stochastic raft models in NEURON give faster AP propagation when channels are clustered than when channels are evenly. The proportional difference is very small when modelled using 54 channels per cluster only 1.3 %. With lower channel density, near the minimum required for conduction, the proportional difference beomes larger, up to 13.8 %. This change is still small compared to the range of AP conduction velocities observed in biological samples. The effect of the channel density is much larger than the differences seen between raft and non-raft models, the conduction velocity being roughly double with 54 channels compared with 26.

When the same models were run with deterministically gated $Na_V1.8$ channels a similar pattern of results was obtained. When modelled deterministically raft models still give rise to higher conduction velocities. Although when there are only 25 channels, the minimum needed to propagated AP in the non-raft model, the conduction velocity is the same in both models. The conduction velocity also decreases as the number of channels is reduced, although there is a slight increase when there are 24 channels in the raft model before conduction fails with fewer channels than this.

When stochastic Hodgkin-Huxley channels are used in the models instead of $Na_V1.8$ the raft models still give faster conduction velocities than non-rafts models. Although the difference was not statistically significant, as only 10 runs of each model were conducted due to the computational time required to run each simulation.

In general clustering of sodium channels leads to fast AP conduction in the Neuron models. AP conduction velocity is also highly dependent on the number of channels, with more channels leading to fast conduction. This would enable a neuron to achieved an critical conduction velocity with fewer channels if they are clustered, as seen with minimum channels numbers this could be advantageous as it reduces the metabolic cost associated with the number of channels.

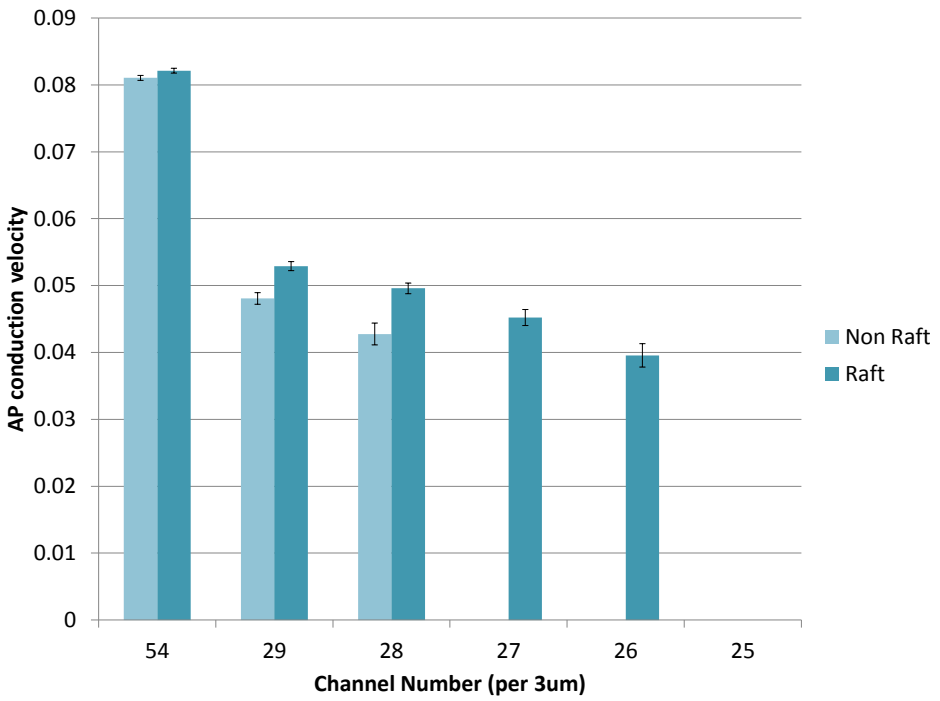

Figure 2-6 Stochastic $Na_V1.8$ channels models AP conduction velocity is higher when channels are clustered. At each channel density modelled in the raft model the conduction velocity was high. At 27 and 26 channels per cluster the AP failed to propagate in the non-raft model and so only the velocity of the raft model is shown.

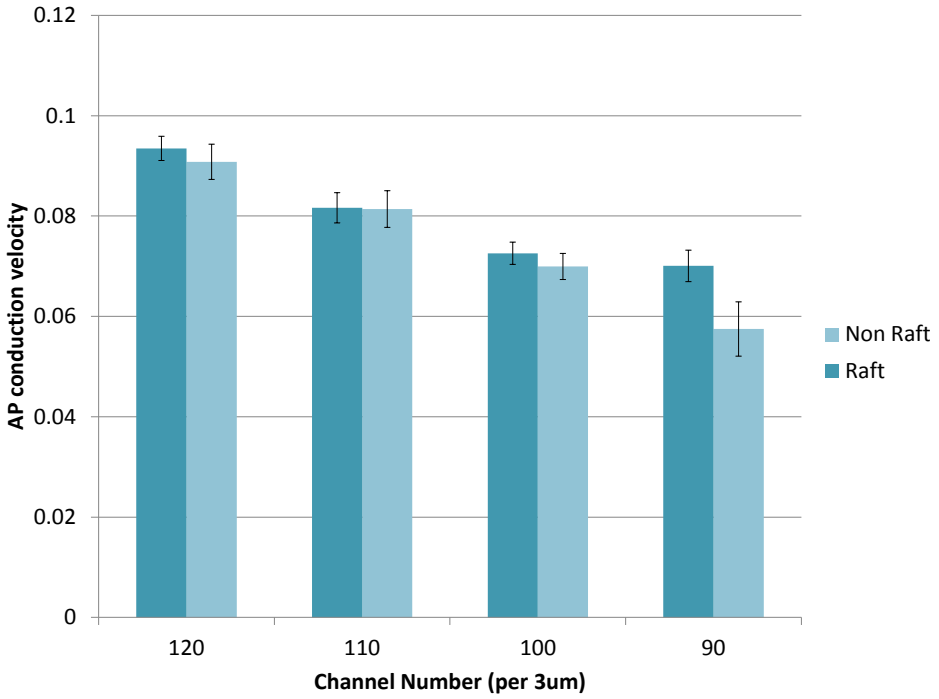

Figure 2-7 Stochastic Hodgkin-Huxley models have higher conduction velocity when channels are clustered. The error bars show the standard error of the mean based on the sample.

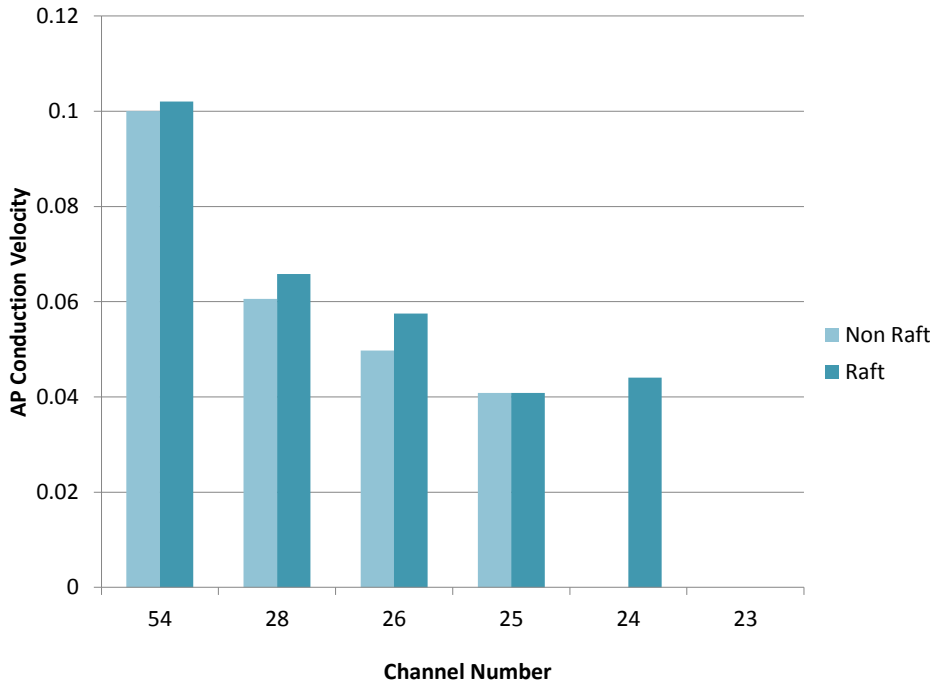

Figure 2-8 Deterministically modelled $Na_V1.8$ channels give higher conduction velocity when clustered in rafts. Near the minimum, when there are 25 channels per cluster the velocity is the same for both raft and non-raft models. No error bars are

shown as each run produces identical results, therefore only one run of each condition was carried out.

Modigliani stochastic and deterministic simulations did not agree with simulations run using NEURON. Here the deterministic model found no difference in the conduction velocity between raft and non-raft models. Conduction velocity increased in both cases when modelled stochastically. However, in this case the non-raft model was faster than the raft model by 27 %.

2.4.3 Efficiency of Action Potential propagation

For each action potential propagated the cell must expend energy in re-establishing the equilibrium concentration of ions across the membrane. During an AP Sodium ions flow into the axon and Potassium ions flow out. Sodium Potassium pumps (NaK-ATPase) remove 3 Sodium ions from the cell and transports 2 Potassium ions in for each molecule of ATP that is used. As more sodium ions are transported by the pumps, it is the current of sodium ions into the cell during the AP that is critical to how many molecules of ATP are required to re-equilibrate, and therefore determine the energetic cost of an AP. The sodium current for each model was recorded from a compartment half way along the length of the axon. The current from each sodium channel in a raft or the equivalent length of axon in the non-raft models was recorded and the total averaged from multiple runs.

In models run with stochastically gated $Na_V1.8$, clustering of channels gives rise to more efficiently propagated AP, Figure 2-9. Raft models with 54 channels required 10 % less sodium current and therefore 10 % less energy to transmit an AP than the non-raft model. Raft model simulations with 29 channels per cluster required on average 18.5 % less current than non-raft models. The minimum current to conduct an AP was 1.02 in the raft model (27 channels) and 1.27 in the non-raft model (29 channels), a difference of 19.3 %.

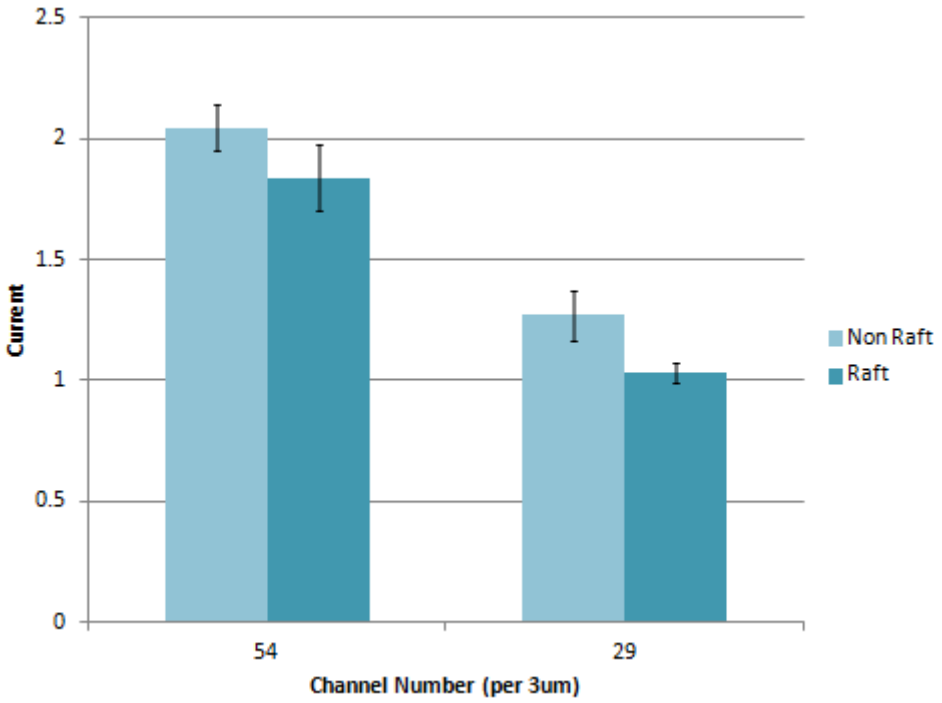

Figure 2-9 $Na_V1.8$ stochastic current passing through the membrane per raft cluster for a single AP. Error bars show estimate of standard error of the mean over 5 runs. For 29 channels mean current is statistically different to 3 standard deviations.

When $Na_V1.8$ was modelled deterministically, less current passed the membrane when channels were clustered and therefore less energy was required, Figure 2-10. The differences were smaller than for the stochastic models. For both stochastic and deterministic the current was higher with greater numbers of channels. This is turns means that higher membrane current is correlated with faster conduction velocity. When stochastically modelled with Hodgkin-Huxley sodium channels clustered channels were generally less energy efficient as more current passed the membrane than when channels were evenly distributed, Figure 2-11. There was no significant difference between them and when there were 100 channels, on average less current passed in the clustered condition. Unlike with minimum channel number and conduction velocity, the energy efficiency does not show the same pattern with both $Na_V1.8$ and Hodgkin-Huxley channels. This may be due to differences in the gating properties between the modelled channels.

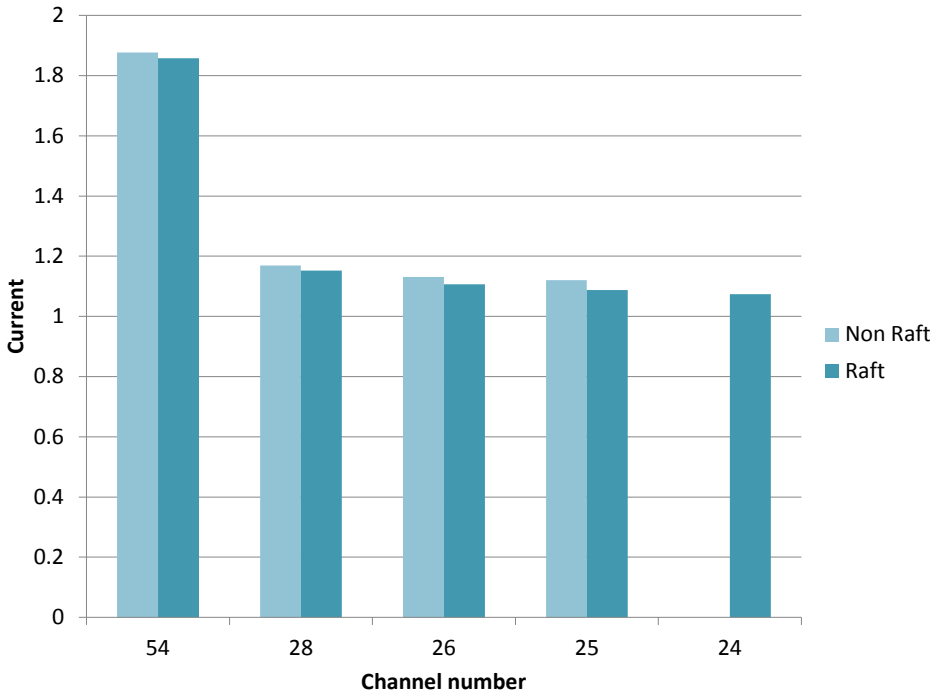

Figure 2-10 Deterministically modelled $Na_V1.8$ channels use less current to propagate AP. AP failed to conduct in the non raft model with less than 25 channels and therefore no current is shown. No error bars are shown as each run produces identical results, therefore only one run of each condition was carried out.

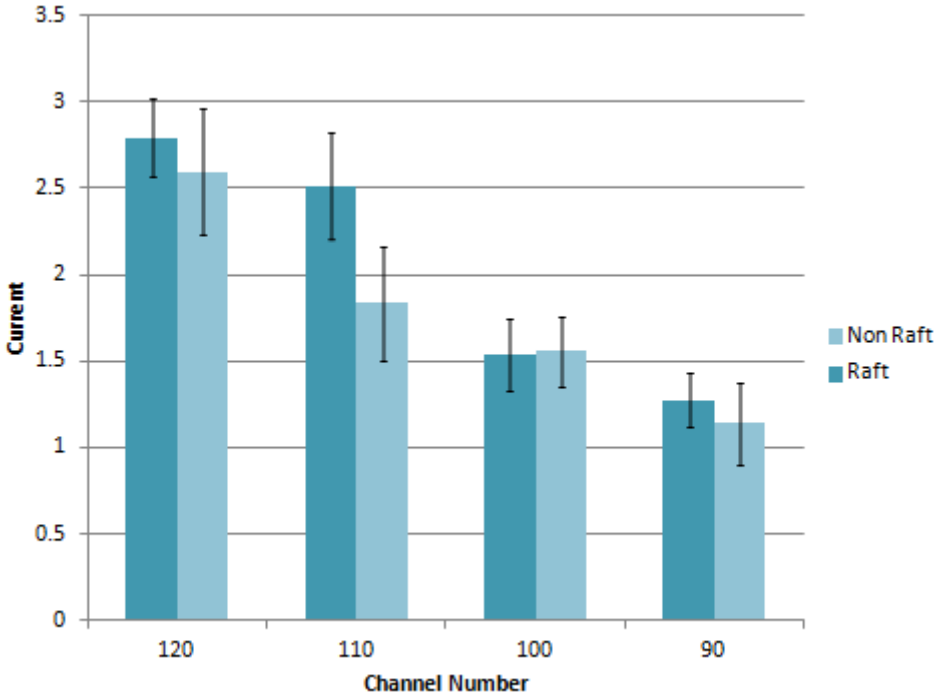

Figure 2-11 Stochastic Hodgkin-Huxley channels current to propagated AP. Error bars show standard error over 5 runs.

The models run using the Modigliani simulator also found that clustered $Na_V1.8$ channels require less Sodium current and energy to propagate and AP than when evenly distributed, Figure 2-12. The difference was considerably more marked when the simulations were run stochastically compared to deterministically modelled channels. The current was higher for stochastically modelled channels than for deterministic ones. This was also the case in the NEURON models that were run. The difference between clustered and evenly distributed stochastic channels is much greater for the Modigliani simulations than the NEURON one. There were very few differences in the setup of the models, the main one being a difference in the potassium channels used, which may account for the differences.

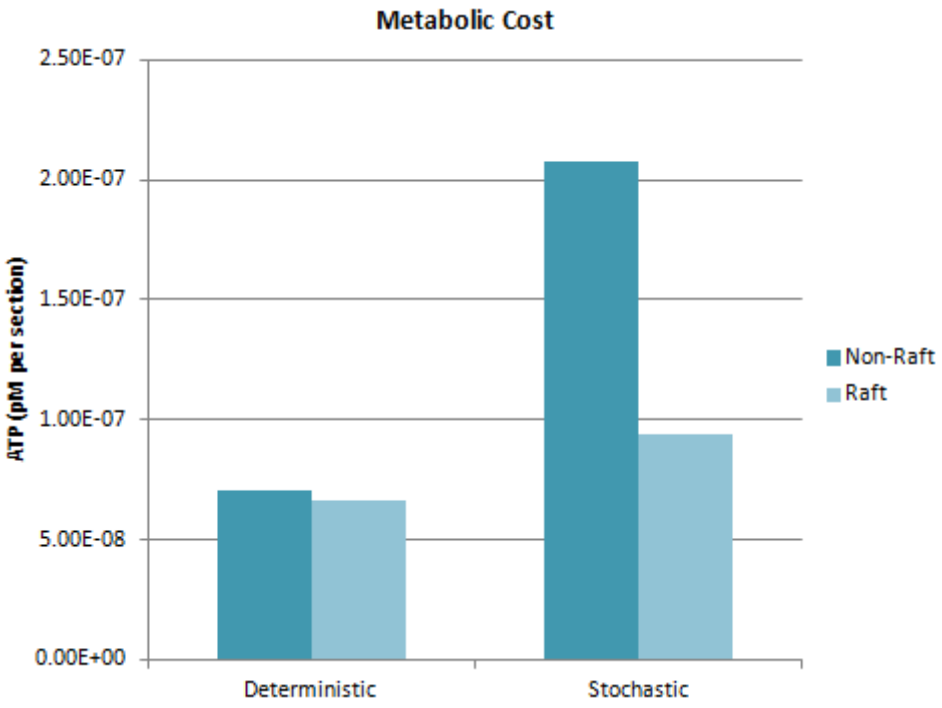

Figure 2-12 Metabolic cost of AP potentials. Modelled using the Modigliani simulator the ATP required to restore the sodium concentration differential following an AP is compared for the raft and non-raft model using $Na_V1.8$ channels modelled deterministically and stochastically.

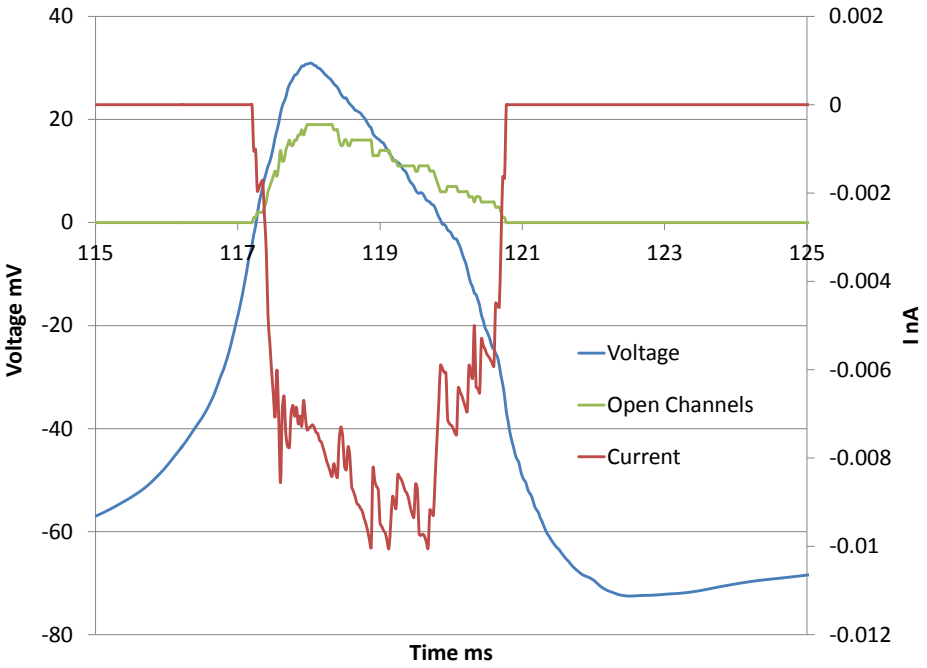

Figure 2-13 Non-raft AP at mid-point of axon. Number of open channels uses the same axis as for voltage. The voltage profile has a noticeable hump on the repolarising phase. The peak of open Sodium channels coincides with the peak voltage. Although peak current is delayed from peak number of open channels and occurs midway through the repolarising phase.

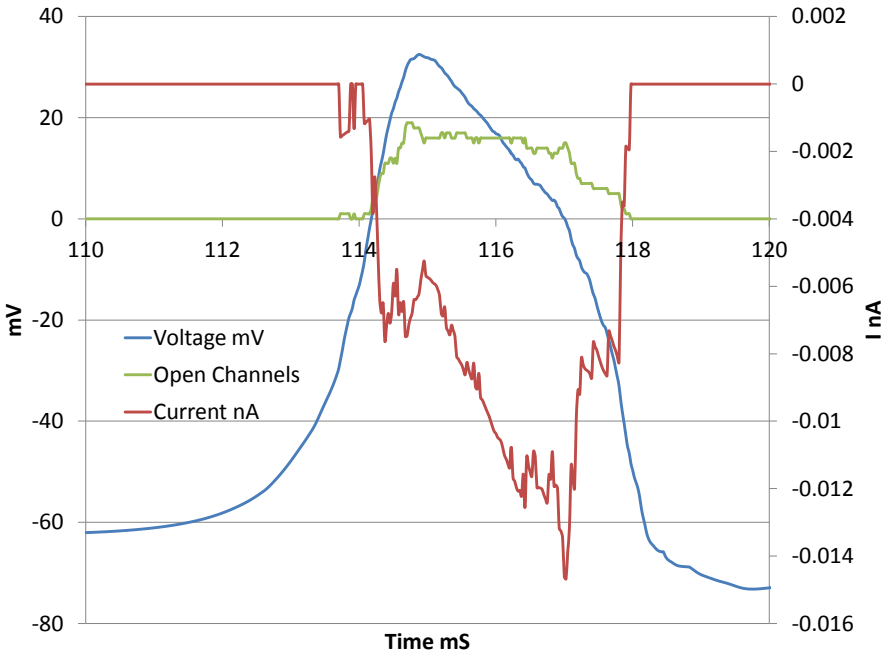

Figure 2-14 Raft model AP at mid-point of axon with KFast channels included in rafts. The voltage profile has a hump in the repolarising phase. The number of open channels remains relatively stable throughout the AP. The peak current occurs towards the end of the repolarising phase.

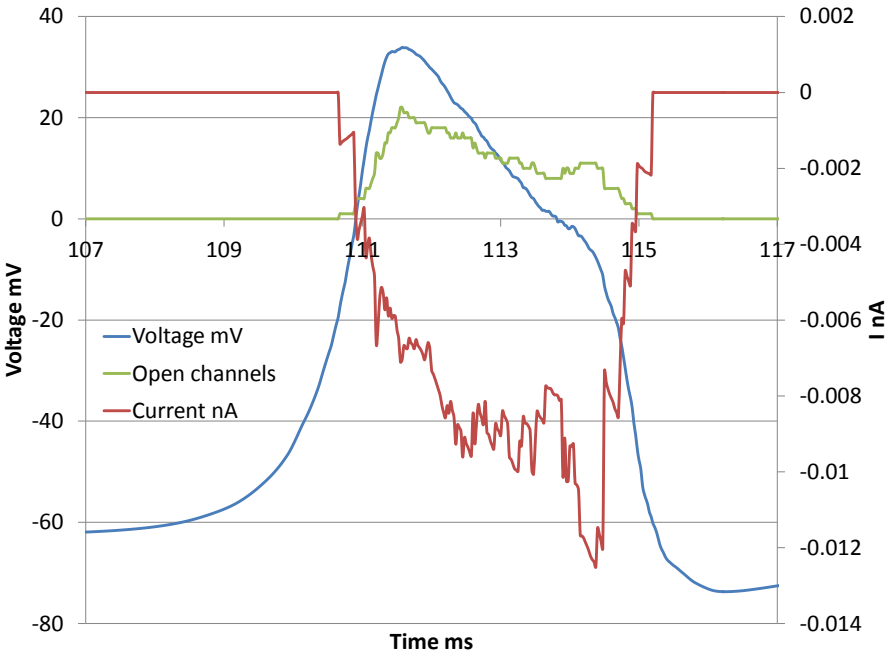

Figure 2-15 Raft model AP at mid-point of axon where KFast channels are excluded from rafts. The hump in the repolarising phase is very marked with KFast channels excluded from rafts. The number of open channels has a main peak coinciding with the peak voltage, but also a smaller secondary peak, which coincides with the peak current and voltage hump near the end of the repolarising phase.

2.4.4 AP shape

The shape of the AP varies between models with and without rafts and depending on whether potassium channels are included in the raft section or not. Raft models (Figure 2-14 and Figure 2-15) give wider AP due to longer repolarising phases. When potassium channels are excluded from the raft (Figure 2-15), the repolarising phase has an additional hump, which is due to more sodium channels being open towards the end of the AP. In raft models, there are two peaks in the number of open channels, one coincident with the AP peak and a secondary peak coincident with the hump in the repolarising phase. The peak current through the channels is during this secondary peak in the number of open channels. This current is not contributing to the regeneration of the AP at the site of the channels.

2.5 Discussion

I aimed to investigate the possible advantages of the clustering of $Na_V1.8$ channels in unmyelinated axons. One of the primary advantages may be an increase in the energy efficiency of the conduction of AP. This can be achieved by reducing the sodium current across the membrane during an AP and therefore the amount of ATP required by NaKATPase to restore the equilibrium concentrations. Increased speed of conduction may also be an advantage to the neuron. Many advantages are seen when sodium channels are clustered in myelinated neurons but clustering in unmyelinated axons has not been thought to be advantageous. Nor is clustering widely observed in unmyelinated axons. However, $Na_V1.8$ has been observed to be clustering in the axons of unmyelinated small diameter DRG neurons. By computationally modelling this system we could investigate the effects of the clustering on the conduction of AP as compared to when the channels were evenly distributed along the axon. We found the clustering of $Na_V1.8$ and other Sodium channels in small diameter fibres is advantageous for the conduction of AP. It leads to a decrease in the minimum number of channels required to conduct an AP, an increase in conduction velocity and an increase in energy efficiency. The minimum energy required to transmit an AP can be reduced by 19.3 % due to the clustering of $Na_V1.8$ channels. This discussion will cover the limitations of the current methods of computational modelling used. The implications of the advantages of clustering that were found. How the current work fits with other research into the effects of channels on AP conduction.

2.5.1 Errors

2.5.1.1 Step size

The equations governing the propagation of AP along axons are differential equations, to which there is no general analytical solution. Therefore to model how these systems work it is necessary to iterate the state of the system through small steps. Most computer simulations require iteration through small time steps. As our model also has spatial extent, through which the signal propagates, it is also necessary to iterate spatially along its length. To this end the spatial step size for time was chosen to be small compared to both the length constant of the axon and the size of clusters, and

the time step size was chosen to be small compared to the time constant of the axon. The length used was 100 nm which is the same as the diameter of the axon modelled. The spatial step size had considerable effects if it was larger than the length of cluster, inhibiting the model from running. Have a larger spatial step size or compartment length than cluster length would in this case be the same as making the size of the clusters larger and therefore destroy the effects of clustering. The step size chosen still was only half that of the default cluster length and therefore an even smaller length would be desirable, but constraints on computational time made this impractical for the current study. A previous study of Sodium channel clustering, (Zeng & Tang 2009), used much longer compartments of 4 µm, which was up to 4 times greater than the width of the axon they were modelling. The width of the axon is proportional to the space constant. The cluster size they used was equal to one compartment, so also 4 µm.

2.5.1.2 Ion Concentration Changes

The modelling methods used assume that the currents involved are small enough not to affect the ion concentration across the membrane sufficiently to change the resting potential following an AP. However, small diameter neurons have a much higher surface area to volume ratio, and so changes in ion concentration are much greater for a given membrane current. In a thin process the change in ion concentration, due to even a single AP, can be large and create significant concentration gradients along the length of the axon. Concentration gradients along the axon can lead to the breakdown of the validity of the cable equations, as they assume constant ion concentrations inside the axon. A total current of 1.3 nA through one cluster, as recorded in the case of 30 $Na_V1.8$ channels, would lead to a change in concentration of 14 mM in a segment of axon 3 µm long. This is the distance between clusters the model uses and the concentration change assumes no diffusion out of the segment during the AP. The resting concentration of Sodium inside the axon is estimated to be around 12 - 15 mM in a typical neuron. Clearly the assumption of constant Sodium concentration is not adequate given these conditions. Table 2-4 gives the ion concentrations and membrane permeabilities (at rest) for a generic neuron. Using these values with the

Goldman-Katz equation (Wright 2004), doubling Sodium concentration from 15 mM to 30 mM would result in only a small change in the resting membrane potential from -65.7 mV to -65.8 mV and a change in the Sodium equilibrium potential from 60.6 mV to 42.1 mV. The change in the resting potential is not substantial so unlikely to have much effect. The change in the Sodium reversal potential means that the peak amplitude of subsequent AP may well be reduced. This would lead to less Sodium current passing the membrane, which leads to less axial current to re-establish the AP at following clusters of channels. $Na_V1.8$ expressing c-type neurons are known to transmit trains of AP, the length of which encodes the intensity of the pain signal, gradual reduction in the AP amplitude could inhibit its ability to transmit intense pain.

Ion	Intracellular	Extracellular	Permeability
Na	15	145	5
K	149	5	100
Cl	10	50	10

Table 2-4 Ionic concentrations and membrane permeabilities of a typical neuron. All values are in mM.

The electro-diffusion model (Qian & Sejnowski 1989) may be more appropriate than the cable model for these simulations due to the small diameter of axon being modelled. The electro-diffusion model is much more computationally demanding than using the cable equation as the basis for simulation. The models used were already very computationally demanding due to stochasticity and small required step size, therefore using the electro-diffusion model as a basis was not feasible.

2.5.2 Sodium Channel Clustering is Advantageous for Action Potential Propagation

Simulations of models where the sodium channels were clustered into rafts had higher conduction velocities, required fewer channels to conduct AP and used less energy to propagate them. The minimum current required to conduct an AP was 19.3 % less when channels were clustered in rafts. These effects were more marked for stochastically modelled sodium channels. This shows that, for thin diameter axons, the probabilistic nature of the gating of channels becomes important. As the diameter is

small the number of channels per unit length is low, with averages of 9-18 in our models.

2.5.3 Minimum Number and Biological Variation

There are only small differences in the minimum number of channels required to propagate an AP between the raft and non-raft models. The minimum number of channels is half as many as the average number of channels expected from observation. Therefore we would expect much larger than the minimum numbers of channels to be present in most axons, such that propagation is reliable. Variability in cells would mean that the density of channels would not be constant along the length of the axons as it is in the models. Even in models with less than the minimum number AP were still often propagated half the length of the axon, such that even if variability lead to a low number in one area of the axon this wouldn't automatically lead to a failure of conduction. The difference in minimum number is small compared with variability in the biological axon.

2.5.4 Effects of Stochasticity

Stochastically gated $Na_V1.8$ channels gave slower conduction velocities than models with deterministically gate $Na_V1.8$ channels. The pattern of the difference in conduction speed between raft and non-raft models was different when modelled stochastically than deterministically, although raft models were still the same or faster. The difference in current between raft and non-raft models was greater when $Na_V1.8$ was modelled stochastically than when it was modelled deterministically.

2.5.5 Axial Current

The largest sodium current passing the membrane during an AP in the raft models is during the repolarising phase. This current is too late to contribute to the regeneration of the AP at the site of the cluster of sodium channels. Therefore it is mainly axial current from previous clusters which regenerates the AP at the present cluster. The current flowing through the membrane at the present cluster regenerates the AP at subsequent clusters along the axon.

2.5.6 Modelling AP in unmyelinated axons

Previous modelling of clustered channels and their effect on AP propagation showed that potassium channels played an important role in the dynamics (Zeng & Tang 2009). Noted differences between the NEURON and Modigliani simulations are likely to be due to the different potassium channels used in the models. When potassium channels are excluded from the areas containing sodium channels, this effectively clusters the potassium channels.

Although not included in our models clustering of channels may lead to or be necessary for cooperative behaviour. Sodium channels in clusters acting cooperatively can improve signal transduction and neuronal encoding (Huang et al. 2012). This cooperation is more likely to occur if channels are densely packed in clusters.

A previous computational model of c-fibres has been used to study activity dependent slowing (ADS), (Erik Fransen 2011). ADS is characteristic of the fibre type, it is reduced excitability due to changes in ion concentration following repeated AP firing. The approach used in this study was to include NaKATPase pumps and keep track of the ion concentrations. As we have seen from our own study this would be important if you want to see the effects on multiple AP. ADS appears to be altered in chronic pain patients, (Orstavik 2003), and is reduced in the axotimised c-fibres of pain model animals, (Mazo et al. 2013), therefore increasing excitability.

2.6 Conclusions

Clustering of $Na_V1.8$ channels can be advantageous for the propagation of AP along the axon of small diameter neurons. C-type DRG fibres can be very thin, near the limit below which the effects of noise make reliable conduction impossible. This means that the number of channels per length of axon can be very low compared to larger diameter neurons. The probabilistic nature of channel gating becomes important in these conditions.

Cable theory assumes constant concentrations of ions across the membrane. Our models, and most commonly used ones, are based on cable theory and as such they may not be as accurate in such thin axons. Models based on the electro-diffusion

models would provide more accurate results for future research if the computational capacity was available. Our models suggest that sodium ion concentrations may double due to the propagation of an AP. Trains of AP, as are common in c-type neurons expressing $Na_V1.8$, would cause even greater changes and their conduction could fail if the concentration gradient was eroded too dramatically. Membrane pumps would be crucial in order to re-establish the ionic gradient allowing for continued conduction.

3 Investigation of the Nanoscale Distribution of $Na_V1.8$

3.1 Introduction

3.1.1 Aims

The hypothesis that $Na_V1.8$ resides within lipid rafts has been supported by their co-localisation with lipid raft markers both in whole cells, as observed with light microscopy, and in sub-cellular fractions. Conventional light microscopy is unable to spatially resolve distances less than a few hundred nanometres, whereas lipid rafts may only be tens of nanometres across. The population of proteins in sub-cellular fractions corresponding to lipid rafts are highly sensitive to the method of fractionation used and may not entirely represent the live cell lipid raft population. Therefore being able to detect where $Na_V1.8$ is located and how it is distributed, on smaller scales than previously observed, in the whole cell condition is valuable to give further support to the theory of $Na_V1.8$ inclusion in lipid rafts.

The inclusion of $Na_V1.8$ in lipid rafts appears to be important for the conduction of signals along small diameter DRG neurons, as lipid raft disruption leads to conduction failure. However, there are many mechanisms which could underlie this function. As explored with computational modelling, the clustering of the channels discretely along the axon may be advantageous for conduction, and disrupting rafts may lead to less clustering of channels. Changes in the clustering of $Na_V1.8$ channels have not been observed with light microscopy after the disruption of lipid rafts. Any Changes in channel distribution may be too small to be observed using this method, due to the limited resolution of light microscopy. Observing the effects of lipid raft disruption on channel distribution at higher magnification will confirm whether any changes occur.

There are different methods available to study biological systems below the limit of light microscopy. These included electron microscopy, atomic force microscopy and a multitude of fluorescence techniques. Our investigation focuses on 2 techniques; scanning electron microscopy (SEM) and Forster resonance energy transfer (FRET). SEM enables the direct imaging of fixed and label samples with resolutions as low as

tens of nm. FRET is used to assess distances between molecules in the nm range and can be used in the live cell condition to assess changes.

3.1.2 Studying lipid rafts

3.1.2.1 Extraction

Lipid raft resistance to non-ionic detergents is one of their defining properties in comparison to the surrounding membrane. This detergent resistance enables their isolation by detergent resistance membrane (DRM) extraction. DRM is extracted from bulk membrane by density gradient centrifugation following ionic detergent treatment of the membrane, such that the un-solubilised membrane floats and can be retrieved (Pike 2003). Triton X-100 is the most commonly used detergent for DRM separation. Tissues or cells are lysed with cold (4 ^{O}C) 1 % Triton X-100 in isotonic buffer. Lipid raft domains are resistant to lysis in 1 % Triton X-100 and therefore remain un-solubilised compared to the rest of the membrane. Lipid raft membrane makes up the DRM, which can be concentrated and separated from the rest of the sample by centrifugation on a density gradient. Originally the method employed sucrose gradients, but now iodixanol (OptiPrep) gradients are also commonly used. Sucrose density gradients are layered over samples which have been adjusted to around 40 % sucrose. Above the sample further discontinuous layers are added, typically consisting of a medium concentration of sucrose, such as 30 % or 35 % and then a low concentration layer of 5 % or 10 % sucrose above that. After ultracentrifugation DRM will have floated to low concentration of sucrose fractions, and in particular are concentrated at the interface between the 35 % and 5 % sucrose fractions. OptiPrep density gradient centrifugation is very similar. Samples are typically adjusted to 40 % OptiPrep, and this is then overlaid with 30 % OptiPrep and a final layer of buffer containing no OptiPrep. Lipid raft membrane floats to low OptiPrep regions after ultracentrifugation and can be collected. There are also lipid raft extraction methods which are detergent free. Detergent free preparations these use either a buffer such as sodium carbonate (pH 11) or purely sonication of purified plasma membrane in order

to disassociate lipid rafts from the membrane and then use density gradient centrifugation to separate them as with other methods.

Although all of these preparations will produce mixtures enriched in known lipid raft constituents, their exact composition varies widely, both in terms of lipid and protein mixtures (Locke et al. 2005). As the composition of lipid rafts varies between the cytoplasmic and exoplasmic leaflets, differences may be due to partial extraction of only the exoplasmic leaflet by DRM extraction techniques.

3.1.2.2 Imaging

Lipid rafts are believed to be smaller than the light microscopy resolution limit, with diameters ranging from a few 10's of nm to 200 nm. In some cases lipid rafts aggregate and therefore become large enough to visualise. This process can be induced in cells by cross linking lipid raft proteins or lipids leading to larger patches of lipid raft on the cell membrane surface. It also happens naturally due to the interaction of raft proteins (Oliferenko et al. 1999). These larger aggregates of lipid rafts can then be visualised by light microscopy.

Alternative imaging techniques can be used to study lipid rafts. Atomic force and electron microscopy have resolution limits far smaller than light microscopy and are therefore able to produce images at the scale of lipid rafts. Planar lipid rafts themselves only differ from the bulk membrane very slightly in their appearance due to being thicker, which make them hard to image directly. Caveolae lipid rafts are easier to identify due to their invaginations and roughly uniform size which is dictated by the radius of curvature due to the inclusion of caveolin. Due to their characteristic shape caveolae have been imaged using scanning electron microscopy and transmission electron microscopy (Thorn et al. 2003). The protein caveolin can also be labelled with gold particles to confirm identification of caveolae in electron microscopy. Atomic force microscopy has been used in model membranes to directly image the phase separation between raft like liquid ordered and liquid disordered regions of membrane (Yuan et al. 2002). This gives some information as to the possible size of rafts, although the lack of membrane proteins and some lipid species in model

membranes, which may stabilise larger lipid rafts, means this may not be applicable to biological membranes.

Others useful tools for studying lipid rafts in membranes use fluorescent labelling and include fluorescence quenching and Förster Resonance Energy Transfer (FRET) imaging studies (Silvius & Nabi 2006). Fluorescence quenching is used to investigate the immediate lipid environment of the labelled molecule. A quencher lipid species enables an excited fluorophore to return to the ground state without emission if it is in contact with the quencher lipid. A reduction in fluorescence intensity or life time is then measured.

FRET enables information about very small separation distances between fluorescent molecules to be gathered using light microscopy. Labelling lipids or proteins of interest with fluorophores means that interactions and proximity to each other can be measured using FRET. FRET is most powerful when the separations involved are a few nm to tens of nm, meaning that is it useful at scales even smaller than electron microscopy. It is used widely to show co-localisation of labelled molecules and so can be used to show restriction of molecules into small areas of the membrane and therefore closer proximity (Zimet et al. 1995).

3.1.2.3 Disruption

As the stability of lipid rafts is dependent on the tight packing of cholesterol in the hydrophobic region of the membrane, depletion of cholesterol from the cell membrane disrupts lipid rafts. Methyl-β-cyclodextrin (MBCD) is a water soluble cyclic oligosaccharide. The centre of the ring of sugars is much less hydrophilic than the outside, and hydrophobic molecules, such as cholesterol, can form inclusion complexes within it. As the hydrophobic molecules are contained within the ring the complex remains water soluble. MBCD can therefore be used to remove cholesterol from membranes, as it shows a high affinity for it over other membrane lipids. It is also possible to use it to enrich membranes with cholesterol, by applying MBCD already saturated with cholesterol (Christian et al. 1997). Cholesterol partitions preferably into the lipid raft portions of membranes, where it is helps to stabilise the constituents into

a liquid ordered phase. Using MBCD to deplete cholesterol from the membrane therefore leads to the disruption of lipid rafts. Known lipid raft proteins, such as Thy1, have been shown to be released from the membrane following MBCD treatment (Ilangumaran & Hoessli 1998). As cholesterol is crucial for raft integrity, inhibition of its synthesis in the cell can also be used to disrupt rafts. Statins inhibit cholesterol synthesis and some have been used to disrupt rafts in this way (Taraboulos et al. 1995). The synthesis of sphingolipids, which are also integral to lipid rafts, has been shown to also lead to disruption. Gylcosphingolipid synthesis has been inhibited using FumonisinB1 to inhibit lipid rafts involved in trafficking to the membrane of raft associated proteins.

Cholesterol and other lipid constituents of rafts are not restricted to rafts but also found in the rest of the membrane. There is some evidence that cholesterol is preferentially removed from non-raft membrane (Ilangumaran & Hoessli 1998). All methods which remove constituents from the membrane may have unwanted effects on the whole membrane and its associated proteins. A different approach, which directly effects the phase separation of lipid rafts into liquid ordered domains, is treatment with 7-Ketocholesterol, a cholesterol analogue. It can replace cholesterol in lipid rafts but does not have the stabilising effect of cholesterol, and so leads to their phase change to liquid disordered.

3.1.3 SEM Theory

Electron microscopy uses electrons in place of photons of light to resolve an image. There are two types of electron microscopy; transmission electron microscopy (TEM) and scanning electron microscopy (SEM). TEM images are produced by electrons being passed through the sample of interest and then being observed, whereas SEM images are composed from the electrons received back from a surface radiated with electrons. In SEM the surface to be observed must be conductive, therefore for non-conducting samples, such as biological samples, the surface is coated with a thin layer of metal. Metals commonly used are gold and chromium, mainly as they are un-reactive. When the conducting surface is irradiated with electrons this causes charging of the material, which then leads to secondary electrons being emitted by the surface. These

secondary electrons are what are usually measured by the detector. However, a small proportion of the radiative electrons are back scattered (reflected by the nucleus) directly, and these can be measured separately. The back scattered electron (BSE) signal is sensitive to the composition of the material in the sample so that different materials can produce a varying strength of signal (Hermann et al. 1996). The signal is also received from deeper within the sample. This means that signals from conducting materials below the surface coating can be detected, as shown in Figure 3-1.

Electron microscopy can resolve at much higher magnifications than conventional light microscopy. This is because electrons can have much smaller wavelengths than visible light and therefore diffraction doesn't occur until much smaller distances. In fact electron microscopy can give images with 250 times higher magnification than light microscopy, with resolution as fine as 1 nm. However, as light is not used there are no colours on the image, instead the three dimensional surface of the sample can be seen when the secondary electron signal is used.

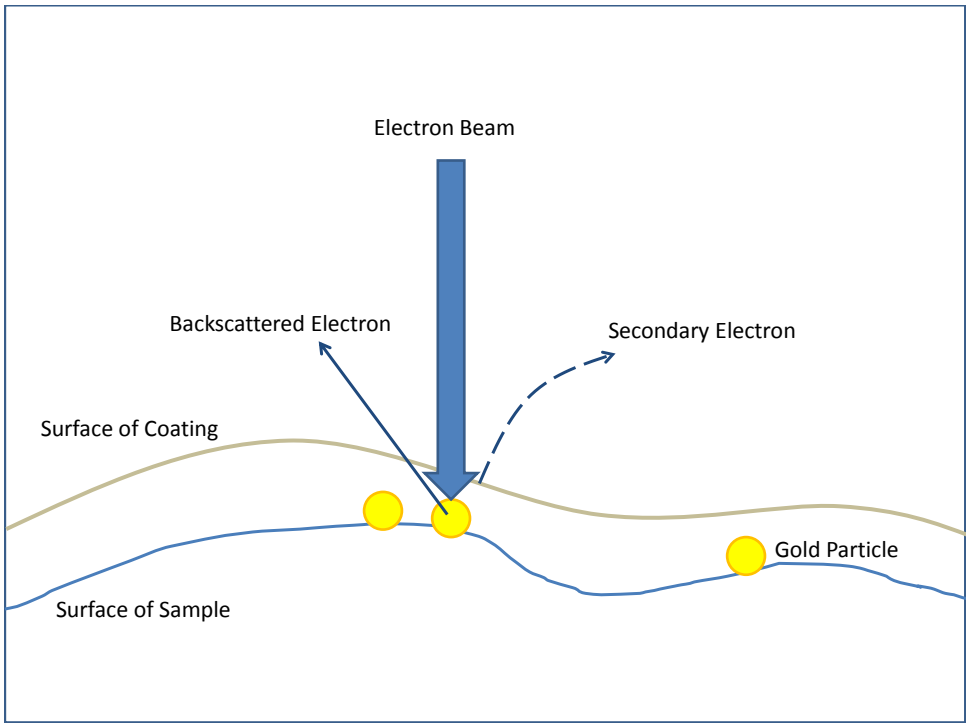

Figure 3-1 Electron signals detectable in SEM using colloidal gold labelling, based on diagram from (Hermann et al. 1996). Gold particles are used to label proteins on the cell surface, prior to sample coating. Electrons are backscattered from the electron beam by the nucleus of the gold particles below the surface coating. The BSE signal shows the composition of the sample. The electron beam produces secondary electrons in the surface coating. The SE signal shows the surface morphology.

To label features of interest, antibodies conjugated to gold particles can be used on biological samples (Horisberger & Rosset 1977). As gold is conductive it will be apparent in the electron microscope image. The choice of gold particle depends on how the sample is to be labelled and imaged. Some large and very uniform gold particles may be apparent from the morphology visible in SE image. Small gold particles may be easily mistaken for surface features in biological samples where the surface is not regular. Small gold particles can be seen using the BSE electron signal as long as the surface coating is of a different conducting metal. Immuno-gold labelling is likely to be more efficient with smaller gold particles as more particles will be able to reach nearby sites very close to each other. Small particles will also be able to reach internal sites more easily following permeabilisation. Even with the BSE signal it may be hard to find which region has good gold labelling at lower magnification with small gold particles, whereas larger gold particles will be more apparent at lower

magnifications. Large gold markers are also less precise in specifying the exact location of the protein of interest. The physical extents of the antibodies used in labelling already cause the gold particle to be displaced from the exact location of the protein of interest, adding an extra layer of inaccuracy.

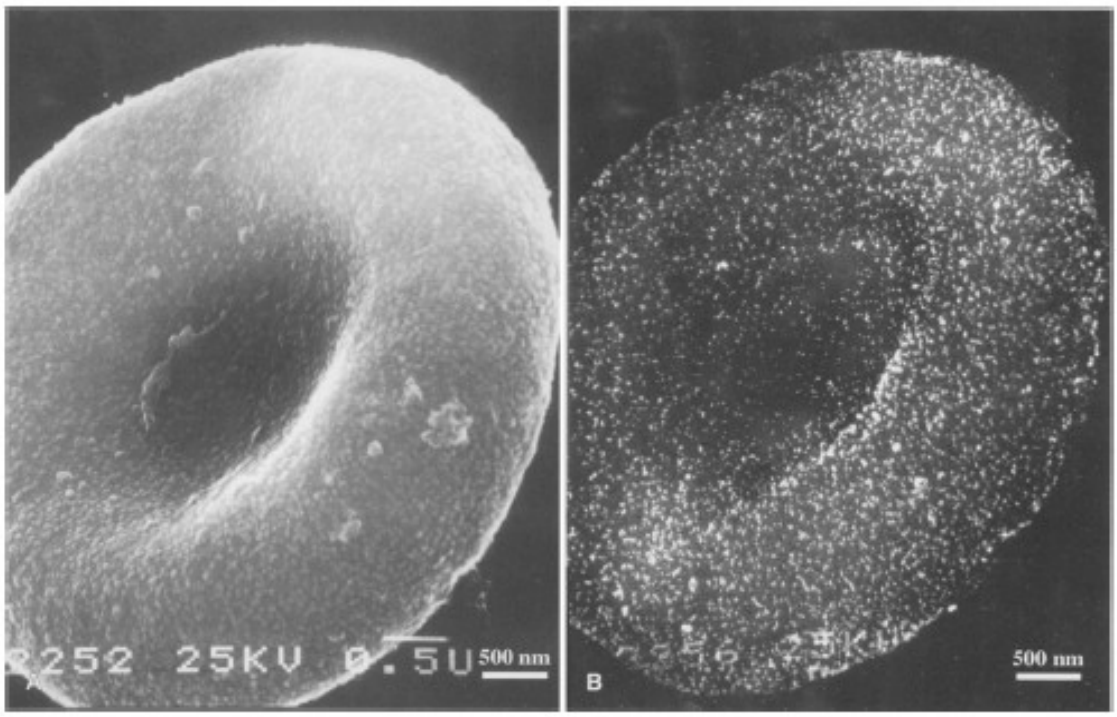

Figure 3-2 SEM images of a red blood cell. The cell membrane is labelled with 15 nm gold against a membrane protein. The cell is freeze dried and coated with 10 nm of carbon. A. The SE image shows detailed 3D surface morphology. B. In the BSE image the gold particles show up clearly. Adapted from (Hermann et al. 1996).

3.1.4 FRET

3.1.4.1 Theory

If proteins are located in lipid rafts they will come into much closer proximity to each other than if they are evenly distributed on the cell membrane. These separations are of the order of a few to tens of nanometres, which are below the level that can be resolved with a light microscope. Proximity and interaction between proteins in cells

can be measured using the technique of Förster (sometimes Fluorescence) Resonant Energy Transfer (FRET). One or two proteins of interest are labelled with chromophores, where the emission spectra of one, called the donor, overlaps with the absorption spectra of the other, called the acceptor. This means that if the two chromophores are close enough to each other the donor will directly excite the acceptor, through a dipole interaction, rather than emit a photon, as shown in Figure 3-3. The efficiency of energy transfer E is given by:

Equation 3.1

$$E = \frac{1}{1 + (r/R_0)^6}$$

where r is the separation and R_0, the Förster Radius, is the distance at which the efficiency is 50%. This inverse 6th power law means the efficiency decreases rapidly with increasing separation, such that small differences in proximity of the fluorophores in the region around the Förster radius result in large changes in the efficiency of energy transfer. Therefore the efficiency of energy transfer is a good measure of the proximity of the chromophores.

The choice of chromophore pair and the environment give the R_0 value by the equation:

Equation 3.2

$$R_0 = [c\kappa^2\eta^{-4}\varphi_d\varepsilon_a J(\lambda)]^{1/6}$$

Where c is a constant = 8.786×10^{-11}, κ is the dipole orientation factor, which depends on the respective orientation of the chromophore dipoles, η is the refractive index of the medium, ϕ_d the donor quantum yield, ε_a the acceptor absorption coefficient and J(λ) is the overlap integral of the donor emission and acceptor absorption spectra. This makes use of the ideal dipole approximation (IDA), which assumes the part of the fluorophore making the transition behaves as an ideal dipole. The dipole orientation factor κ is important for determining the Förster radius, but the orientations of the dipoles is difficult to ascertain. It is generally assumed that the dipoles will be randomly isotropically arranged, this leads to an average value of κ^2 of 2/3. However, this assumption may not hold when fluorophores are attached to membrane bound proteins, which by definition are not isotropically distributed. It is estimated the κ^2 for membrane associated fluorophores can be in the range of $0 \leq \kappa^2 \leq 4$ (Loura 2012). However, even in membranes the average value for κ^2 is still close to 2/3 and therefore it is generally used.

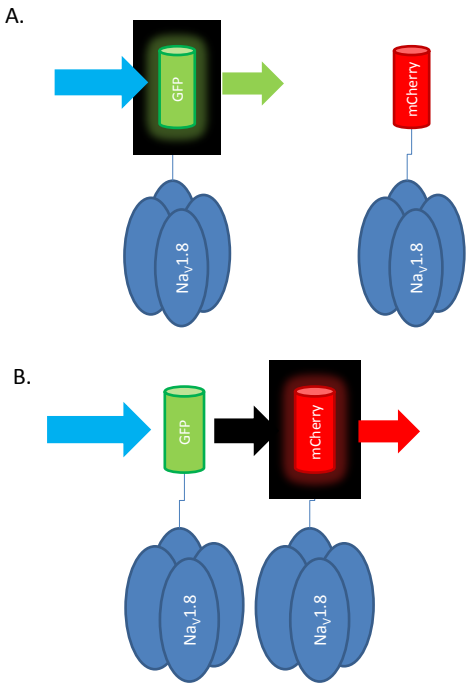

Figure 3-3 Diagram of FRET A. When fluorophores are spatially separated excitation of the donor (GFP) leads to direct emission of light. B. When fluorophores are located close together the donor can directly excite the acceptor (mCherry) leading to emission by the acceptor.

3.1.4.2 Sources of Error

Distinguishing a true FRET signal from background fluorescence is one of the main challenges faced in FRET studies. The donor emission and acceptor excitation spectra are unlikely to overlap exactly. The ability to detect the increased acceptor fluorescence due to FRET is reduced if the donor emission overlaps with the region of acceptor emission being measured. Also if the acceptor's excitation spectra overlaps with the donor's there can be direct excitation of the acceptor at the same wavelength used for donor stimulation.

3.1.4.3 Pair selection

A good overlap of donor emission and acceptor excitation spectra leads to a higher overlap integral J(λ) and a longer R_0. For this reason the pair of green fluorescent protein (GFP) and mCherry, a monomer red fluorescent protein, were chosen (Albertazzi et al. 2009) for our investigation, their spectra are shown in Figure 3-4. Compared with the widely used CFP-YFP pair used they have a longer R_0,

approximately 5-6nm, and may therefore be more suitable for the proximity measurements we need which should have a similar separation. UV light can be damaging to cells, and therefore using GFP rather than CFP will reduce the risk of damage, as it is excited by a longer wave length.

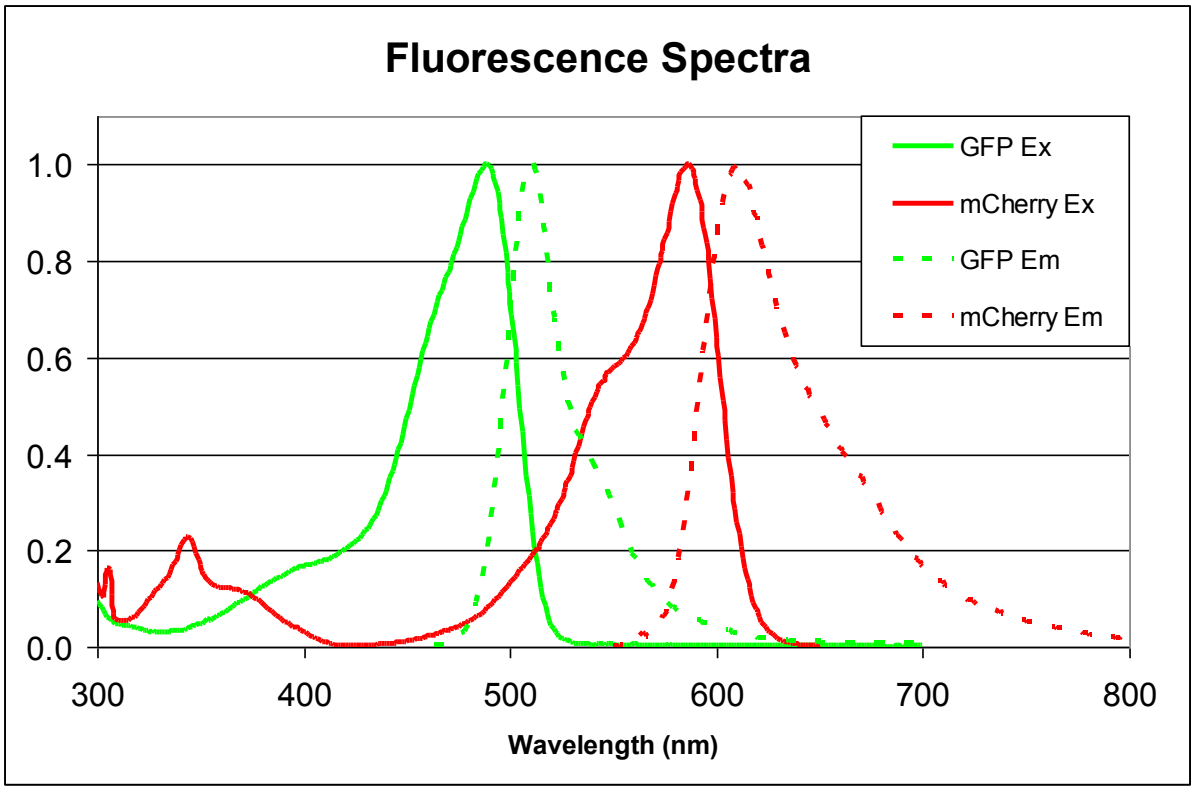

Figure 3-4 Absorption and emission spectra for GFP and mCherry fluorophores. Spectra data sourced from Fluorescence SpectraViewer (Life Technologies) (Anon n.d.). Y axis shows relative intensity in arbitrary units, with spectra normalised such that they have a peak amplitude of 1.

FRET has been used to study the sodium channel $Na_V1.8$ previously (Liu et al. 2006), in order to asses binding of potential blockers for the treatment of pain.

3.2 Methods

3.2.1 Cloning

PCDNA 3.1 containing mCherry (Roger Y. Tsien, University of California) was amplified by transforming XL1-blue competent cells, growing overnight and extracting DNA by miniprep (Qiagen). Primers were designed for $Na_V1.8$ with HindIII and AgeI restriction sites at the 5' and 3' ends respectively. $Na_V1.8$ was amplified from the $Na_V1.8$ expressing PRK5 plasmid (Okuse) using the primers in Table 3-1 to add the restriction sites. For amplification Taq DNA polymerase (Fermentas) was used. After initial denaturation for 1 minute at 98 ^{O}C, 30 cycles of PCR were used, consisting of 30 seconds denaturation at 98 ^{O}C, 30 seconds annealing at 72 ^{O}C and 2 minutes 20 seconds extension at 72 ^{O}C, followed by a final extension of 10 minutes at 73 ^{O}C. The plasmid PCDNA3.1 (containing mCherry) and insert ($Na_V1.8$) were cut with HindIII and AgeI fast digest restriction enzymes (Fermentas) at 37 ^{o}C for 20 minutes and denatured at 80^{o}C for 20 minutes. The insert was ligated into the vector using the ligase enzyme for 1 minute at 37^{o} followed by two hours at 22^{o}C and denatured at 65 ^{o}C for 10 minutes. The ligation product was transformed into competent cells and plated on LB agar ampicillin (100 µg/ml) plates, which were incubated overnight at 37 ^{o}C. Successfully transformed colonies were picked and grown overnight in LB media at 37 ^{o}C with shaking. DNA was then extracted by miniprep, cut with restriction enzymes and run on a 1% agarose gel to check for inserts. The plasmids were sequenced to confirm correct insertion and the cells containing them grown on for endo-toxin free maxi-prep (Qiagen) for transfection of mammalian cells.

Product	Direction	Restriction site	Sequence
Flotillin	Forward	HindIII	ACTGAAGCTTACCATGTTTTTCACTTGTGGCC
Flotillin	Reverse	AgeI	AATAATACCGGTCGCGCCGTCCTTAAAGG
$Na_V1.8$	Forward	HindIII	ACTGAAGCTTACCATGGAGCTCCCCTTTGCGTCCGT
$Na_V1.8$	Reverse	AgeI	TCGAACCGGTCGTAACTGAGGTCCAGGGCTGTTTCC
GFP	Forward	AgeI	ACTGACCGGTCATGAGTAAAGGAGAAGAACTTTTCACTGGAGTT
GFP	Reverse	XbaI	CTGATCTAGATTATTTGTACAATTCATCCATACCATGGGTAATACC

Table 3-1 Primers used for cloning of DNA to be inserted in to plasmid vectors.

3.2.2 DRG Culture

Adult female Wistar rats, weighing approximately 150 g, were culled by CO_2 asphyxiation. DRGs were dissected out and placed in 10 ml of ice cold DMEM (Gibco, Life Technologies) + 1 % Penicillin Streptomycin (Gibco, Life Technologies) and the remaining nerve roots removed by micro-dissection. They were incubated at 37^{o}C for 90 minutes in 2 ml DMEM with 0.125% collagenase XI (Sigma) and 0.1mg/ml DNase II (Sigma). Cells were triturated with a 1ml pipette tip until the solution appears homogeneous and passed through a 70 µm sieve (BD Biosciences), which was then washed through with 2ml DMEM. 4 BSA cushions of 2ml were prepared with 10 % BSA in DMEM, 1ml of cell suspension was layered over each. Layered cushions were centrifuged at 800 rpm for 7 min. All supernatant was removed starting with the interface (containing the debris) followed by the rest of the BSA cushion and finally the DMEM on top. The DRG cells remaining in the pellet were re-suspended in 2ml DMEM. 12 µl of cell suspension were taken to count the cells with a haematocytometer and the rest centrifuged at 1200 rpm for 3 minutes. Cells were re-suspended to the desired concentration and plated in dishes pre-coated with poly-L-Lysine (Sigma) and Laminin (Life Technologies). Cells were cultured in the presence of NGF (50 ng/ml, Peprotech), to promote neurite outgrowth and Aphidicholine (10 µM, Sigma) to suppress Schwann cell proliferation.

3.2.3 Cell Line Culture

Immortal cell lines; PC12, HEK293 and ND7, were cultured in 10cm cell culture dishes (BD Falcon) in complete media (DMEM, 10% FBS, 1% Penicillin/Streptomycin). To passage the cells the plates were washed with 10 ml pre-warmed ($37^{O}C$) PBS and then incubated with 1 ml of 0.25% Trypsin (Gibco) for 1 minute whilst gently tapping the side of the dishes. The Trypsin was neutralised and the cells re-suspended by the addition of 9 ml pre-warmed DMEM and centrifuged at 1200rpm for 3 minutes. The supernatant was aspirated and the cells re-suspended in 1ml complete media. Cells were counted in a 12ul sample of cell suspension using a haemocytometer and plated at the desired density. For transfection cells were plated on 13mm glass coverslips, pre-coated with poly-L-Lysine, in a 24 well plate.

3.2.4 Cell Fixation and Staining

For localisation of lipid raft marker GM1 ganglioside, DRG cultured neurons were treated first with biotinylated Cholera Toxin Beta Subunit (CTB) prior to fixation. Cultures were washed twice with PBS and incubated with 1:1000 biotinylated CTB in PBS at room temperature for 20 minutes. Cultures were washed twice with PBS and incubated with 1:1000 streptavidin-Alexa488 in PBS at room temperature for 20 minutes before fixing.

Cultures were washed twice with PBS and fixed with Para-Formaldehyde 4% in PBS for 10 minutes at room temperature, or 15 minutes on ice. Fixed DRG cultures for treatment with antibodies were washed twice with PBS and incubated with the primary anti-body in PBS with 10% Goat Serum for 1 hour. Primary anti-bodies used and their concentrations were mouse anti-Ankyrin G and Annexin A2, and rabbit anti-$Na_V1.8$ 1:200. They were washed twice with PBS and incubated with the appropriate secondary fluorophore conjugated anti-body for 1 hour. They were washed twice and mounted on slides with glycerol PBS to be viewed.

3.2.5 Transfection by Electroporation

Transfection of DNA into cells by electroporation was carried out using the Neon transfection system (Invitrogen). DRG cultures were electroporated before plating. Rather than resuspend cell pellets in complete media they were cleaned by

resuspension in 10ml pre-warmed PBS and centrifuged at 1200rpm for 3 minutes. The PBS was removed and the cells resuspended in buffer R (Invitrogen) at a concentration of approximately 5000 cells per ul. 20ng/ul plasmid DNA was added and 10ul of cell suspension was taken up into a Neon gold tip and electroporated with 2 pulses at 1200 volts of 20 msec each. Cell were then added directly to dishes containing pre-warmed DMEM with 10% FBS. The following day media was replaced with complete media with NGF and Aphidicholine for DRG cells.

3.2.6 Optical Injection

Optical transfection is a technique that is being developed to help transfect plasmids and other molecules into cell types that are traditionally difficult to transfect. It involves using a laser beam to form a temporary pore in the membrane of a cell, which allows molecules in the surrounding media to enter the cell.

One day before transfection cells were plated on glass bottomed dishes in complete DMEM. Before transfection cells were washed twice with pre-warmed OptiMEM (Gibco) solution and the media replaced with pre-warmed optiMEM containing plasmid DNA. To test for viability following photoporation test runs were carried out without DNA but in media containing propidium iodide (PI). Photoporation was carried out using a femtosecond titanium sapphire laser in conjunction with the St Andrews University Biophotonics group as part of a joint Photonics for Life project (Praveen et al. 2011).

3.2.7 Transfection by Lipofection

One day before transfection cells were plated at 10^5 cells per well on a 24 well plate or glass bottom dish of the same area, in 500 µl complete DMEM. Cells were incubated at 37 ^{O}C with 5 % CO_2. 1 hour prior to transfection wells were washed once and the media replaced with pre-warmed Opti-MEM, and returned to the incubator. For each well to be transfected 50 µl Opti-MEM was mixed with Lipofectamine 2000 and another 50ul Opti-MEM mixed with 1 µg of plasmid DNA in Endotoxin free buffer, these were incubated at room temperature for 10 minutes. The Lipofectamine and DNA solutions were mixed and incubated for 20 minutes at room temperature to form the transfection complexes. 100 µl of complex mixture were added to each well and

then incubated at 37 ^{O}C. After 4 hours 30 % FBS in Opti-MEM was added to make a final concentration of 10 % FBS in each well.

3.2.8 Magnetic Transfection

One day before transfection cells were plated on glass coverslips in a 24 well plate. Stock solutions of $Na_V1.8$-GFP and $Na_V1.8$-mCherry were made up to a DNA concentration of 0.2 µg/µl. 10 µl of each solution was added to 120 µl of PBS, to which was added 28 µl of NeuroMag (nanoTherics) nano particle solution and mixed by pipetting. This was added to 500 µl of CDMEM culture media. Cell cultures were washed 2 times with culture media and then the media contain the DNA and nano particle was added. Cultures were place in the magnefect machine (nanoTherics), which was run at 5 Hz for one hour with an oscillation of 0.2 mm, whilst incubated at 37 ^{O}C and 5 % CO_2. After transfection the media was replace with 500 µl CDMEM culture media.

3.2.9 Scanning Electron Microscopy

One week before imaging DRG cultures were prepared as previously described on glass coverslips in a 24 well plate. The day before imaging cell cultures were fixed and stained as necessary. Cultures were washed three times with PBS before and after fixation. Different fixation methods were compared to determine the best method for preserving the morphology for SEM imaging. Methods compared were: methanol fixation for 5 minutes on ice, followed by either direct evaporation or washing with water and drying at 50 ^{O}C; or fixation with PFA for 10 minutes at room temperature, washing with water and drying at 50 ^{O}C. In order to label DRG cells with gold particles for SEM detection they were stained with primary anti-bodies and then treated with gold particles conjugated to secondary anti-bodies. Fixed cultures, before being dried, were washed twice with PBS and then incubated with primary anti-body as previously described. Cultures were washed twice with PBS and then incubated with 40 nm gold particles conjugated to anti-rabbit IGG anti-bodies (KPL) in the provided buffer for 1 hour. Cultures were then washed twice with water and left to dry at 50 ^{O}C overnight. Cultures were mounted on electron microscope stumps and a bridge of silver painted between the sample and the stump. Samples were coated with chromium using the

sputter coater for 1 minute at 75 mA under vacuum. Images were taken using the LEO Gemini 1525 FEGSEM, in both SE and BSE modes, with the help of Dr Mahmoud G Ardakani from the Harvey Flower Microstructural Characterisation Suite, Imperial College**.** Before samples are loaded into the microscope imaging chamber the vacuum is purged. For imaging samples were loaded once firmly mounted in an eight stump holder and the imaging chamber closed. The microscope pump is turned back on and air is removed from the compartment until the system vacuum reaches 1.5 x 10^{-5}.

3.2.10 FRET

For FRET studies, 100 µl of HEK 293 cell suspension was placed in 35 mm glass bottom dishes (MatTek) overnight at a plating density of 1.5 x 10^5 cells per well. On the following morning, the medium was replaced with 100 µl of Opti-MEM Reduced Serum Medium prior to cell transfection with 0.6 µg of our flotillin constructs (either individually or combined in a co-transfection) using 1.5 µl of Lipofectamine 2000 transfection reagent according to the manufacturer's instructions (Invitrogen). FBS was added back to the cells to final concentration of 10% FBS 4 hours post-transfection and the medium was replaced with fresh pre-warmed MEM the following morning. Immediately prior to FRET imaging, the medium in each 35 mm dish was replaced with 1.5 ml of sterile-filtered Normal solution (140 mM NaCl, 5 mM KCl, 2 mM $MgCl_2$, 1.8 mM $CaCl_2$, 10 mM glucose and 10 mM HEPES in cell culture grade H_2O, pH 7.4). FRET was performed by the sensitised acceptor emission method [31] at 37 ˚C under a Leica SP5 MP inverted microscope. After recording the absorption and emission spectra of GFP and mCherry, green and red fluorescence were initially excited separately at 488 nm and 543 nm, with the corresponding fluorescence emission recorded using 500-550 nm and 576-657 nm filters, respectively. Subsequently, fluorescence was excited at 488 nm, with both green and red fluorescence emission recorded. The FRET experiment was repeated for co-transfected cells following 30 minute incubation in 7.5 mM methyl-β-cyclodextrin in normal solution to disrupt lipid rafts. Image recording and analysis was performed using Leica Application Suite Advanced Fluorescence (LAS AF) software.

3.3 Results

3.3.1 Investigation of Protein Distribution by Scanning Electron Microscopy

DRG cells were cultured for a week with NGF to produce cultures with a high proportion of small diameter cells with fully extended neurites. Cultures were fixed using either 4 % PFA in PBS or methanol in PBS. Methanol fixation followed by washing with water resulted in cells that retained their shape and neurites which were clearly visible when imaged using SEM, Figure 3-5(A). There were cracks in the surface of methanol fixed cells, particularly where the cell body membrane meets the plate surface. The cell body shape also appears shrivelled and deformed. Methanol fixation immediately followed by drying almost completely destroyed the morphology of the cells, Figure 3-5(B). As the methanol was in a solution of PBS, salt crystallised on the plate surface during drying, particularly nucleating around cell bodies. PFA fixation followed by washing with water and drying at 50 ^{O}C, resulted in the best retention of morphology, Figure 3-5(C). The cell bodies of PFA fixed cells were clearly defined and not deformed. Their eurites were visible and clearly defined including processes with diameters of 20 nm or less, Figure 3-6. In all samples, and particularly clear in the samples dried from water, were a range of sizes of cell bodies from 10 µm to 50 µm across, as would be expected from a DRG cell culture. The range of cell size and morphology also closely matched what was observed when the same cultures were observed with an upright light microscope in the lab prior to fixation, such that minimal disruption had been caused by culture fixation and treatment.

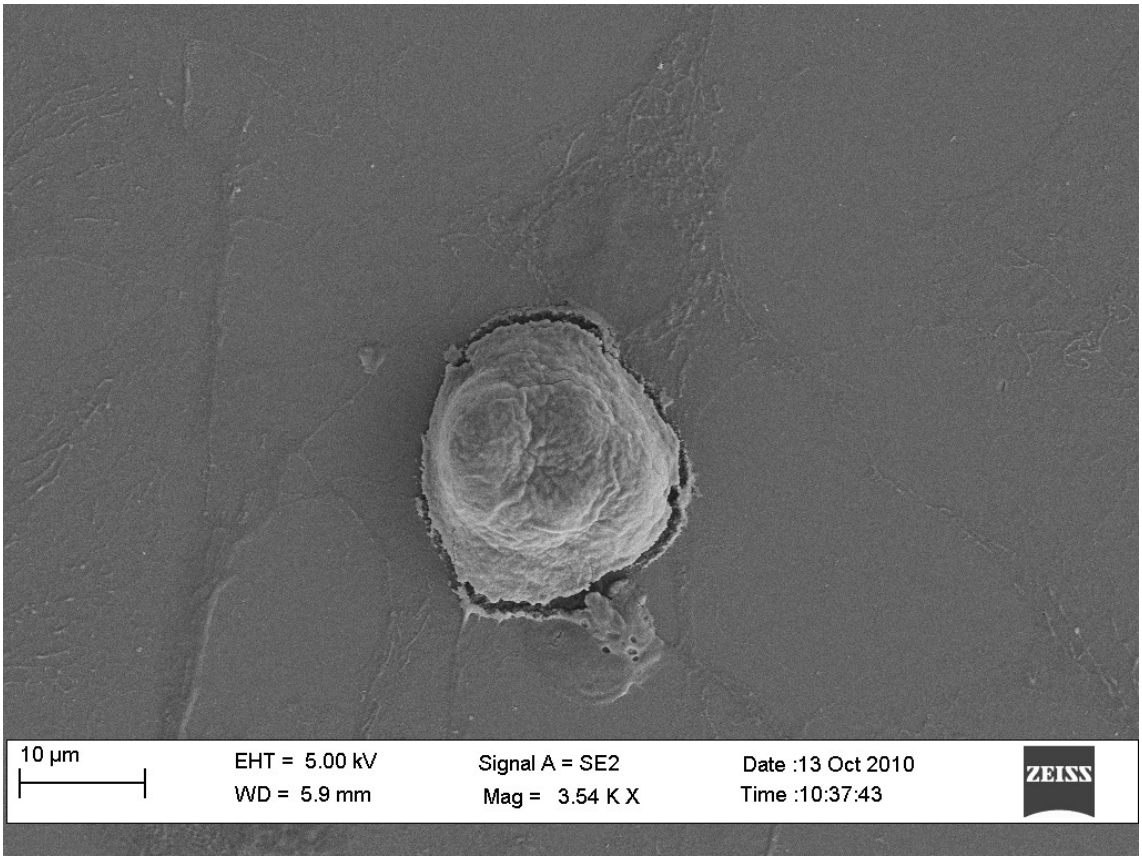
10 µm
EHT = 5.00 kV
WD = 5.9 mm
Signal A = SE2
Mag = 3.54 K X
Date :13 Oct 2010
Time :10:37:43
ZEISS

A.

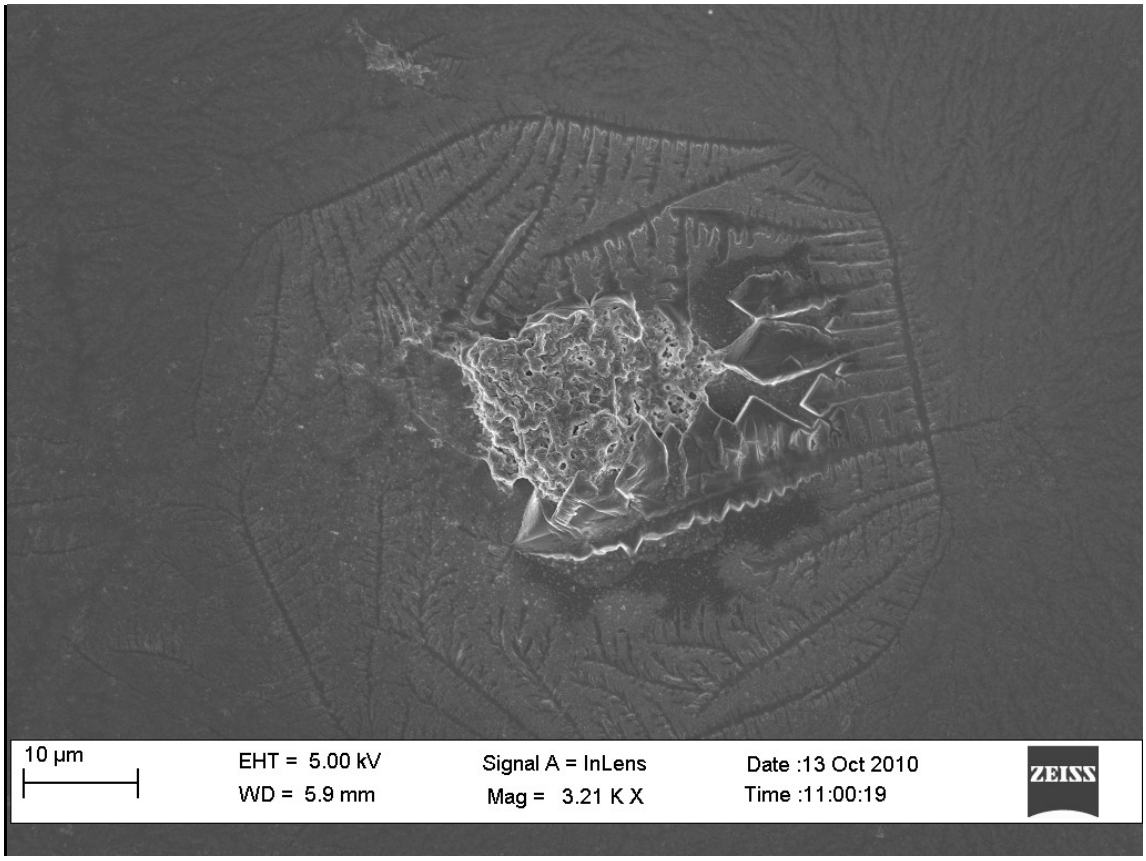
10 µm
EHT = 5.00 kV
WD = 5.9 mm
Signal A = InLens
Mag = 3.21 K X
Date :13 Oct 2010
Time :11:00:19
ZEISS

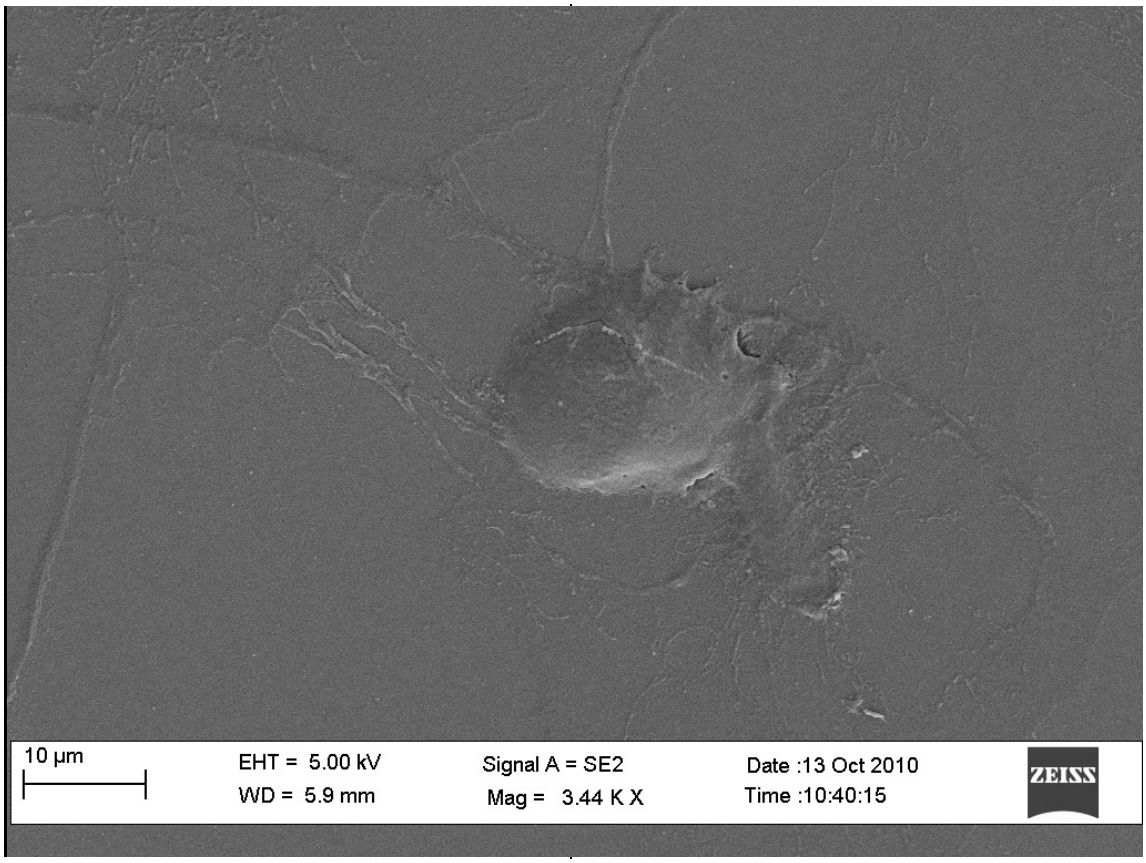

Figure 3-5. Comparison of fixing methods for scanning electron microscopy. A. Methanol fixation, washed with H_20, dried at 50^OC. B. Methanol fixation, dried by immediate evaporation. C. PFA fixation, washed with H_20, dried at 50^OC.

DRG morphology was well preserved following fixation and preparation for SEM imaging. Small diameter DRG neurons, which correspond well with the population expressing $Na_V1.8$, were abundant and different aspects of their morphology were easily distinguished, Figure 3-6(A). The nucleus of the cells in often very clear as it can stand proud of the surface. As is also observed with light microscopy the nucleus makes up a large proportion of the cell body, which in these images can be seen as a larger envelope surrounding the nucleus and which lies much flatter to the surface by comparison. This can be seen clearly in Figure 3-6(B), to the left of the cell nucleus. Neurites originating from the cell body are visible radiating out from the cell. These vary in thickness and tend to be thickest closer to the cell body. Many neurites branch and these become some of the thinnest neurites, Figure 3-6(D).

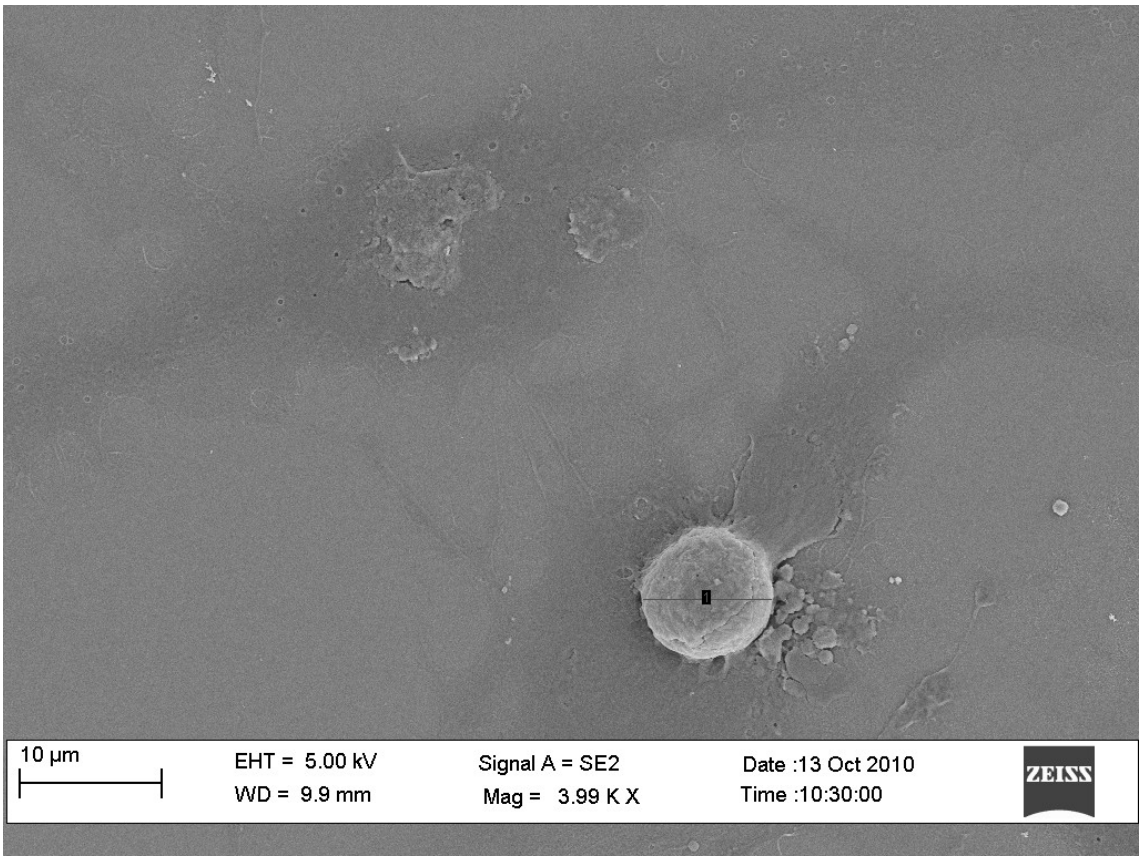
10 µm
EHT = 5.00 kV
WD = 9.9 mm
Signal A = SE2
Mag = 3.99 K X
Date :13 Oct 2010
Time :10:30:00
ZEISS

A.

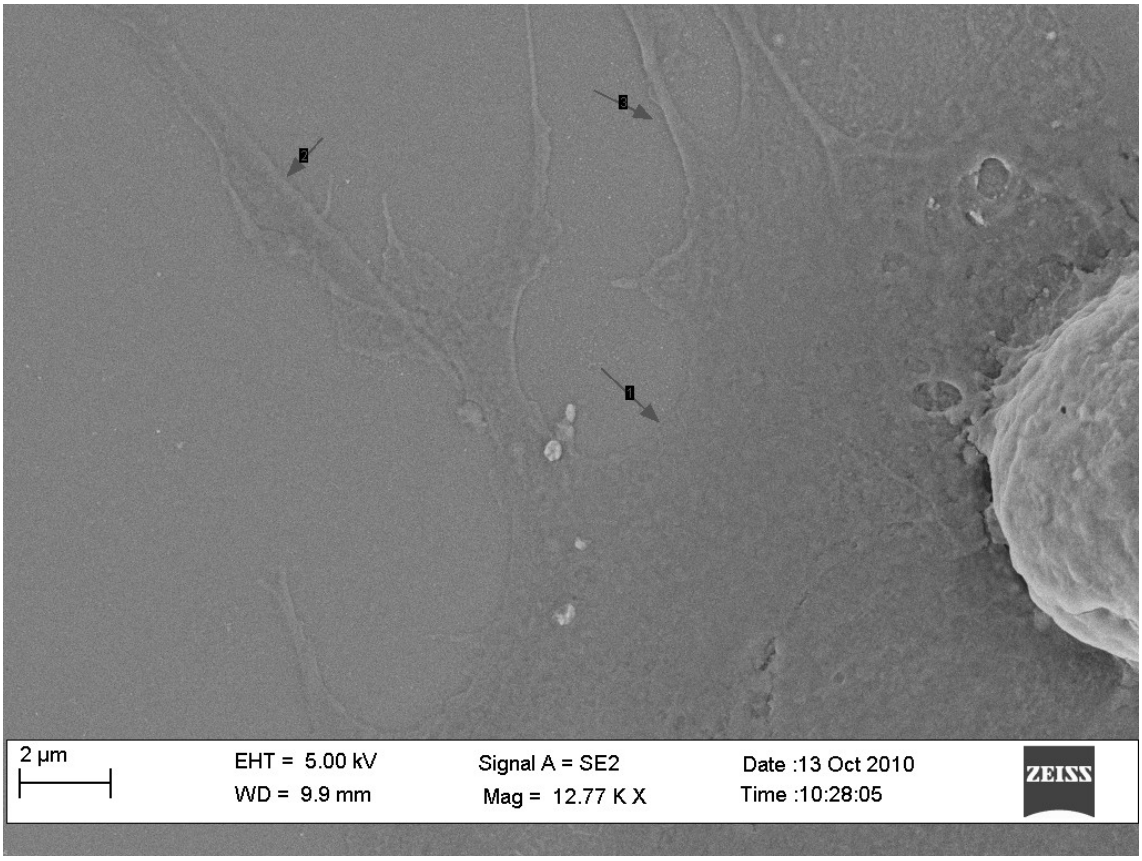
3
2
1
2 µm
EHT = 5.00 kV
WD = 9.9 mm
Signal A = SE2
Mag = 12.77 K X
Date :13 Oct 2010
Time :10:28:05
ZEISS

B.

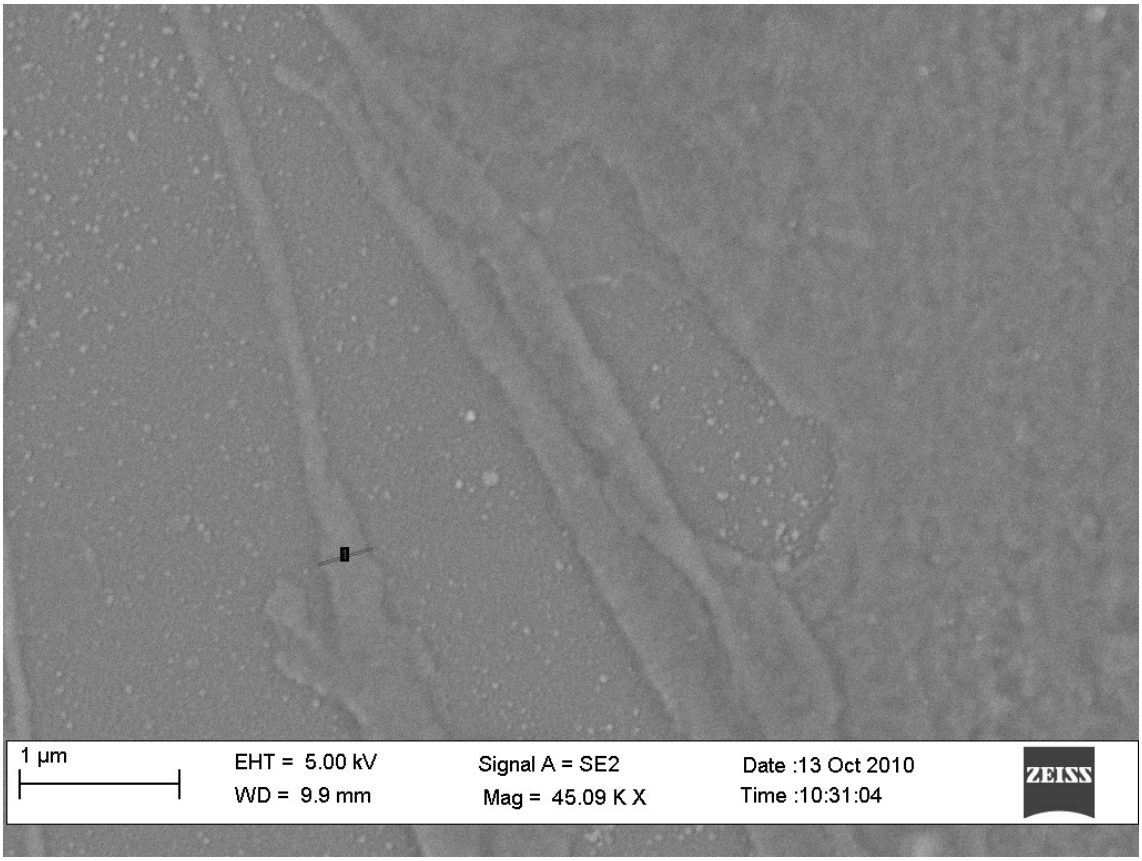
1 µm
EHT = 5.00 kV
WD = 9.9 mm
Signal A = SE2
Mag = 45.09 K X
Date :13 Oct 2010
Time :10:31:04
ZEISS

C.

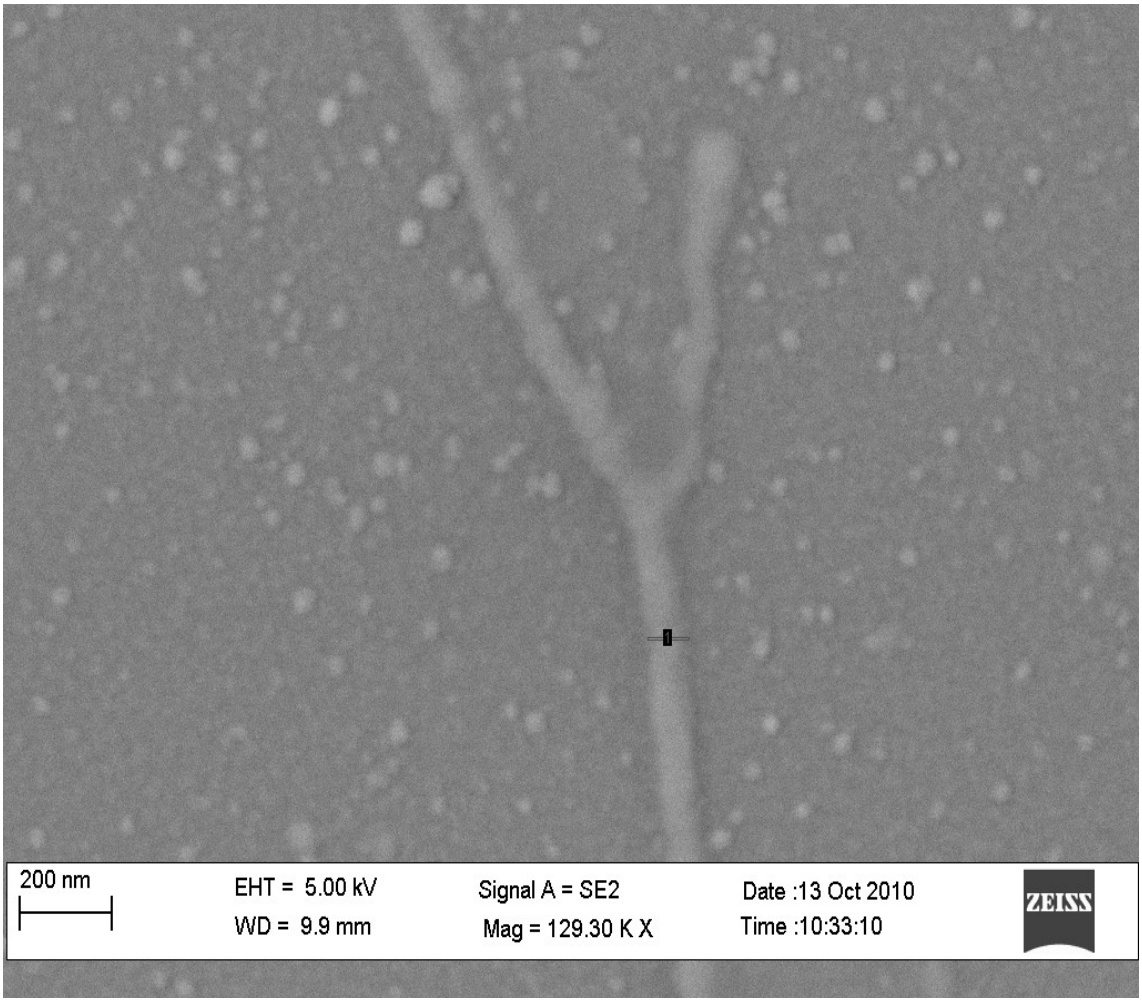

D.

Figure 3-6. DRG cultured neuron imaged by scanning electron microscope. A. Shows whole DRG with cell body. The diameter measurement labelled 1 is 9.2 µm. B. Higher magnitude image of the same cell as in A, with arrows showing the edge of the cell body membrane envelope and neurites originating from the cell body. C. At higher magnification neurites are shown to be well defined and visible, neurite diameter labelled 1 is 340nm. D. Very thin neurites can be imaged. The labelled neurite diameter is 88 nm.

3.3.1.1 Lipid raft marker labelling on the neurites of DRG neurons

Membrane proteins of can be labelled with gold particles by the use of anti-bodies. Although gold particles may be visible morphologically even after sample coating with chromium, they can be hard to distinguish and analyse due to the uniform colour of the surface. Where surface morphology is itself uneven, they are often not distinguishable from other surface features. In this case the BSE signal, which

elucidates the composition of the material below the surface, is used to good effect to show the distribution of labelling with gold particles. The back scattered electron (BSE) signal from scanning electron microscopy originates from deeper within the sample and varies depending on the composition of the sample. Lipid raft marker proteins were labelled with 40 nm gold particles and samples were coated with chromium. Gold labelling was hard to observe with the commonly used secondary electron signal, Figure 3-8(A). The gold particles are difficult to distinguish from surface features based on morphology alone. As can be seen in Figure 3.10, some gold particles are visible in the morphology of the secondary electron signal but this only becomes apparent due to comparison with the BSE signal. There are other features in the secondary electron signal image which could be easily mistaken for gold particles but are in fact just the cell surface. Although the labelling is beneath the chromium coating the gold particles can be detected using the BSE signal. In the BSE signal gold particles labelling the surface appear as bright dots and hence where there is a lot of labelling this is apparent even at lower magnifications. Gold particle labelling was observed for CTB labelling of GM1 ganglioside, known to reside in lipid rafts, Figure 3-7, Figure 3-8 and Figure 3.10. Gold labelled CTB shows GM1 located on the membrane of small diameter neurons. It is located on the cell body and the neurites, although the density varies widely. Some areas show high levels of labelling with particles every only tens of nm apart or forming larger groups. Other areas show very little or no labelling. This may be due to in efficient labelling or highly variable levels of the protein expressed on the membrane. Not many areas within the same field of view showed these large differences in labelling. In Figure 3-7(D) the neurite shown has little labelling whilst a small patch of neighbouring membrane show much higher levels. Crucially we were unable to observe neurites with patches of high labelling for GM1 interspersed with low levels of labelling, which would correspond to the patterns observed with light microscopy.

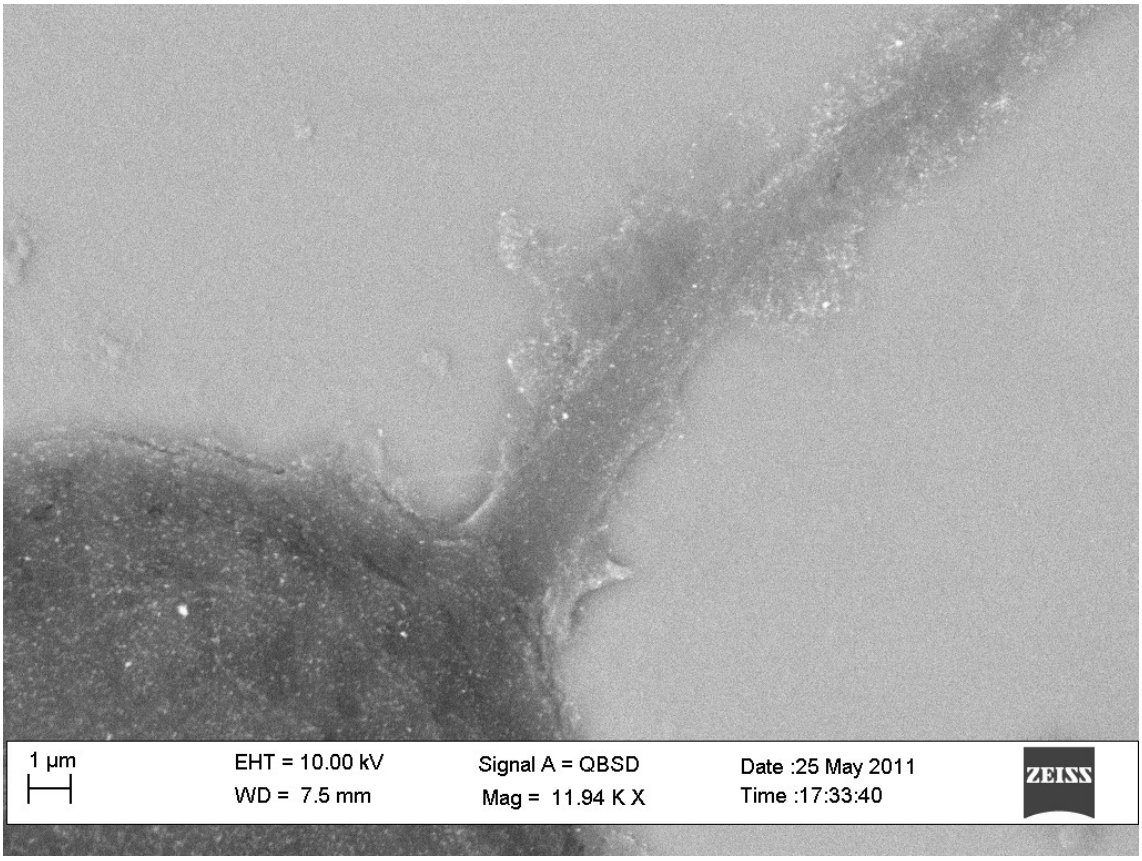
1 µm
EHT = 10.00 kV
WD = 7.5 mm
Signal A = QBSD
Mag = 11.94 K X
Date :25 May 2011
Time :17:33:40
ZEISS

A.

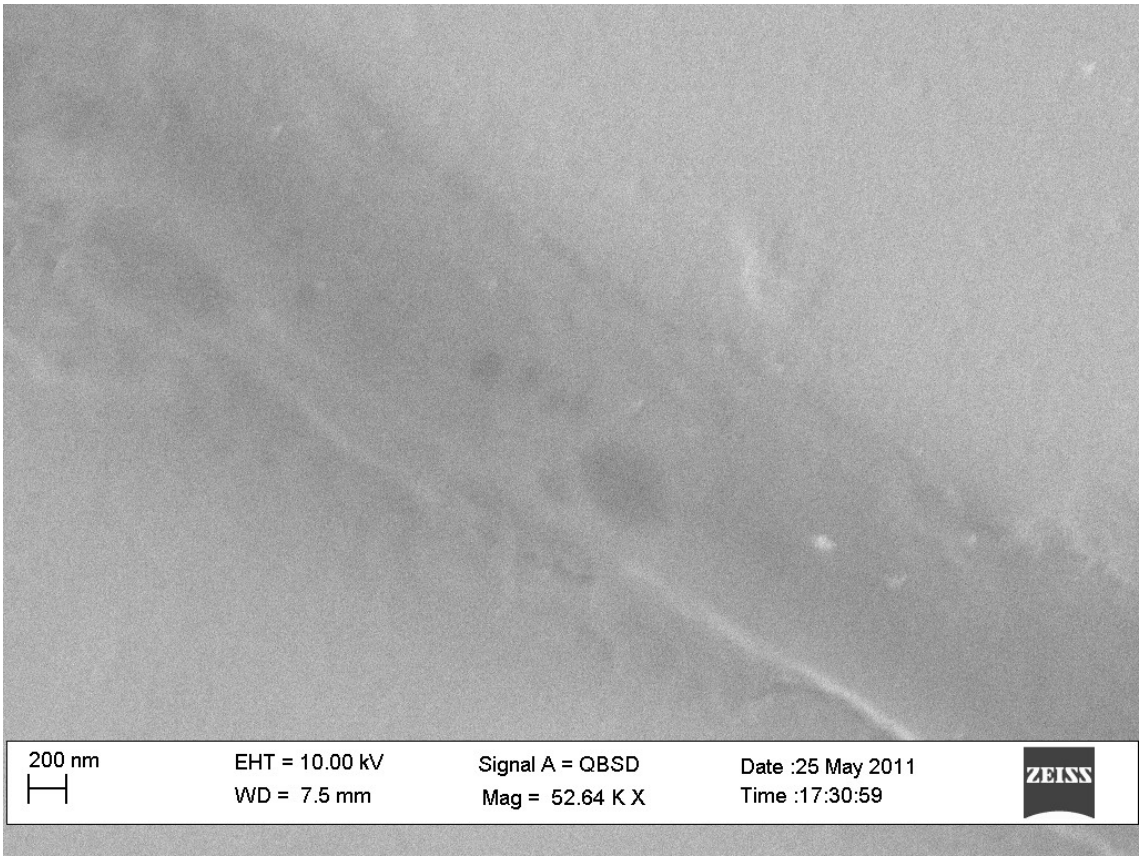
200 nm
EHT = 10.00 kV
WD = 7.5 mm
Signal A = QBSD
Mag = 52.64 K X
Date :25 May 2011
Time :17:30:59
ZEISS

B.

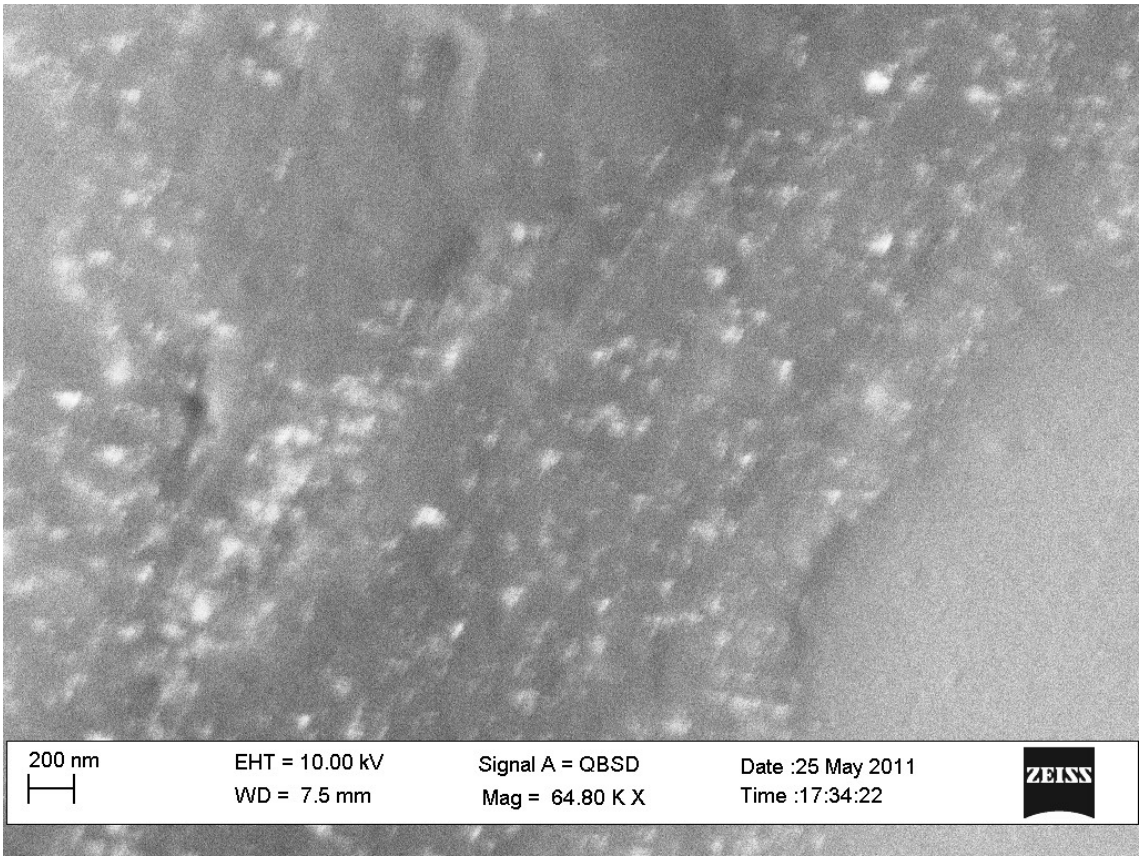
200 nm
EHT = 10.00 kV
WD = 7.5 mm
Signal A = QBSD
Mag = 64.80 K X
Date :25 May 2011
Time :17:34:22
ZEISS

C.

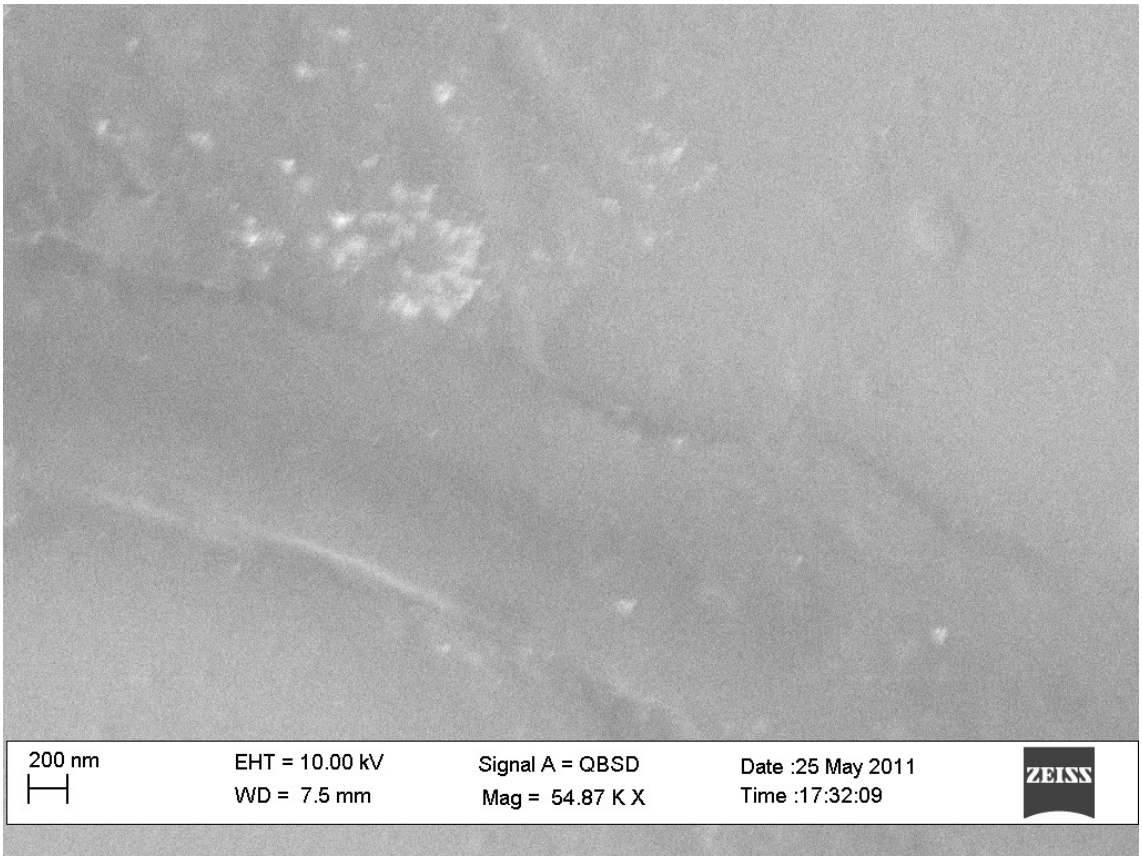

D.

Figure 3-7 CTB staining with gold particles on DRG neuron culture. CTB staining for GM1 shows very efficient labelling in some areas of neuronal membrane in A and C, but only moderate labelling for GM1 on some neurites as seen in B and D.

Some areas of neuronal membrane showed abundant labelling with CBT, whilst other showed minimal labelling, even on the same cell, Figure 3-7(D). High density labelling can be seen in a lower magnification image of a cell body and neurite, Figure 3-7(A), as the high intensity. However, lower intensities would not be visible at lower magnifications and so are harder to find on a sample. More disperse labelling can be seen in Figure 3-7(B).

3.3.1.2 Distribution of lipid raft marker proteins

Lipid rafts are thought make a minority of the total membrane surface area in most cells. Therefore the proteins used to mark for them would be expected to be mainly confined to only certain areas of the membrane corresponding to rafts. The size of these areas could vary considerably in accordance with the large variability in the size

of lipid rafts, from as small as patches 50 nm across to hundreds of nm and even larger for aggregations of rafts.

Spatial distribution of gold particles labelling for lipid raft marker proteins was analysed using ImageJ and the Spatial statistics 2D/3D tool from the 3D ImageJ Suite plugin, (Andrey et al. 2010).

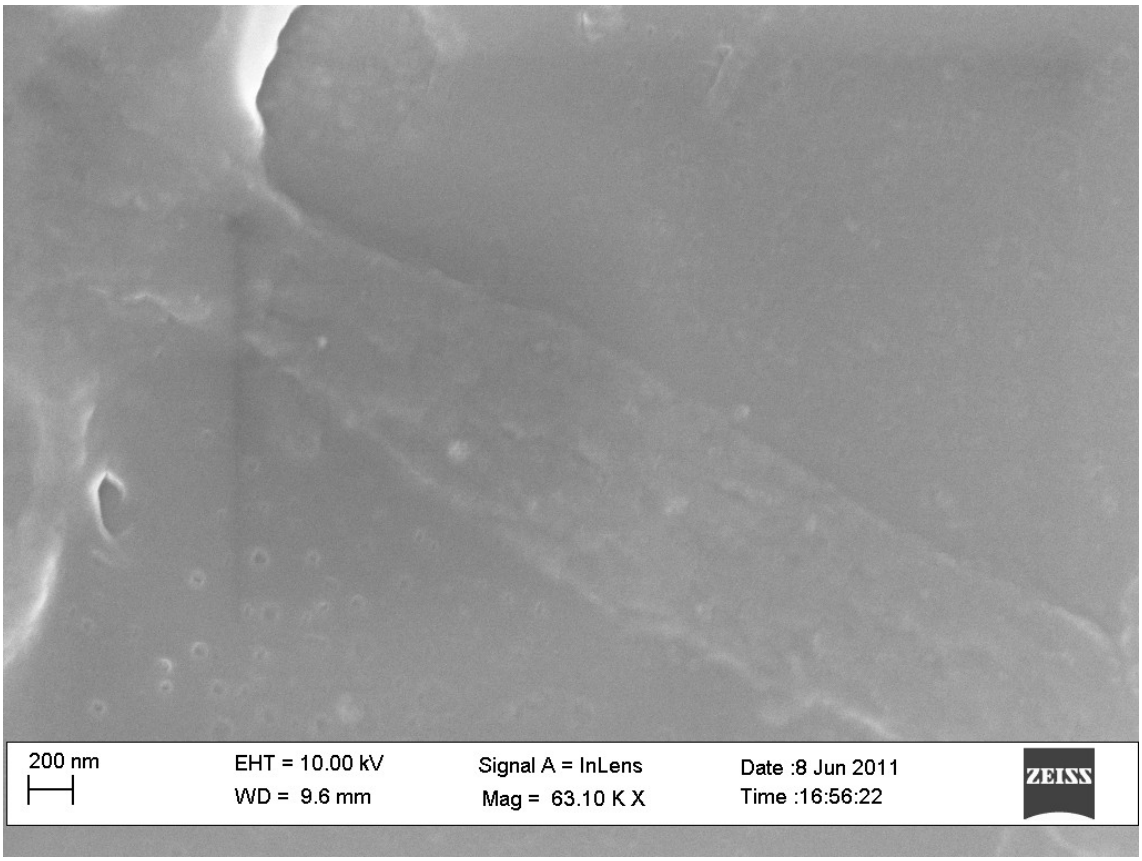

A.

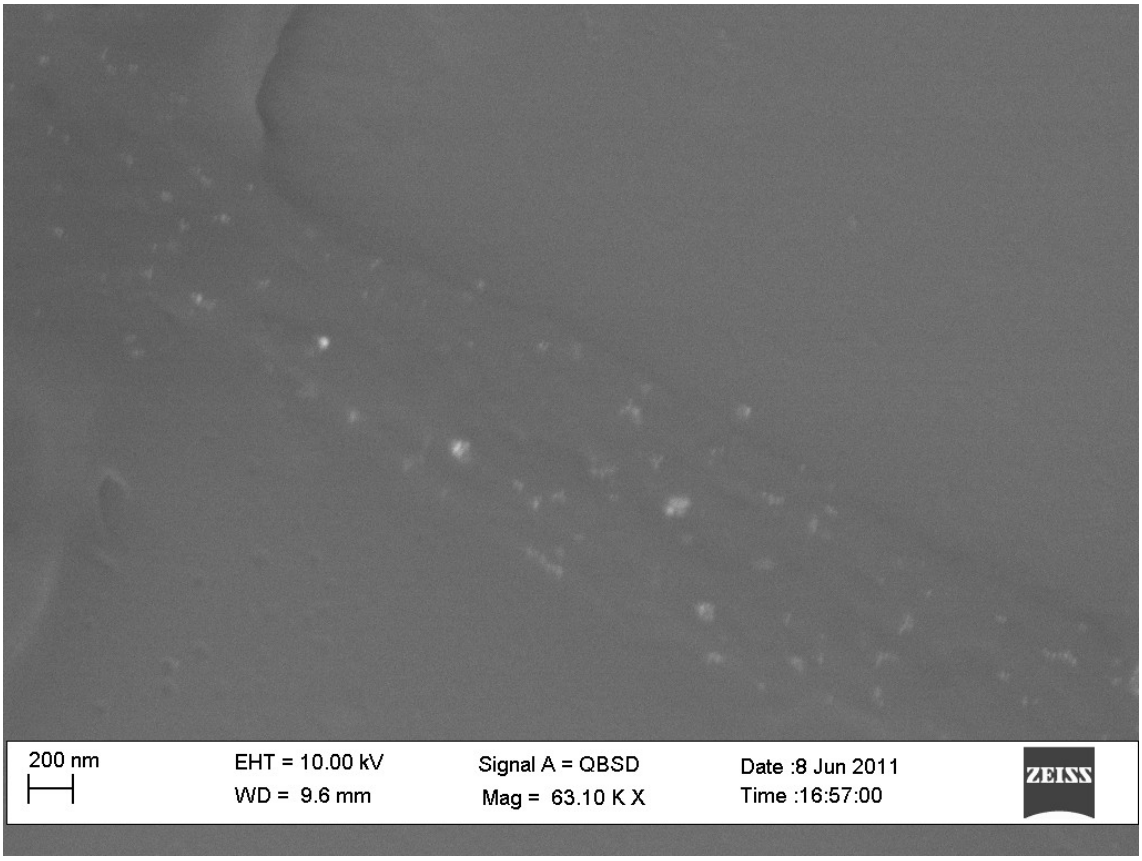
200 nm
EHT = 10.00 kV
WD = 9.6 mm
Signal A = QBSD
Mag = 63.10 K X
Date :8 Jun 2011
Time :16:57:00
ZEISS

B.

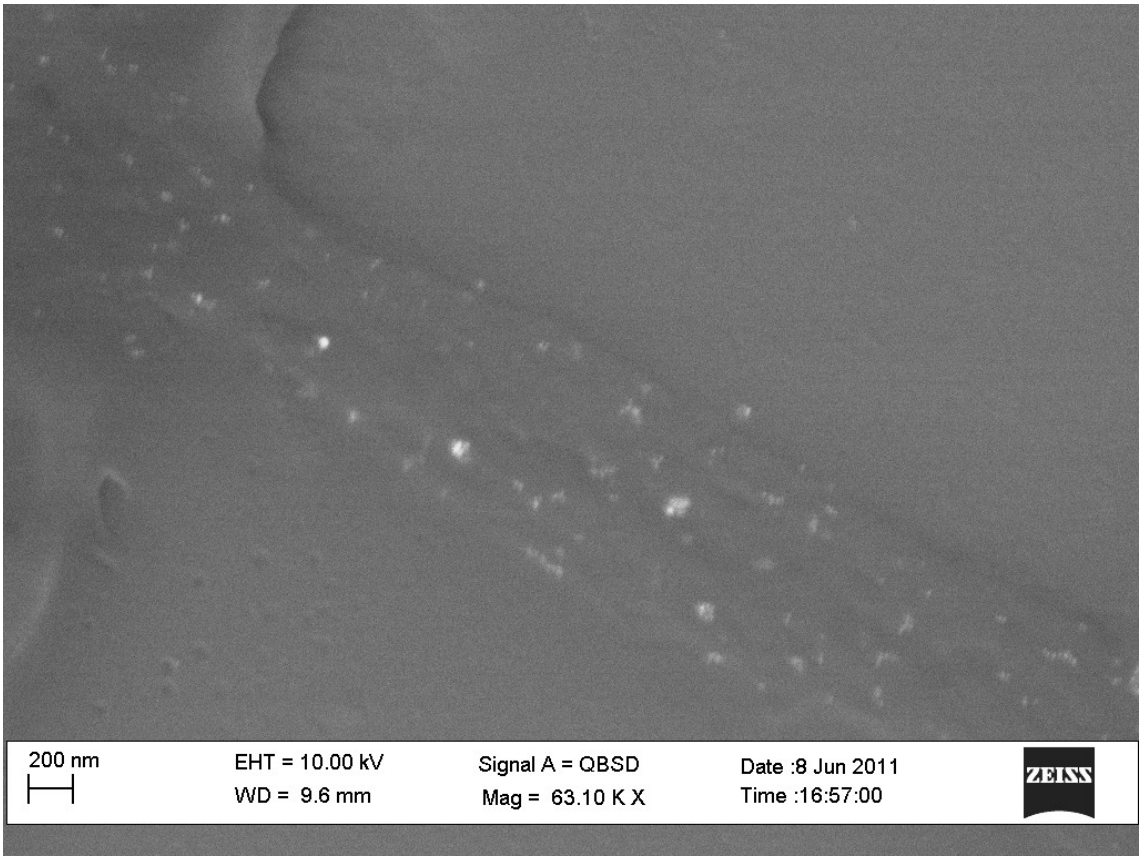
200 nm
EHT = 10.00 kV
WD = 9.6 mm
Signal A = QBSD
Mag = 63.10 K X
Date :8 Jun 2011
Time :16:57:00
ZEISS

C.

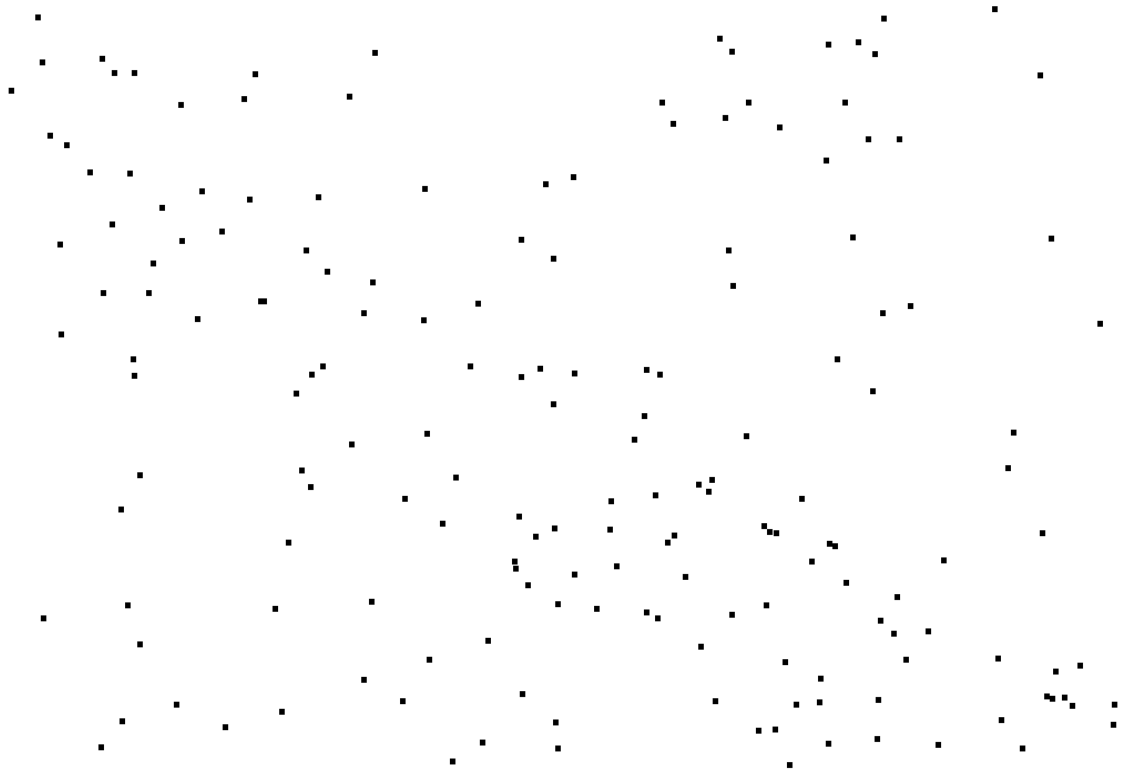

D.

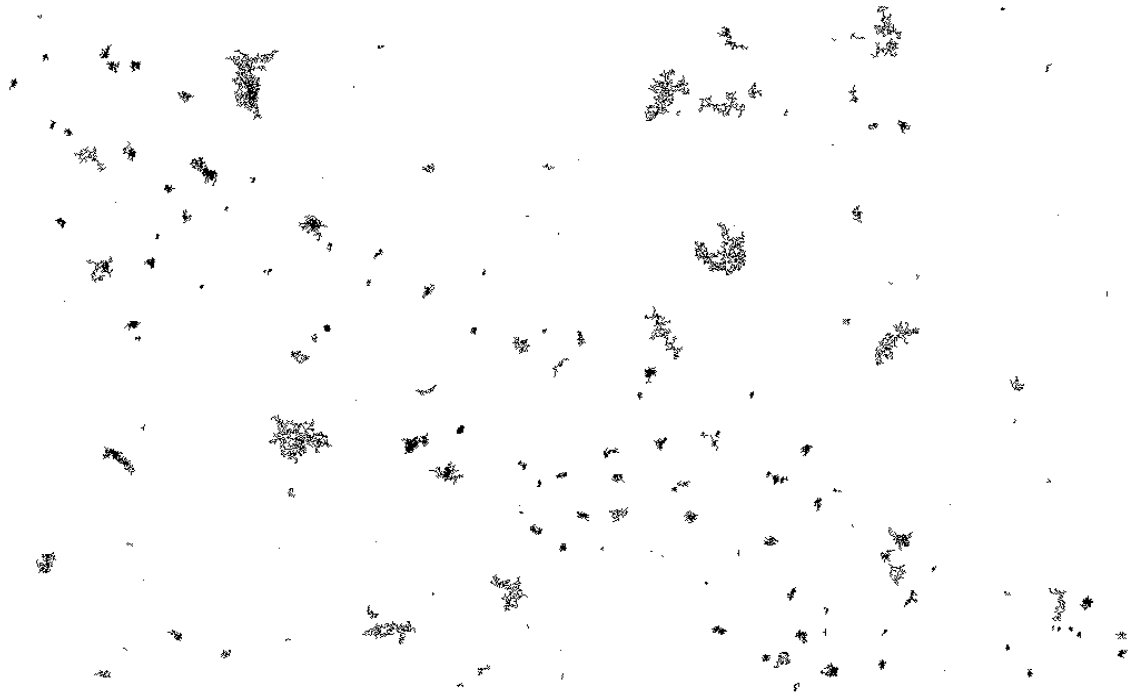

E.

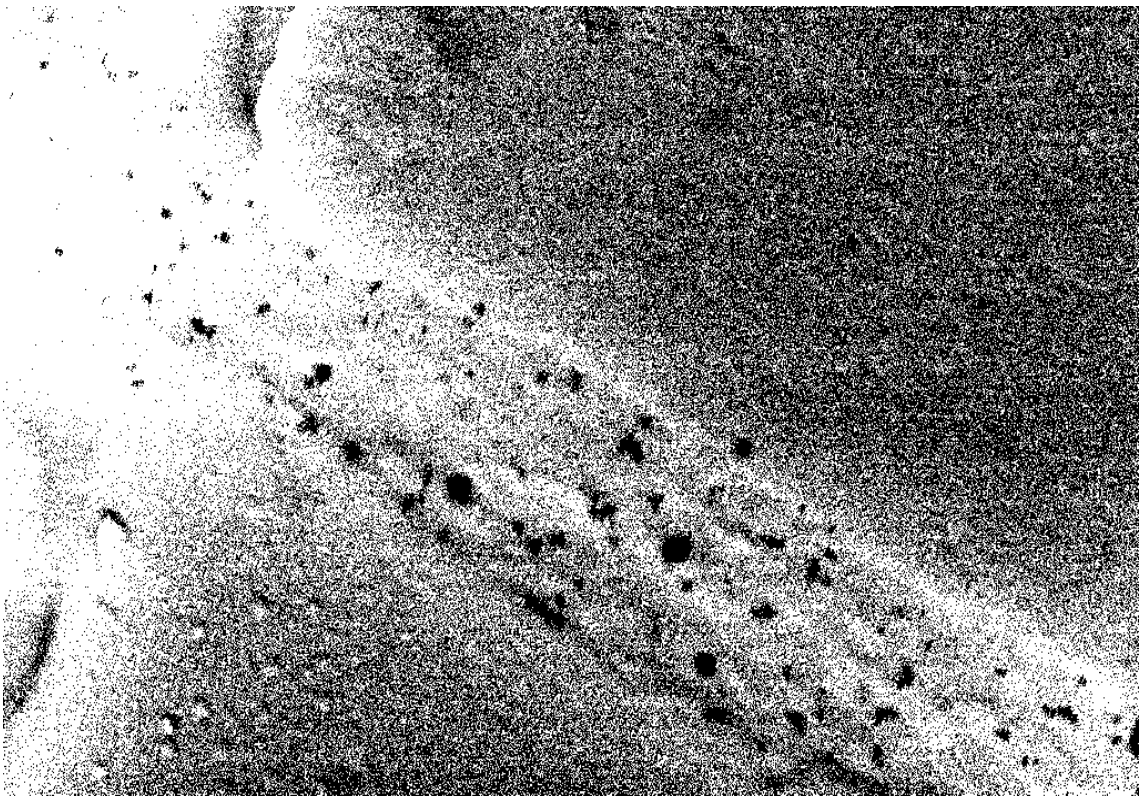

F.

Figure 3-8 Cultured DRG neurite labelled for GM1 using CTB and 40nm Gold particles. Different image processing techniques for analysis the distribution of particles. A. The SE image showing the surface morphology of the neurite and the region of the cell body from which it emerges. B The BSE signal showing the labelling of the lipid raft marker protein GM1 as white particles mainly localised to the surface of the neurite. C. Autocorrected version of B which enhances the signal from the labelling. D. The maxima extracted from C using imageJ. The maxima correspond well the labelling seen in B and C. E. Another way of viewing the maxima from imageJ, this time giving all the points within each supra-threshold region rather than just the brightest as given in D. F Threshold image of C given by imageJ, using the moments cut off. This method enable the size of the particles to be more easily analysed, although also contains considerable noise.

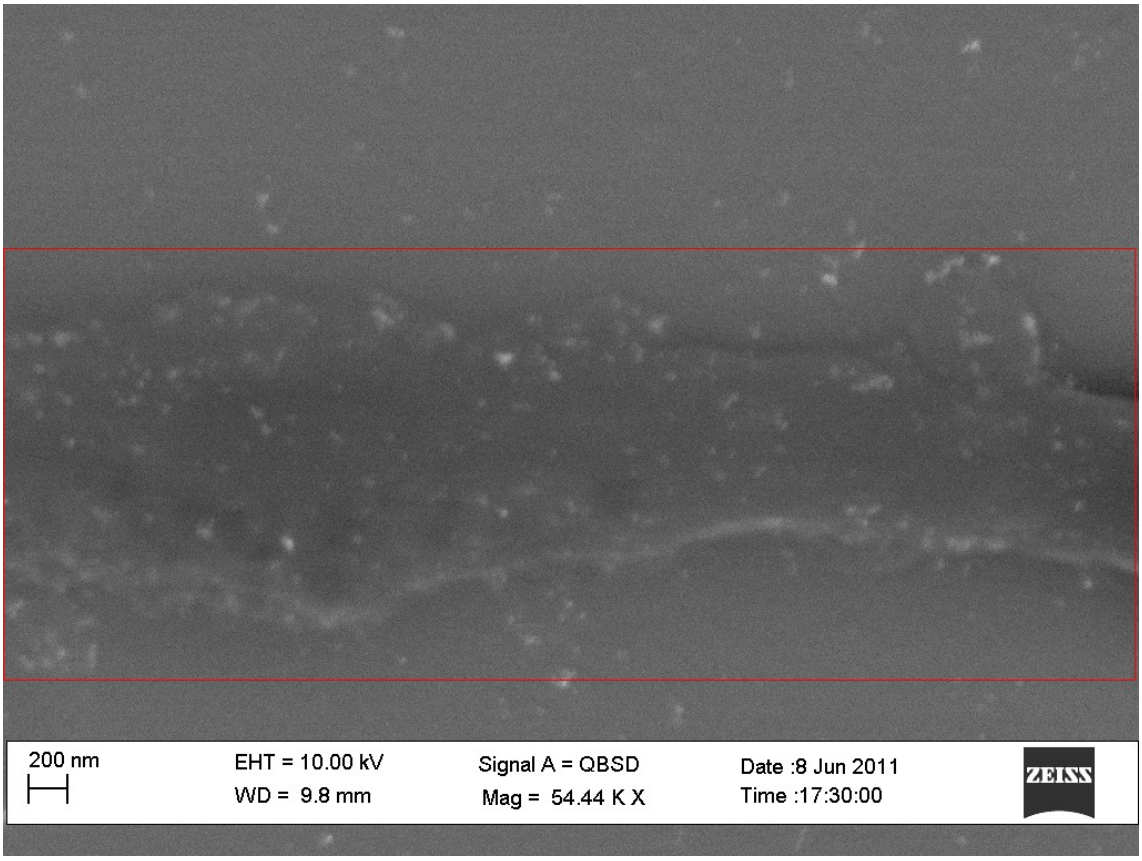
200 nm
EHT = 10.00 kV
WD = 9.8 mm
Signal A = QBSD
Mag = 54.44 K X
Date :8 Jun 2011
Time :17:30:00
ZEISS

A.

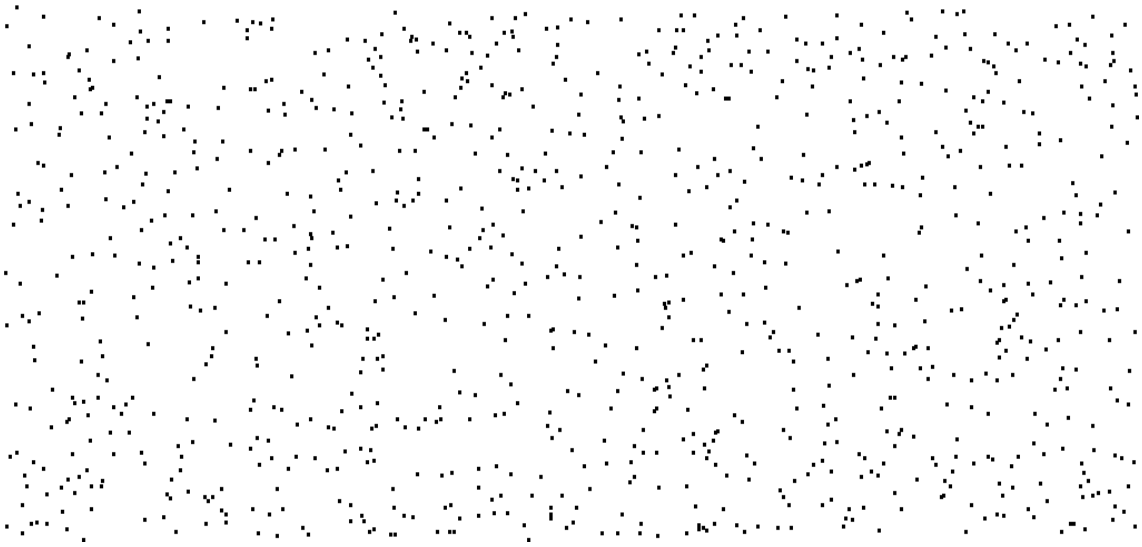

B.

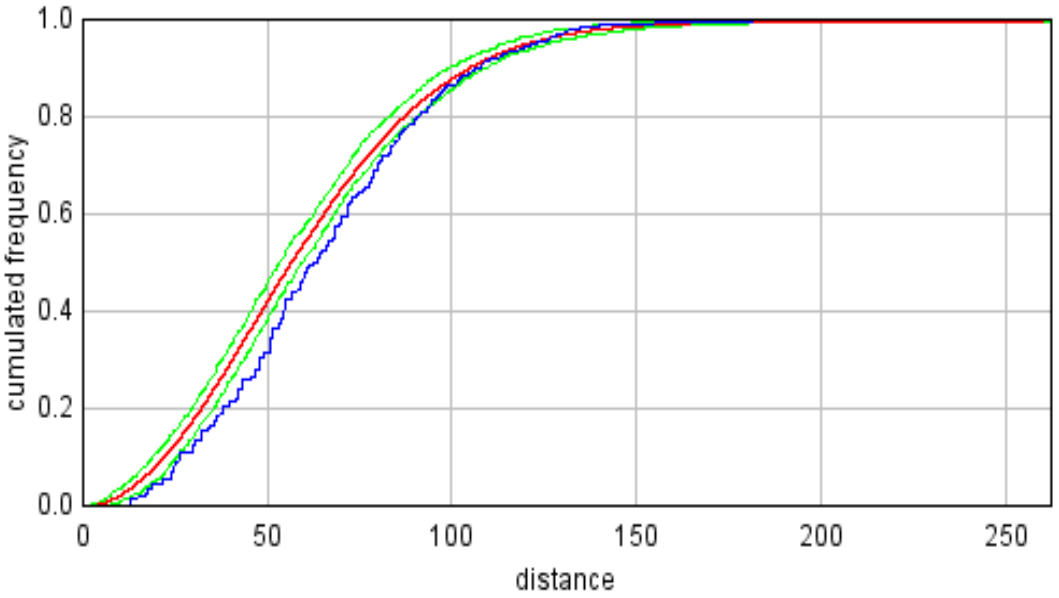

C.

Figure 3-9 Distribution of CTB labelling for GM1 on cultured DRG neuron treated with MBCD. A. BSE signal of a small diameter neurite showing labelling with 40 nm gold particles for GM1, selection shown in red is used for analysing the distribution of particles. B. The maxima from the area cropped in red from A. C. Graph of the G distance function based on the maxima shown in B. The blue line shows the G function for the sample. The red line shows the average G function for randomly distributed particles, with the green lines either side showing the 5% confidence interval for the average. To the right of the line indicates particles are more evenly spaced than a random distribution. The distances are in nm. The sample is evenly distributed outside of the to 95% confidence for distances between 25nm and 90nm.

Thy1 was labelled using gold particles conjugated to secondary antibodies following primary anti-body treatment. Both individual gold particles and clusters of particles were visible on neurites. Clustering was apparent on two scales. Small dense clusters consist of a few labelling gold particles immediately adjacent to each other, with the appearance of a large particle. Larger clusters consist of individual and tight clusters all in one area of membrane.

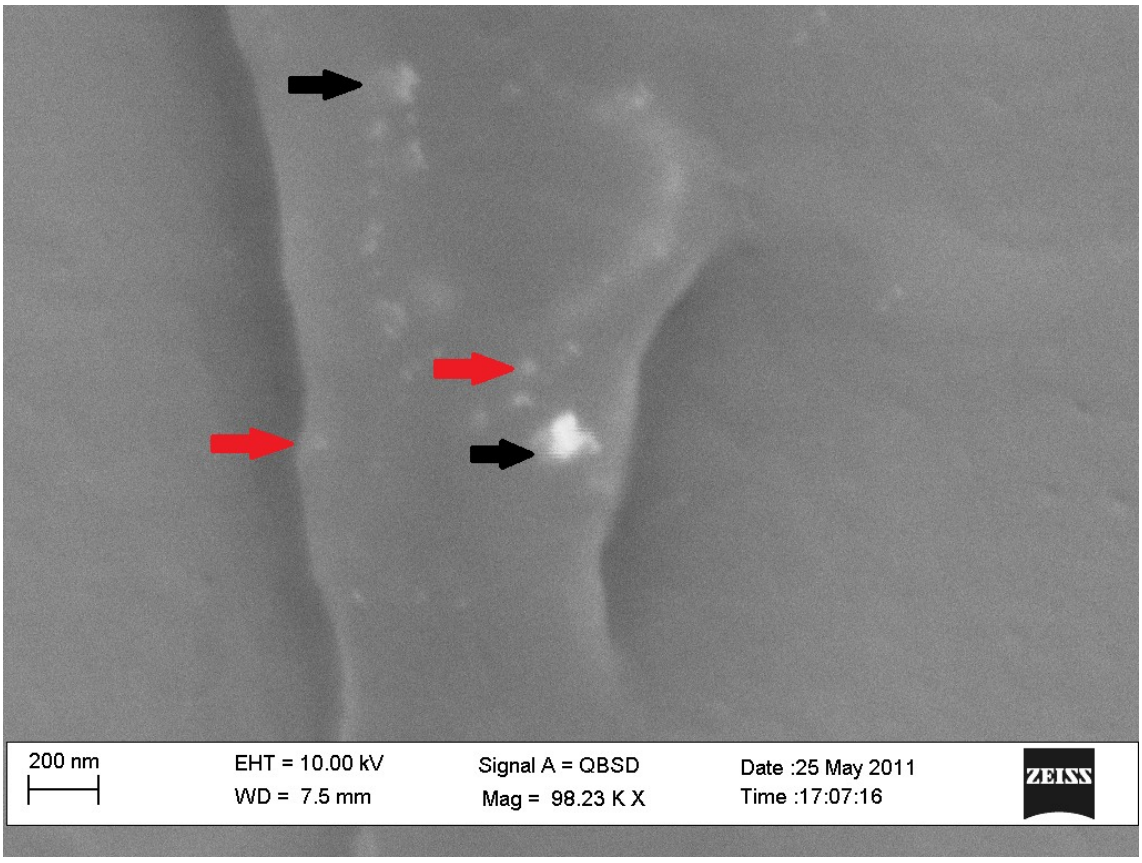

A.

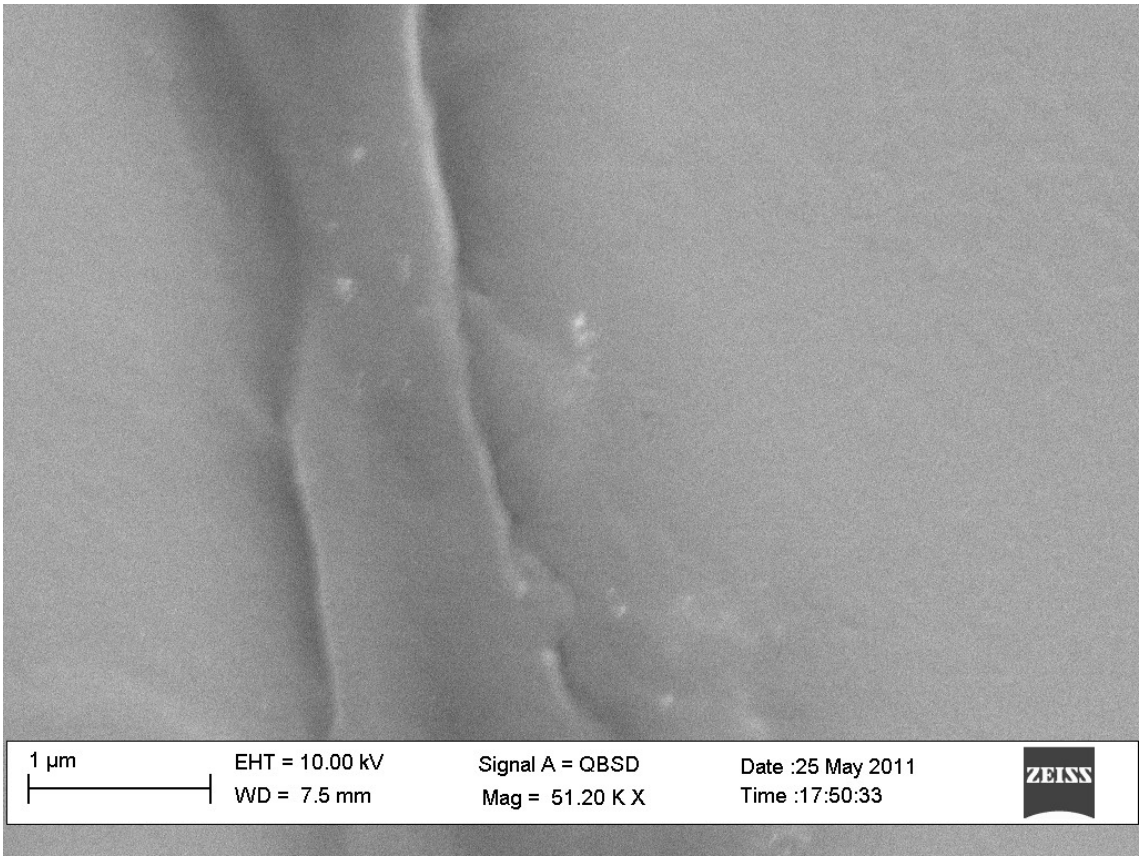
1 µm
EHT = 10.00 kV
WD = 7.5 mm
Signal A = QBSD
Mag = 51.20 K X
Date :25 May 2011
Time :17:50:33
ZEISS

B.

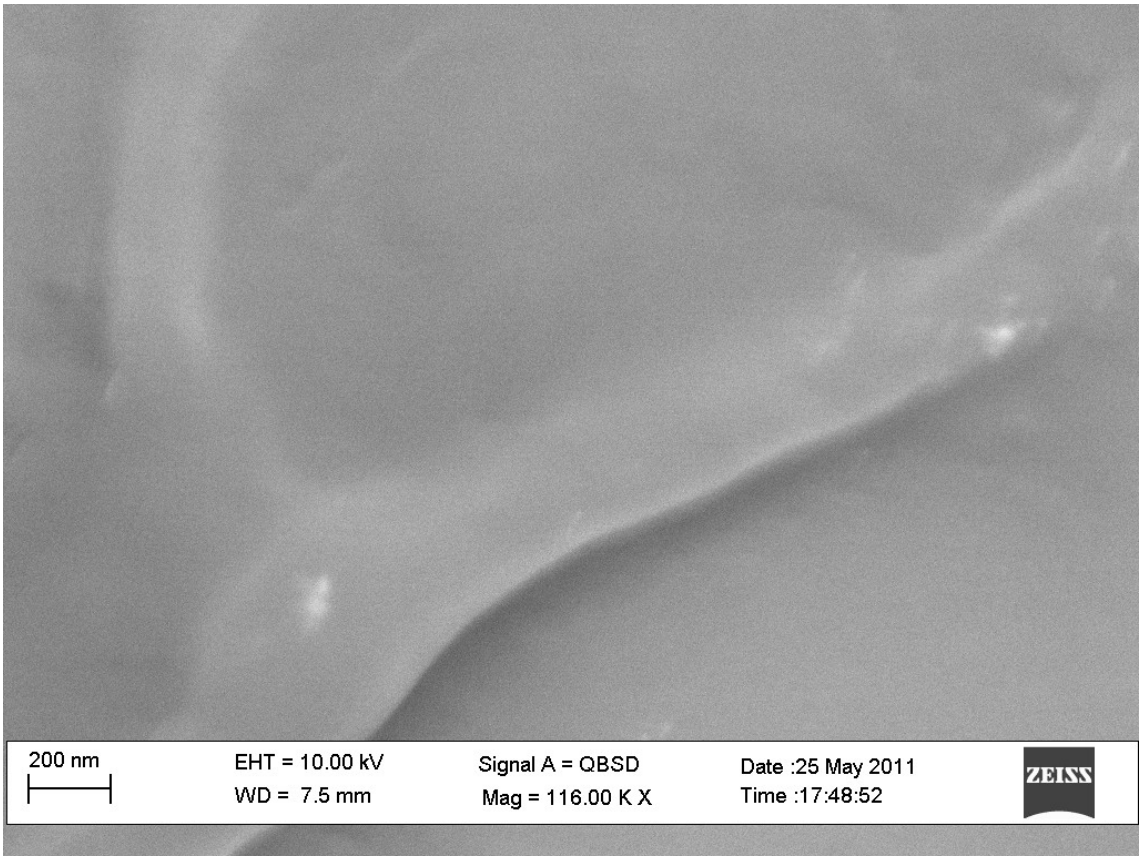

C.

Figure 3-10 Thy1 labelling with gold particles on DRG neuron culture. A. Region of a neurites showing labelling the size of single particles (black arrows) and clusters of particle (red arrows). B. Gold labelling of Thy1 on a neurite and on membrane extended to the side of the neurite. C. Two clusters of labelled Thy1 (red arrows) along the length of a neurite.

Where neurites are well labelled GM1 appears to form small clusters as well as individual proteins labelled which a spatially separated from other labelled proteins. On the larger scale the distribution is fairly uniform. The marker Thy1 is also found labelled on the surface of the neurites of DRG neurons. It is distributed in both small and large scale clusters. The small clusters are similar in size to that of lipid rafts postulated by other investigations, with diameters of up to 200nm (Pike 2003). The larger clusters, which contain both smaller clusters and individually labelled proteins and which may be visible using light microscopy, could correspond to clustering previously reported in DRG neurons (Pristerà et al. 2012).

3.3.1.3 $Na_V1.8$ labelling on DRG neurites

$Na_V1.8$ was labelled on the surface of DRG cells by 40 nm gold particles, Figure 3-11. Labelling was very restricted for $Na_V1.8$. Only 5 images were captured showing any labelling. Where gold labelling was observed there were patches the correct size for individual particles. Labelling was observed on one neurite, which was 200-500 nm wide, over a distance of 1400 nm that consisted of at least 7 particles, some of which appear to be larger than a single gold particle, Figure 3-11(A). This is similar to the larger clusters observed with Thy1 staining, Figure 3-10A. The distribution of of particles labelled was analysed using imageJ and the 2D/3D spatial statics plugin. The pattern of points for analysis was extracted using the imageJ maxima tool, to give roughly the same number as estimated by eye, shown in Figure 3-11(B). The outline of the membrane in the image was used to give the boundary for the possible distribution of particles. The nearest neighbour cumulative distribution function (CDF) was measured from the pattern, this is refered to as the G-function, and compared to the case of completely randomly distributed particles and the 5% confidence interval. This is shown for the most clear example of gold labelling in Figure 3-11(E). The sample G-function starts below and to the right of the random distribution, indicating an evenly distributed pattern of particles on scales below 300 nm. The sample then rapidly increases and continues above the random distribution, indicating a clustering of particles with around 300-500 nm seperations. However, the sample distribution

remains within the 5% confidence interval boundaries showing that these variations are not statisically significant and could be due purely to random positioning.

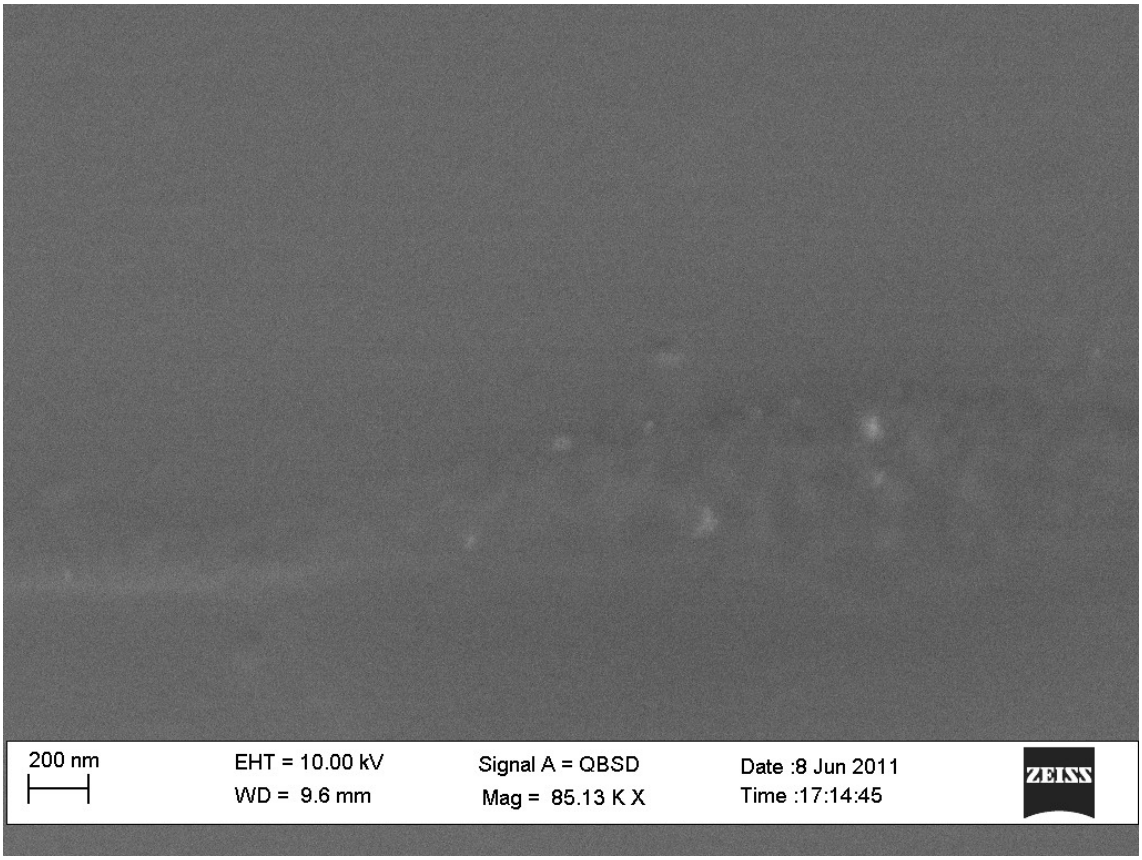

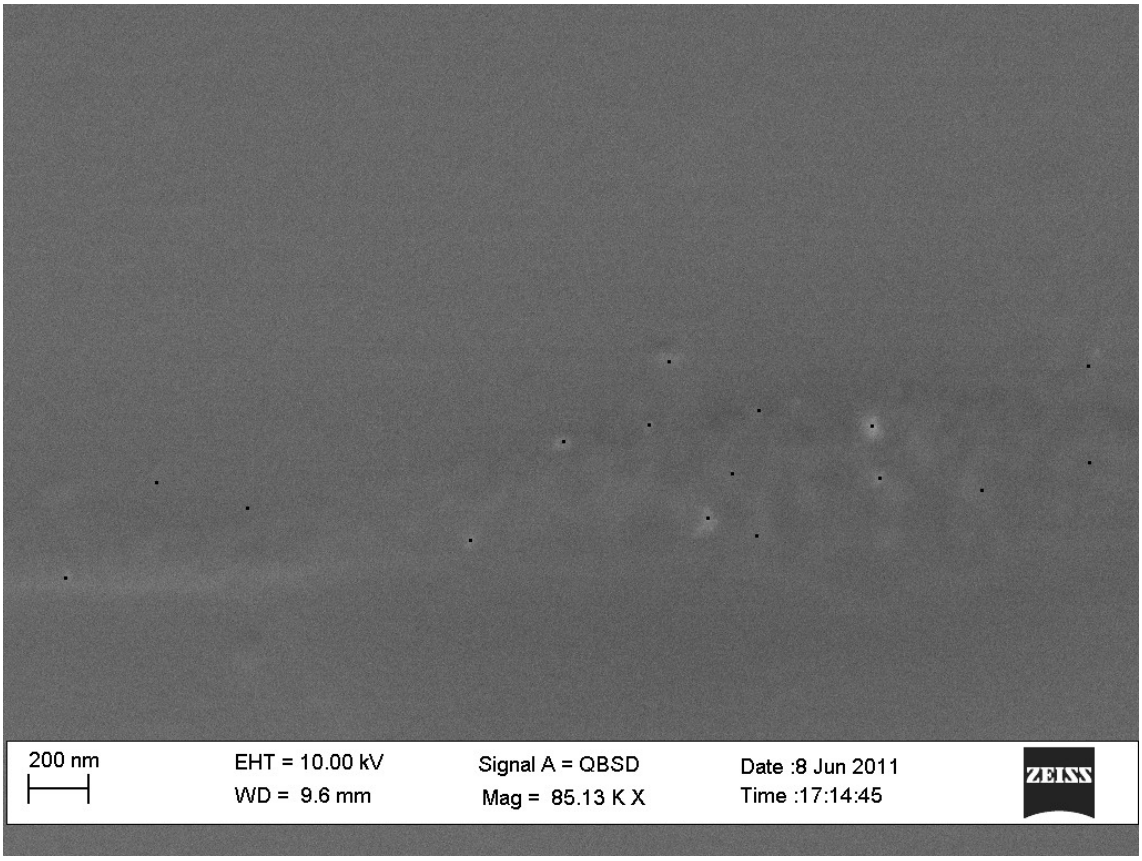
200 nm
EHT = 10.00 kV
WD = 9.6 mm
Signal A = QBSD
Mag = 85.13 K X
Date :8 Jun 2011
Time :17:14:45
ZEISS

B.

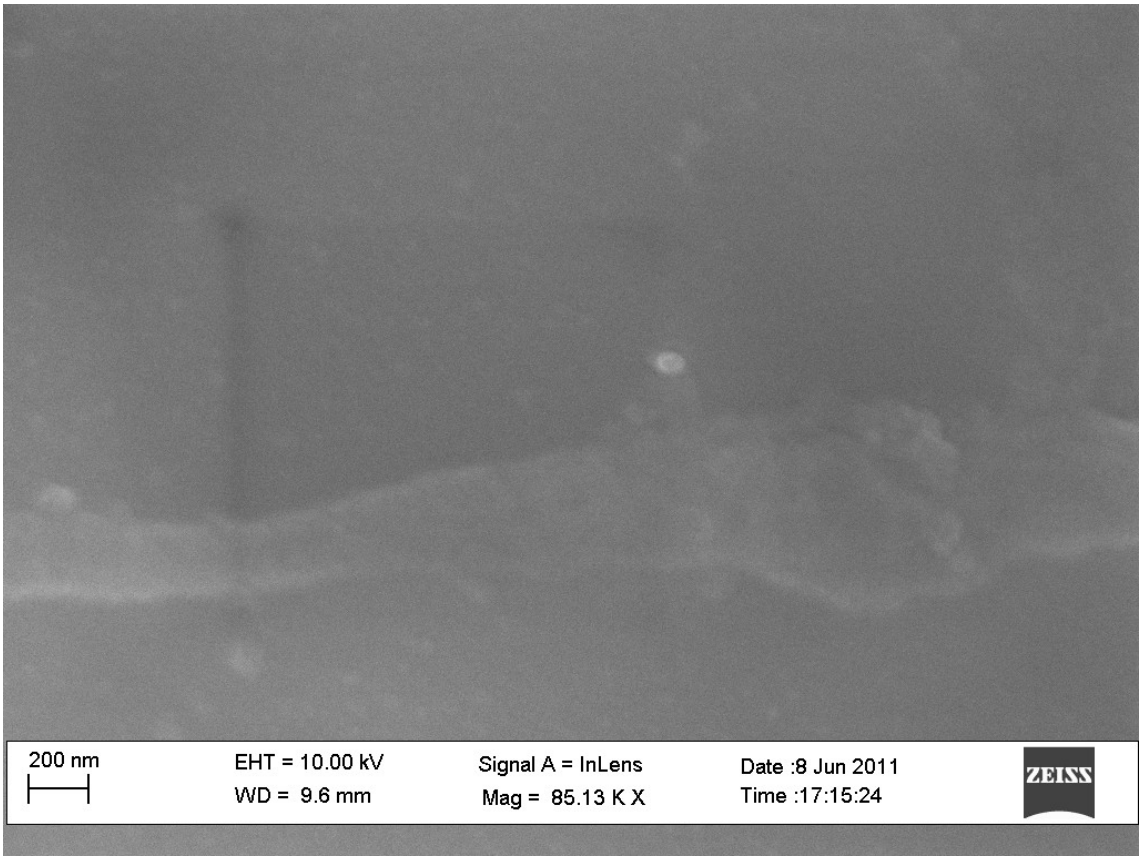
200 nm
EHT = 10.00 kV
WD = 9.6 mm
Signal A = InLens
Mag = 85.13 K X
Date :8 Jun 2011
Time :17:15:24
ZEISS

C.

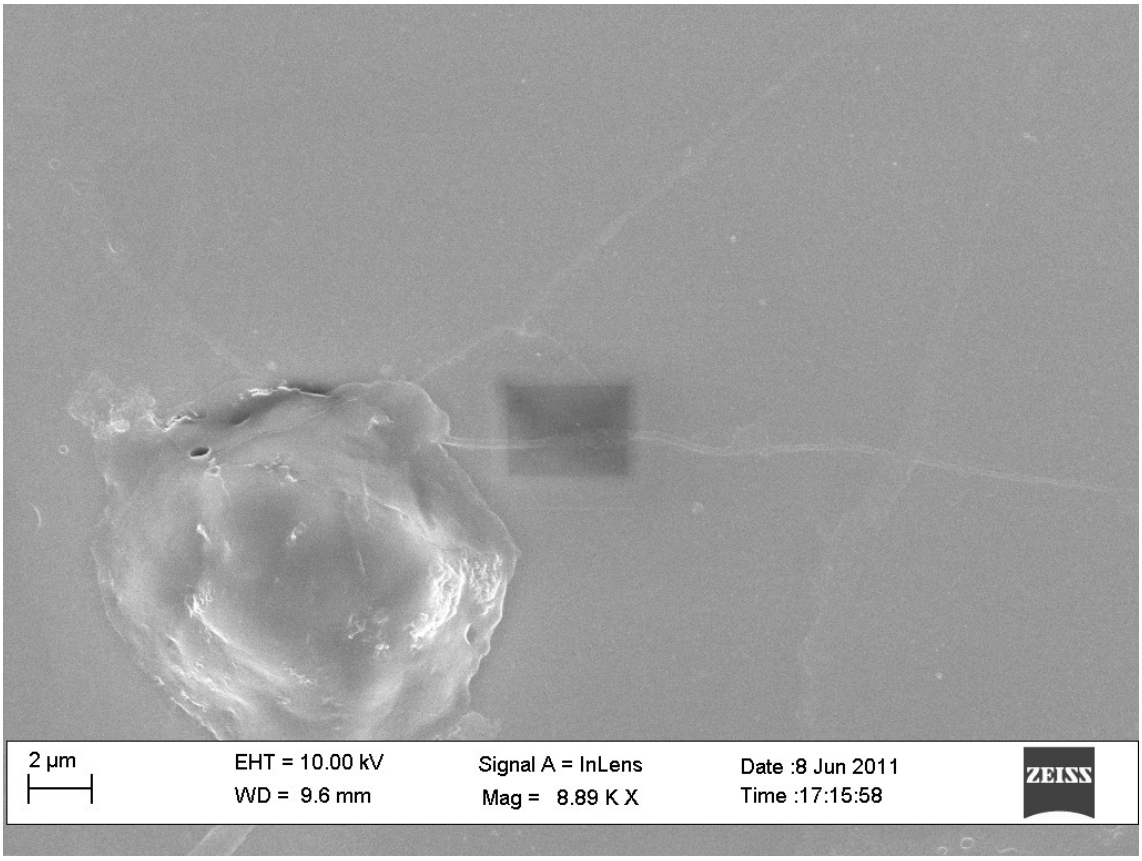

D.

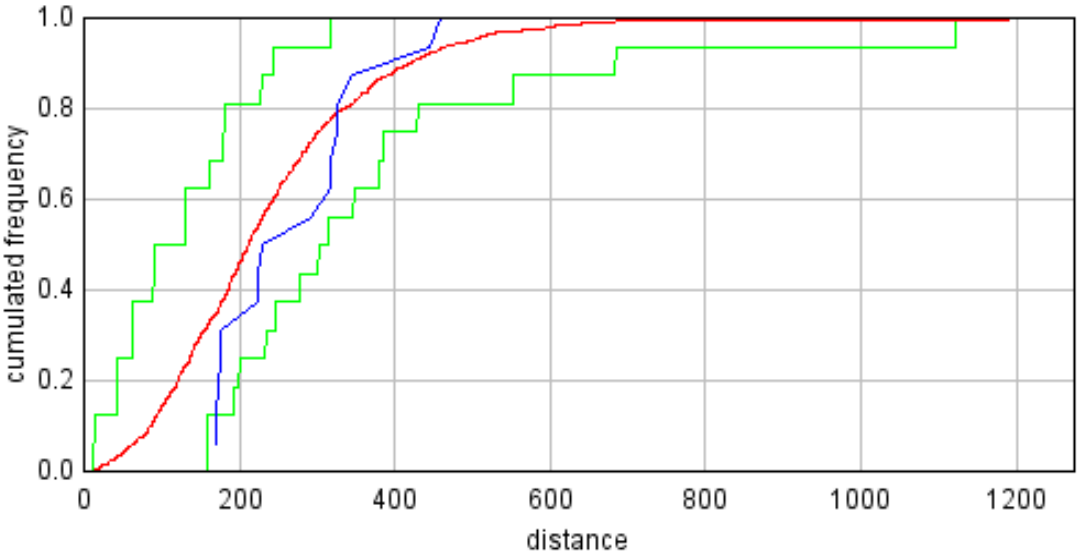

Figure 3-11 $Na_V1.8$ labelled with gold particle imaged using SEM. A. Backscatter signal shows labelling of $Na_V1.8$ using 40 nm diameter gold particles. B. Black points show the maxima found using ImageJ from the image in A. C. Secondary electron signal for the same areas as A, showing neurite morphology. D. Secondary electron signal showing the whole cell. Shaded area is areas shown in A, B and C.

3.3.1.4 Effect of lipid raft disruption on protein distribution

Less gold labelling for NaV1.8 was observed on treated samples than in untreated ones, 6 labels for 3 images combined as apposed 13 labels for 3 images combined. Due to the general low observation of labelling it is unclear whether this represented any real difference. Gold labelling for GM1 showed no marked difference in the distribution in cultures treated with MBCD compared with untreated cultures, Figure 3.10. On MBCD treated cultures gold labelling was observed on the surface of the plate, where there was no apparent cell membrane. This was observed near some labelled neurites but not others and was not seen in the untreated samples. This is mostly likely due to labelling adhering to the laminin coating of the glass slip. Although it could be due to fragments of membrane remaining on the surface of the coverslip where there had previously been membrane. MBCD is generally thought not to disrupt the integrity of the entire membrane. However, combined with subsequent treatment with PFA for fixation damage to the morphology of the membrane may be caused. Alternatively, MBCD may cause release of lipid raft marker proteins from the cell membrane, which could subsequently become attached to the poly-L-Lysine and Laminin coating of the coverslips.

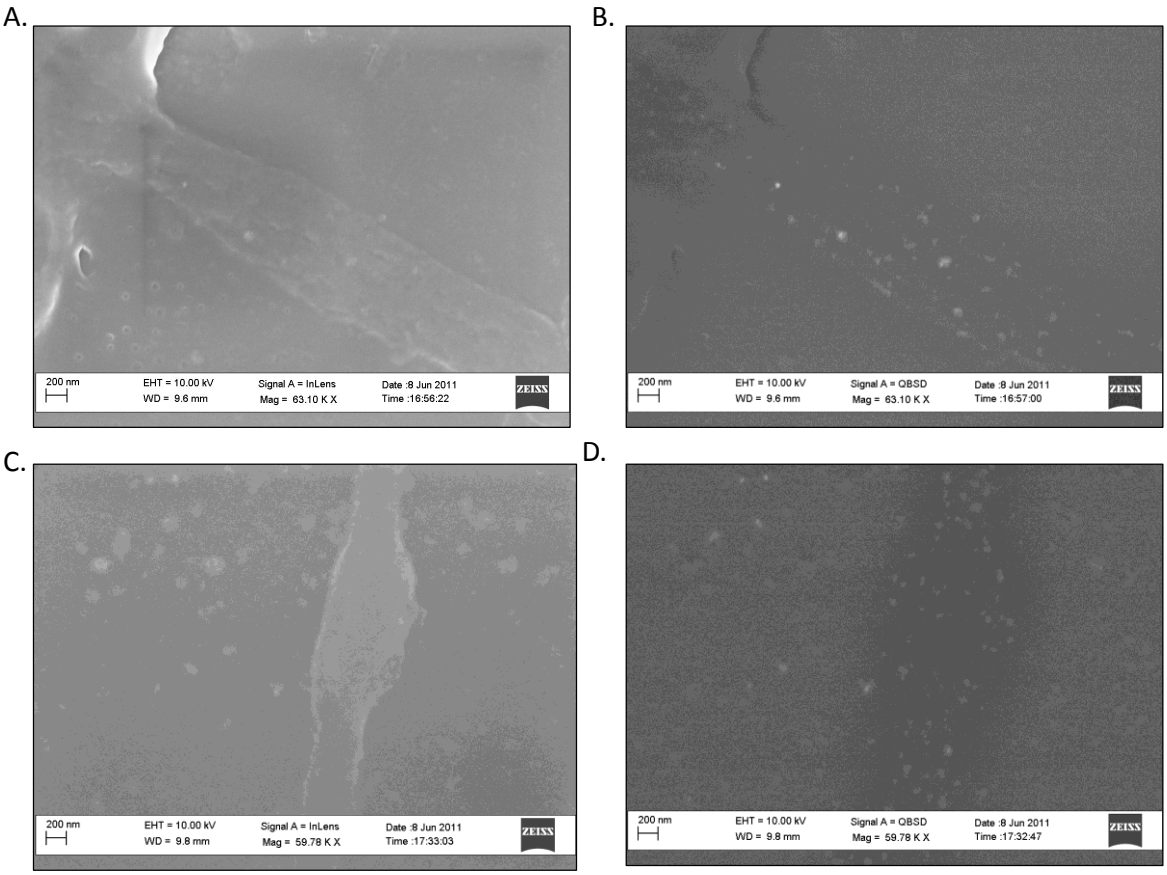

Figure 3-12 CTB staining with gold particles A. and B.Untreated, C. and D. Treated with MBCD. A and C secondary electron signal, B and D BSE signal.

To quantify the distribution of the proteins in the images taken they were analysed with the imageJ plugin 2D/3D spatial statistics. In total 8 GM1 untreated, 4 GM1 MBCD treated, 5 Thy1 untreated and 4 Thy1 MBCD treated images were analysed. The analysis consisted of finding the maxima using imageJ, defining the area of cell membrane in the image and then running the analysis of the distribution of particles. Two cumulative distance functions (CDF) were found for each sample. One was the nearest neighbour CDF, the G function, and the other the point event CDF, the F function. These were then compared to the case of the same number of randomly distribute within the area defined. A random distribution would produce values from 0 to 1 with the expected average of a number of images to be 0.5. The average values of the F and G function for the different conditions is given in Figure 3-13. For a clustered distribution of particles a consistently high value of the F function and a low value of

the G function would be expected. Exactly the reverse is true in this case. This leads to the conclusion that the distribution is more ordered than a random distribution. All conditions on average showed distributions which are statistically significantly different from random. The only exception was Thy1, in the condition without lipid raft disruption. In this case it appears to be due to outliers showing a more clustered distribution and lack of observed areas of labelling for analysis. The distribution observed may be due to method of labelling and analysis making clusters difficult to detect or the presence of an underlying mechanism keeping particles distributed in an ordered fashion.

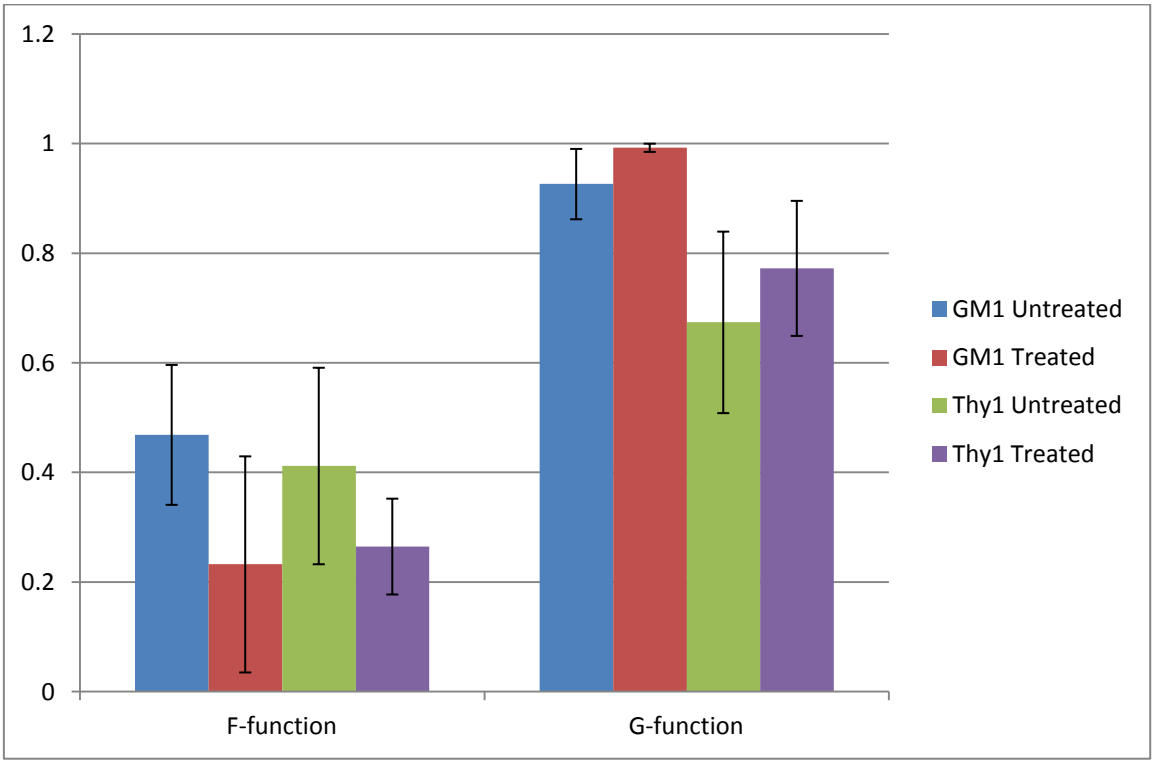

Figure 3-13 Cumulative distance function averages for the any point to nearest labelled protein (F-function) and distance to nearest neighbour (G-function). If labels were completely randomly distributed points would give functions uniformly distributed between 0 and 1 and therefore an average of 0.5 would be expected. Low values of the F-function and high values of the G-function imply evenly distributed labelling (more ordered than completely random). Errors bars show the standard error of the average from the multiple measurements made. The high G-function values imply lipid raft markers observed are arranged in a regular manner. The number of

analysed images for each condition were; GM1 untreated: 8, GM1 treated: 4, Thy1 Untreated: 5, Thy1 Treated: 4.

3.3.2 Investigation of Protein Separation Distance using FRET

In order to investigate protein clustering using FRET, 4 constructs were created to be transfected into cells. These consisted of 2 pairs; Flotillin-mCherry (red fluorescence) and Flotillin-GFP, and $Na_V1.8$-mCherry and $Na_V1.8$-GFP. The Flotillin pair were cloned, to test whether FRET signals could be measured due to the clustering of established lipid raft proteins and ablated by lipid raft disruption. To test for clustering of $Na_V1.8$, the GFP and mCherry conjugated constructs were cloned. The clones were inserted into the plasmid PCDNA3.1+, which was used to transfect them into cells. FRET measurements were taken using confocal microscopy and the sensitised emission method, .

3.3.2.1 HEK cells transfected with Flotillin constructs

Cells from the immortal cell line HEK were plated at a density of 150,000 cells on 35 mm glass bottom dishes. They were transfected with 0.6 µg of one or both DNA constructs with 1.5 µl Lipofectamine 2000 (Invitrogen). For imaging the media was replaced with normal media. For FRET measurements the sensitised acceptor emission method was used. Measurements were taken using a Leica SP5 MP inverted microscope at 37 ^{O}C. Flotillin-GFP was excited with a laser at 488 nm and Flotillin mCherry was excited with a laser at 543 nm. Green fluorescent emission was measured from 500-550nm and red fluorescent emission was measured at 576-657 nm.

Flotillin-GFP and Flotillin-mCherry, green and red fluorescences were initially excited separately at 488 nm and 543 nm, with the corresponding fluorescence emission recorded using 500-550 nm and 576-657 nm filters, respectively. Subsequently, fluorescence was excited at 488 nm, with both green and red fluorescence emission recorded. The FRET experiment was repeated for co-transfected cells following 30 minute incubation in 7.5 mM methyl-β-cyclodextrin in Normal solution to disrupt lipid rafts. Image recording and analysis was performed using Leica Application Suite Advanced Fluorescence (LAS AF) software.

Flotillin constructs were expressed on the membrane of the cell body, and processes extending out from it, of cultured HEK cells, Figure 3-14**.** This expression appears unevenly on the membrane, possibly due to aggregated lipid rafts.

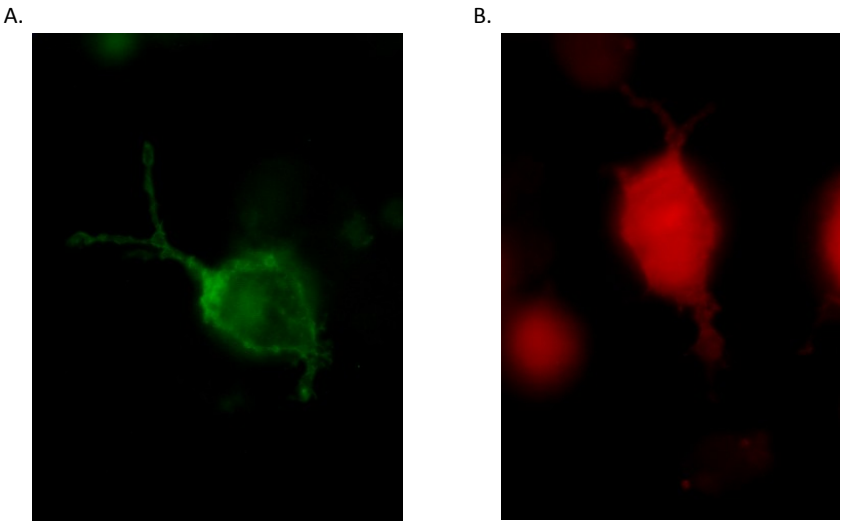

Figure 3-14 HEK cells transfected with fluorescent Flotillin constructs. A. Flotillin-GFP B. Flotillin-mCherry. The Flotillin construct is clearly expressed on the membrane and prominences of the cells.

The sensitised emission method measures the acceptor emission due to direct excitation by the donor. The red fluorescence measured upon exicitation in the GFP absorption spectra at 488 nm was normalised against direct excitation in the mCherry absorption spectra at 543 nm. When the donor (mCherry) is present in the double transfection samples excitation at 488 nm was higher than in the absence of the donor. This increase emission may result from FRET between the donor and acceptor due to Flotillin proteins coming into close proximity on the membrane of the cells. A possible source of error is the small amount of red light emitted directly from GFP, in other words the GFP emission spectra within the red fluorescence measurement range of 576-657 nm. The expected contribution of this can be estimated and corrected for

using the measurement of red fluorescence from the donor (GFP) in the absence of the acceptor mCherry. This is normalised against the emission in the green range of 500-550 nm.

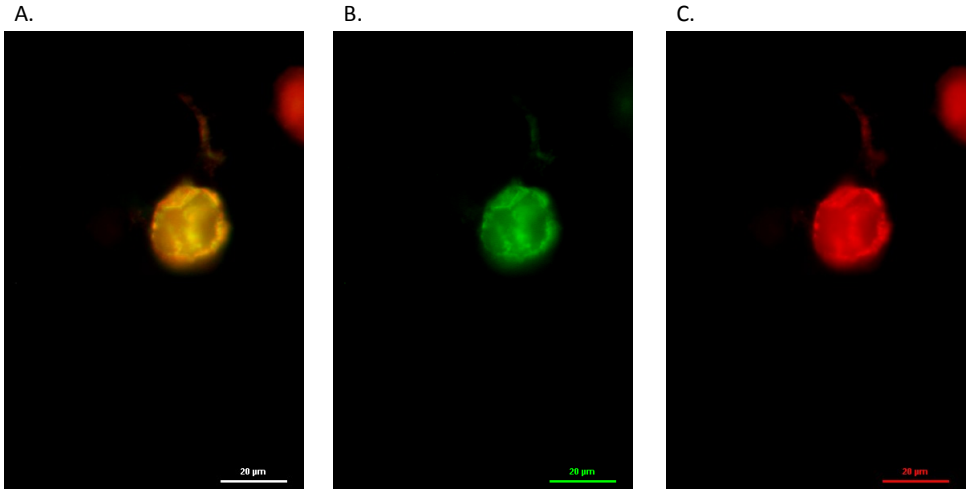

Figure 3.10 Co transfected Flotillin-GFP and Flotillin-mCherry in HEK cells. A. Merge showing both fluorescence from Flotillin-GFP and Flotillin-mCherry in the same cell. B. Green fluorescence from Flotillin-GFP. C. Red fluorescence from Flotillin-mCherry.

The FRET measurements resulting from the study are shown in Figure 3-15. The absolute fluorescence intensity measured at 543 when exciting in the absorption spectra of GFP is normalised against the red fluorescence at 543 with mCherry is directly excited. This normalise value is shown. For each condition multiple cells were measured and the values are all shown to give a sense of the spread. Alongside this the mean with the standard error is shown. As well as the normalisation the measurements were also corrected for the amount of fluorescence expected to be emitted from GFP where we measured in the emission spectra range of mCherry. Red fluorescence detected from Flotillin-mCherry was greater when in the presence of Flotillin-GFP than without. This may well be due to energy transfer when as the fluorfores are maintained at close proximity due to their containment in lipid rafts.

However the difference in fluorescence measure between this case and the in the absence of Flotillin-mCherry is not statistically significant and therefore may be purely due to small samples size. Doubly transfected cells were also measured following treatment with MBCD to try to disrupt lipid rafts in the live cell membranes. No significant difference between this and untreated cells was found. Although in this case the difference between the samples and untreated cells only transfected with Flotillin-mCherry was significant. As the disruption does not appear to have affected the degree of energy transfer occurring, it may be the case that the distribution of Flotillin is remaining the same after treatment with MBCD (at least within the remaining proportion). In this case the significant difference lends support to the fact that Flotillin proteins in the membrane are coming into very closely proximity as would be expected if they are constrained within lipid rafts.

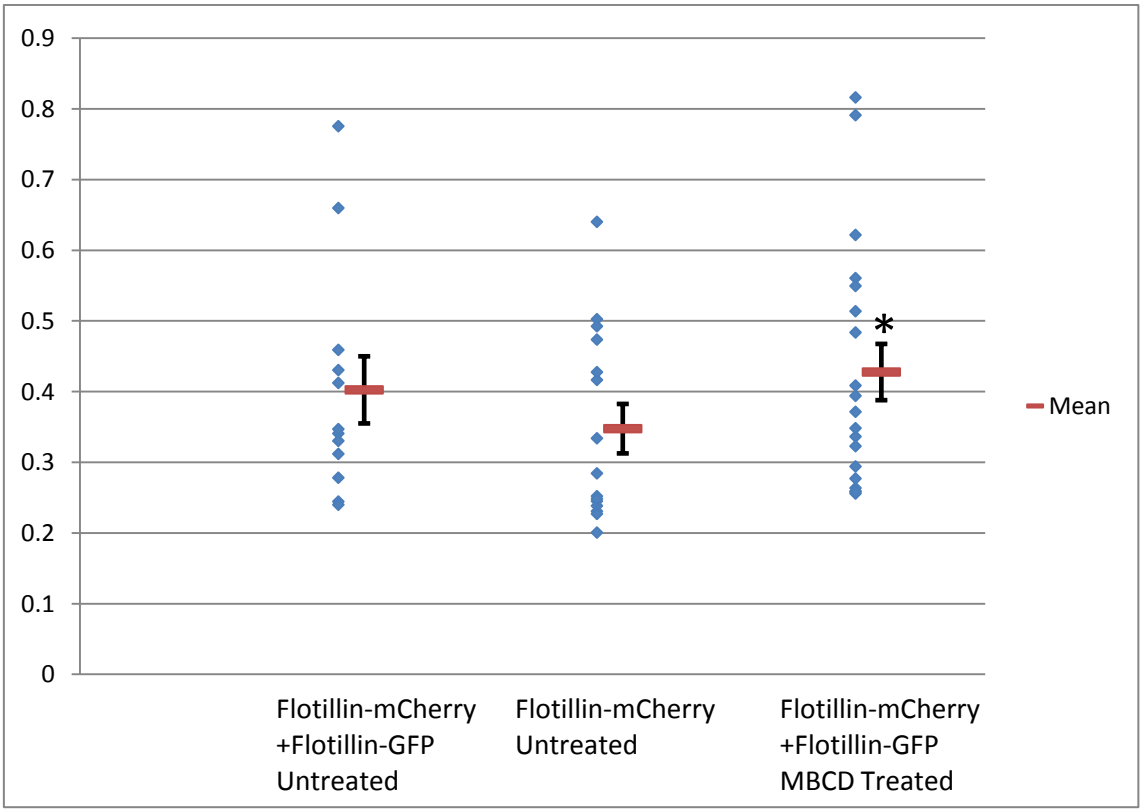

Figure 3-15 Relative fluorescence of Flotillin-mCherry with excitation at 488 compared to 543. The fluorescence values are corrected for the contribution of mCherry to when stimulated in the range for GFP. When Flotillin-mCherry is co-expressed with of Flotillin-GFP more red fluorescence is emitted upon excitation in the absorption spectra of GFP, compared to when it is expressed alone. This difference

was not abolished by treatment with MBCD to disrupt lipid rafts. After corrections were taken into account only the significant difference is between Flotillin-mCherry Untreated and Flotillin-mCherry + Flotillin-GFP Treated with MBCD.

3.3.2.2 Fluorophore linked $Na_V1.8$ is expressed on the membrane

In order to measure FRET signals in DRG neurons between $Na_V1.8$ proteins, to determine their distribution, they need to be fluorescently labelled. As labelling with antibodies was not possible for these proteins in the live cell condition, fluorescently label proteins were cloned. Constructs encoding the sodium channel $Na_V1.8$ conjugated to either the GFP or the red fluorescent protein mCherry were cloned. The $Na_V1.8$-mCherry construct was transfected into cells from the ND7 cell line. Transfection efficiency was low but some cells showed clear red fluorescence with absence of any green fluorescence, Figure 3-16. The $Na_V1.8$-mCherry construct is expressed mainly on the cell membrane, as can be seen by the ring pattern of expression in Figure 3-16(C). It is also expressed at a low level in the cytosol of the cell, but excluded from the nucleus.

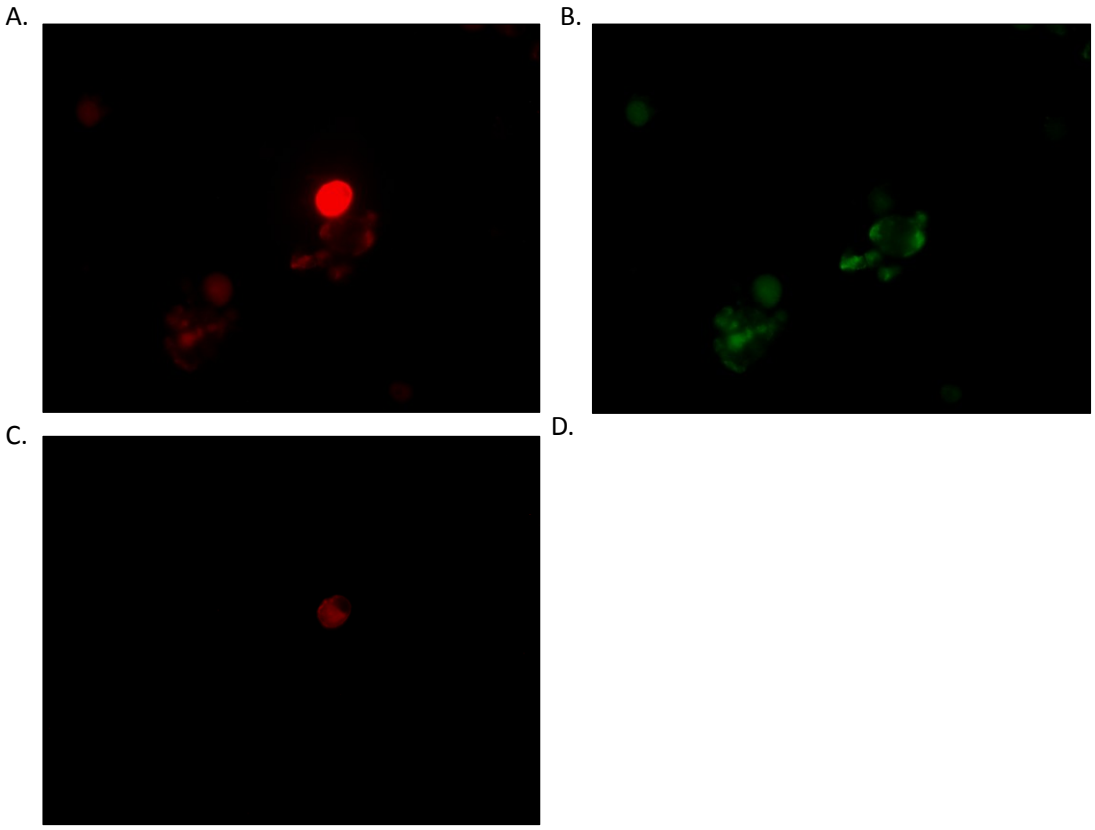

Figure 3-16 $Na_V1.8$-mCherry expressed in ND7 cells. A. cell expressing the red fluorescent $Na_V1.8$-mCherry construct and no green fluorescence (B). C is a lower intensity image of the of the red fluorescence of the same cell in order to make the cellular features more defined.

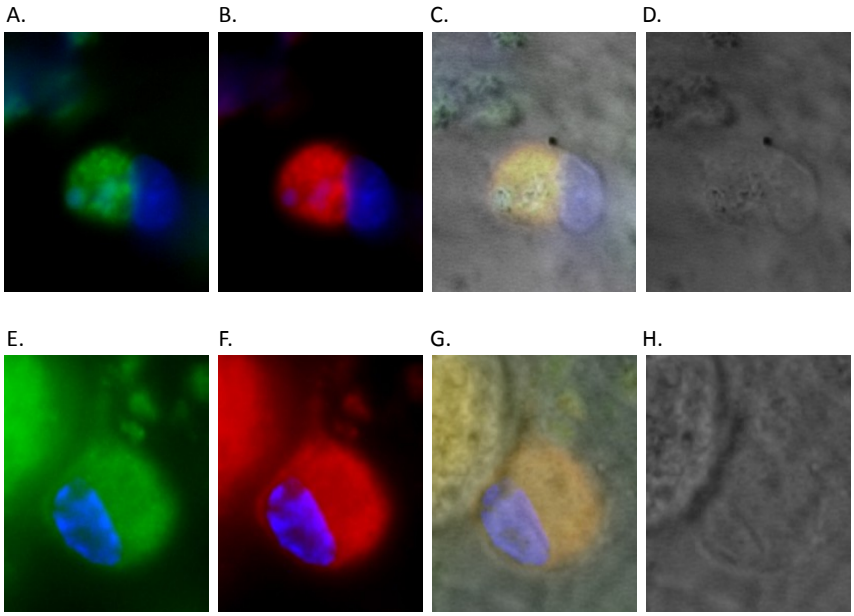

Figure 3-17 DRG neurons co-transfected using magnetic transfection with $Na_V1.8$-GFP and $Na_V1.8$-mCherry. A. And E. DRG cell showing green fluorescence due to $Na_V1.8$-GFP expression. B. And F. DRG cell showing red fluorescence due to $Na_V1.8$-mCherry expression. C. And G. Green and red fluorescence are co-localised. D. And H. Cell visualised using bright field illumination.

3.4 Discussion

In this study we set out to observe the spatial distribution of $Na_V1.8$ below the resolution limit of light microscopy, and how this compared with the distribution of lipid raft marker proteins. SEM was used in order to directly observe the location of proteins via gold labelling on the surface of culture neurons. From previous light microscopy studies, we would expect to see $Na_V1.8$ and lipid raft proteins form discrete large clusters along the length of the axon. We haven't previously observed the pattern of proteins within or between these clusters and the current study aims to elucidate this distribution. Observations of the lipid raft markers GM1 and Thy1 were made using SEM. Many regions showing extensive labelling for GM1 were analysed. The distribution observed did not correlate well with previous observation with light microscopy. Below the light microscopy resolution both GM1 and Thy1 showed a

clustered distribution. Observation of $Na_V1.8$ was very limited. It was not possible to determine the overall distribution of $Na_V1.8$. This was due to a low amount of labelling for $Na_V1.8$ in the samples. We will discuss the obstacles of the current study due to the labelling of $Na_V1.8$. The choice of methods to analyse particle distribution and their limitations will be discussed.

A FRET study was also undertaken with the aim of measuring any changes in the distance between proteins due to lipid raft disruption.

3.4.1 Lipid Raft Marker Distribution

SEM imaging allows the resolution features and visualisation of protein labelling at magnifications above the limit of light microscopes. We used SEM to observe the distribution of lipid raft marker proteins and $Na_V1.8$ of DRG neurons. Lipid raft marker proteins were observed to be more evenly distributed at small scales than would be expected from a completely random distribution. This could be an artefact of the labelling or analysis process or due to mechanisms controlling their distribution on the cell surface.

DRG neurons can be fixed and prepared for SEM imagining in a way which preserves their morphology. Furthermore membrane proteins of interest can be labelled with gold particles by the use of anti-bodies. These gold particles can be visible morphologically following sample coating with chromium. However, where surface morphology is itself uneven, they are often not distinguishable from other surface features. In this case the BSE signal, which elucidates the composition of the material below the surface, is used to good effect to show the distribution of labelling with gold particles.

Using scanning electron microscopy the labelling of a variety of lipid rafts markers and their distribution is seen. The lipid raft marker CTB, which binds to GM1 ganglioside, was found on the membrane of DRG neurons. Its distribution varies, with some areas

of high density labelling and others with sporadic labelling. Where neurites are well labelled it appears to form small clusters as well as individual proteins labelled which a spatially separated from other labelled proteins. On the larger scale the distribution is fairly uniform. The marker Thy1 is also found labelled on the surface of the neurites of DRG neurons. It is distributed in both small and large scale clusters. The small clusters are similar in size to that of lipid rafts postulated by other investigations, with diameters of up to 200 nm (Pike 2003). The larger clusters, which contain both smaller clusters and individually labelled proteins and which may be visible using light microscopy, would correspond to clustering previously reported in DRG neurons (Pristerà et al. 2012). Disruption of lipid rafts with MBCD didn't clearly cause any change to the cell membrane distribution of lipid raft markers.

Analysis of the distribution of the lipid raft markers GM1 and Thy1 did not show clustering of the particles, and the distribution was not altered by treatment with MBCD. The method of analysis was to look at the nearest neighbour and point event distribution functions of the particles, (Dixon 2001). This has previously been used to look at nuclear centromere distribution, (Andrey et al. 2010). Other researchers have used the Hopkins' statistic in order to analyse the degree of clustering of particle in lipid rafts, (Wilson et al. 2004). The chosen algorithm chosen for distribution analysis would only make a small difference, and only in the cases where the distribution was nearly random. Information on the distribution of the particles is lost when finding the maxima using ImageJ. It is not able to find 2 particles when they are in touching one another. In this case only one maxima is given. In some images there appear to be many particles touching one another and forming clusters. Although with the BSE signal particles were generally distinguishable from the background, there was still a high degree of noise when finding the maxima. This can lead to false positives and some particles with weak signal being excluded. This would add a random element to the distribution, thereby decreasing the detection of patterns.

The localisation of lipid raft markers below the resolution of light microscopy has rarely be attempted below the limit of conventional light microscopy and yet it is at exactly

these scales at which rafts are thought to ordinarily reside (Owen et al. 2012). Scanning electron microscopy allows the direct imaging of the membrane surface of a cell. It was chosen over transmission electron microscopy as the membrane rather than a cross section could be viewed and a single neurite could be followed along its course to see how the distribution varies. Transmission electron microscopy would have the advantages of being able to sample directly from ex-vivo tissue, easy access to epitopes for antibodies and there would be no need to coat the samples as is required for SEM. Another study has used SEM in order to image the labelling of proteins thought to be associated with lipid raft, (Hogue et al. 2011).

FRET results support the accepted view that Flotillin is clustered into rafts. The transfer of energy between the different fluorophores require Flotillin proteins to be in close proximity to each other as would be expected from dense packing within lipid rafts. Treatment by MBCD does not appear to change the efficiency of energy transfer between the fluorophores attached to the Flotillin proteins. This indicates that the average separation between proteins is largely unchanged following treatment. This could be due to only small amounts of Flotillin being released from rafts upon treatment, such that the majority remains in the same distribution as untreated cells. In this case the average separation would not change. Also lipids rafts and their constituents have been found to be anchored to the cytoskeleton, which may stabilise their distribution following raft disruption.

3.4.2 $Na_V1.8$ Distribution

$Na_V1.8$ gold labelling as imaged by SEM was very limited on DRG cell culture samples. This is most likely due to the epitope for the $Na_V1.8$ antibody being intracellular. Methanol permeabilisation was used to maximise labelling efficiency as this allowed the anti body to access intracellular membrane. This had limited success due to the large gold particle size used for a labelling. Further permeabilisation distorted the morphology of the cells.

The labelling of $Na_V1.8$ that was achieved show clustering of channels on small and large scales. This was similar to Thy1 labelling but the low efficiency of labelling means

it is not possible to be sure $Na_V1.8$ is generally clustered in this way. No labelling was seen in cultures that had been treated to disrupt lipid rafts. However, as only low levels of labelling were seen in untreated cultures this may well only be due to low labelling efficiency.

FRET signals from $Na_V1.8$ weren't recorded due to insufficient co-expression in cells. Some co-expression was possible using a recently developed magnetic transfection system. $Na_V1.8$ has been very difficult to transfect due to the large size of the plasmid once it has been inserted of 12 KB. DRG neurons are also difficult to transfect cells. Due to these restrictions we have tried novel transfection methods as double expression of both constructs in a single cell with electroporation, which is usually used to transfect DRG neurons, was not feasible given single transfection rates of roughly in a few hundred thousand cells.

3.4.3 Conclusions

The distribution of particles observed using SEM does not appear to be a good indication of whether or not they reside in rafts. Therefore persevering with observing the distribution of $Na_V1.8$ is unlikely to confirm any raft association. Lack of NaV1.8 labelling in the current study meant we were unable to confirm and refine the clustered distribution previously observed with light microscopy. Refining labelling techniques by trying further permeabilisation, smaller gold particles or by using gold directly conjugated with antibodies may help clarify the distribution. No difference was observed in FRET measurements for the lipid raft marker Flotillin when rafts were disrupted. Lack of transfection of $Na_V1.8$ constructs into cells meant FRET measurements weren't taken. However, as no difference was observed with markers then it wouldn't be clear what to expect if $Na_V1.8$ was or wasn't associated with rafts. If we had successfully expressed the constructs more efficiently we would have moved on to looking at FRET signals between $Na_V1.8$ and lipid rafts markers and other proteins which may interact with $Na_V1.8$.

4 Investigating the Proteome of DRG Neuron Lipid Rafts

4.1 Introduction

4.1.1 $Na_V1.8$ Interactions

Lipid rafts are rich in the variety of proteins they contain. They are important platforms for the interaction of proteins (Simons & Toomre 2000). Proteins can partition into rafts either due to preference due to hydrophobic matching or by association with other raft targeted proteins. Disrupting the integrity of rafts along $Na_V1.8$ expressing neurons prevents signal propagation (Pristerà et al. 2012). If $Na_V1.8$ requires other lipid raft proteins for its function then disrupting rafts may prevent this interaction leading to signal failure. The population of proteins resident in the lipid rafts of un-myelinated DRG neurons is mostly unknown other than some lipid raft markers and a few other proteins.

$Na_V1.8$ is known to bind to Annexin A2 light chain, also known as p11, and this association is required for functional expression of $Na_V1.8$ on the membrane (Okuse et al. 2002; Foulkes et al. 2006). The primary binding partner of p11 is AnnexinA2I, which is also a lipid raft associated protein and is involved in the aggregation of lipid rafts. As the binding sites for Annexin A2 and $Na_V1.8$ are different on p11 it is possible that they could both bind simultaneously. The Annexin A2-p11 complex is responsible for the stabilisation of other proteins, such as CD44, in lipid rafts and these lipid rafts interact with the actin cytoskeleton to anchor them in place (Oliferenko et al. 1999). $Na_V1.8$ interacts with the marker for caveolae type lipid rafts, Caveolin 1 (Ohman et al. 2008). This binding implies that $Na_V1.8$ may be found in Caveolae, a sub type of lipid raft.

Known and predicted interaction partners of a given protein can be found in STRING, which is a database of proteins and their predicted interactions (Müller et al. 2011). These interactions are based on the known interactions from published literature as well as predictions from the data of high throughput studies, genomic information and conserved co-expression. STRING gives a list of predicted interaction partners for $Na_V1.8$ (using it gene name SCN10A). STRING has recently been updated and this has changed most of the proteins that it predicts intact with $Na_V1.8$. In the old version,

STRING 9.0, the top 10 interacting proteins identified are shown in Figure 4-1. Unsurprisingly S100-A10, another name for p11, has the highest score (0.93) for confidence of an interaction. The protein interactions which are given by STRING are ranked by score, reflecting the evidence available for the interaction. The protein interactions provided by the latest version, STRING 9.05, are given in Figure 4-2. The lists of top protein interactions given by the current and previous version of STRING are largely different. This appears to be due to a change in the scoring method used and increased use of the gene ontology (GO) database as evidence for interactions between proteins. Now proteins involved with the Clathrin assembly, which is responsible for the removal of $Na_V1.8$ from the membrane, feature highly. Sodium channel Clathrin linker 1 comes top of the list as this acts as a linker to bind $Na_V1.8$ to Clathrin heavy chain 1 for its removal (Liu et al. 2005).

Gene	Protein	Experiments	Database	Text mining	Score
S100a10	Protein S100-A10	•		•	0.903
Sort1	Sortilin Precursor			•	0.817
Sclt1	Sodium channel and clathrin linker 1			•	0.772
Pdzd2	PDZ domain-containing protein 2	•		•	0.676
Taok2	Serine/threonine-protein kinase TAO2	•		•	0.676
Trpv1	Transient receptor potential cation channel subfamily V member 1			•	0.659
Anxa2	Annexin A2			•	0.653
Msn	Moesin	•		•	0.501
Gls	Glutaminase kidney isoform, mitochondrial Precursor			•	0.452
Gja1	Gap junction alpha-1 protein	•		•	0.45

Figure 4-1 $Na_V1.8$ interaction partners from STRING 9.0. Top 10 scoring proteins, which are known or predicted to interact with $Na_V1.8$, from a previous version of STRING. Known binding partner p11 (S100-A10) and its partner Annexin A2 are featured.

Gene	Protein	Experiments	Database	Text mining	Score
Sclt1	Sodium channel and clathrin linker 1		•	•	0.939
Slc18a3	Vesicular acetylcholine transporter		•	•	0.9
Synrg	Synergin gamma		•		0.899
Cltc	Clathrin heavy chain 1		•		0.899
Aak1	AP2-associated protein kinase 1		•		0.899
Epn2	Epsin-2		•		0.899
Cltb	Clathrin light chain B		•		0.899
Ap2s1	AP-2 complex subunit sigma		•		0.899
Clta	Clathrin light chain A		•		0.899
Tmed3	Transmembrane emp24 domain-containing protein 3 Precursor		•		0.899

Figure 4-2 $Na_V1.8$ interaction partners from STRING 9.05. Top 10 scoring proteins, which are known or predicted to interact with $Na_V1.8$, from the current version of STRING. Proteins from the Clathrin Assembly responsible for removing $Na_V1.8$ from the membrane feature highly.

4.1.2 Lipid Raft Proteins of DRG Neurons

Other channels have been found to be functionally dependent on interaction with other proteins within lipid rafts. The potassium channels $K_V7.2$ and $K_V7.3$ in DRG neurons require co-localisation with the muscarinic receptor within lipid rafts to produce their characteristic M current (Oldfield et al. 2009). A similar mechanism may be responsible for $Na_V1.8$ functional dependence on lipid rafts.

Nerve growth factor (NGF) stimulates the translocation of its receptor TrkA into lipid rafts (Limpert et al. 2007). This translocation is required for the neurite outgrowth seen upon NGF treatment and is mediated by a direct association between TrkA and the lipid raft marker protein Flotillin.

P2X3 is a receptor for ATP and is important in pain pathways, it has also been shown to partition in to lipids raft in the neurons of the trigeminal ganglion, which like the DRG contains C-types neurons.

4.1.3 Studying Proteomes

Proteomics is the study of an entire population of proteins. Traditionally this has been the population of proteins in a whole organism or specific tissue. As separation and detection methods have become more sensitive individual cell type and sub-cellular organelle proteomics is becoming possible. Even single cell proteomics has become possible (Jensen & Mouritsen 2004). The work flow involved in proteomics generally consists of biological sample preparation, protein digestion into peptides, mass spectrometry (MS) identification of peptides and protein matching from a database based on the peptides present (Mann et al. 2001). The proteome can then be further analysed. Often findings are verified by other techniques such as western blot and immunostaining. The prepared biological sample is required to be free from contaminant proteins and many substances, such as detergents and solvents, which can interfere with either digestion or MS analysis. Digestion is usually carried out with the enzyme trypsin, but another alternative is chymotrypsin. Trypsin cleaves polypeptides where there is a lysine or arginine (unless followed by proline). Chymotrypsin cleaves where there is a tyrosine, tryptophan or phenylaline amino acid in the protein.

4.2 Methods

4.2.1 Raft Sample Preparation Considerations

Lipid rafts on the axons of DRG neurons contain putative functional partners of $Na_V1.8$, which might be necessary for its function. The sciatic nerve contains the axons of DRG neurons. It contains a heterogeneous mix of axons from different subsets of DRG neurons including Aβ and Aδ as well as C-type. It also contains the Schwann cells that myelinate the larger diameter fibres. Therefore the sample will need to be processed in order to separate the lipid raft fractions. It is also possible to use cultured neurons

as the sample. Cultured cells are still a heterogeneous mix of different DRG neurons and Schwann cells. However they can be treated to suppress Schwann cell proliferation with aphidcholine and small diameter c-type DRG neurons survive longer in culture and therefore there is a higher proportion in longer term cultures. Cultured DRG neurons have no neurites when they are plated and NGF is used to promote neurite outgrowth. In order to have a higher proportion of neurite and small diameter neurons a longer culture is desirable. $Na_V1.8$ only seems to be distributed in a punctuate manner on the axon and not soma plasma membrane. Also depletion of cholesterol by MBCD treatment of small diameter cultured DRG neurons does not reduce soma currents as record by patch clamp (data not shown). This may be due to the rafts on the axon being more aggregated and therefore more easily distinguished by light microscopy or a difference in the partitioning of $Na_V1.8$ into rafts between the soma and axon. This may be due to different binding partners in the different cellular compartments. Cell culture can allow the physical separation of these cellular components by barriers. Compartmental culture allows the cell bodies to be seeded in one compartment of a culture dish but for the neurites to grow out into separate compartments, this would then allow the neurites to be collected but not the cell bodies. It also creates a barrier to prevent the spread of Schwann cells into the neurite chamber. It also allows for different culture media to be used in different compartments.

4.2.2 Cell Culture and Membrane Isolation

DRG cells were cultured as previously described. The DRG's of five adult female rats weighing 150g were used for each sample. The cells harvested were plated onto 5 wells of a 6 well plate, which were pre-coated with poly-L-Lysine and Laminin. For the serum free condition instead of DMEM based complete media Neurobasal media (Gibco) with 2% B27 Neuromix serum free supplement (PAA) and 1% Penicillin/Streptomycin was used. Cells were cultured in the presence of NGF, to promote neurite outgrowth, and Aphidicholine, to suppress Schwann cell proliferation, for 6 days. The wells were washed 3 times with pre-warmed sterile filtered PBS. 350ul of sterile filtered, ice cold PBS, 20% Glycerol was added to each well and the cells were

suspended using a cell scrapper. The suspension from all the wells was combined and homogenised by sonication with 9 pulses at power level 50 for 6 seconds each with 10 second pauses in between each pulse. Mammalian protease inhibitor was added at 1:100 concentration and the homogenate and centrifuged in a TLA45 rotor at 5000 rpm for 10 minutes at 4 ^{o}C to remove nuclear components and debris. The supernatant was collected and centrifuged in at 40000 rpm in a TLA45 rotor for 30 minutes at 4 ^{o}C to spin down the membrane fraction. The supernatant was removed and the membrane pellet was used for further separation.

4.2.3 Compartmental Culture

Round 35 mm diameter polystyrene culture dishes had 2 cm long scratches made in them with a sterile pin rake. The scratched area was pre-coated with poly-L-lysine solution for 2 hours. The scratched area was washed 3 times with cell culture graded water and allowed to dry. 30 µl of 1 % methylcellulose, laminin and 25 ng/ml NGF, is added to the centre of the scratched area. The Teflon divider is greased with high-vacuum grease using a blunted 23g needle attached to a sterile grease loader. The grease is applied around the outer rim and cell body compartment. The cell culture plate is applied to the greased side of the Teflon divider and pressed on gently outside of the area covering the divider. The dishes are turned over and incubated at 37 ^{o}C for 1.5 hours for the grease to settle and form a seal. Media is added containing penicillin to both side chambers and incubated over night. Any dishes with compartments that leak are not used for cultures. DRG cultures are prepared as previously described. All compartments of the dishes are washed three times with DMEM 1 % penicillin-streptomycin. Final media is added to the side compartments. Cells are plated in the central compartment and allowed to settle for 15 minutes. Cultures are incubated overnight at 37 ^{o}C and 5 % CO_2. To encourage neurite growth into side chambers NGF is added to these but not the central compartment.

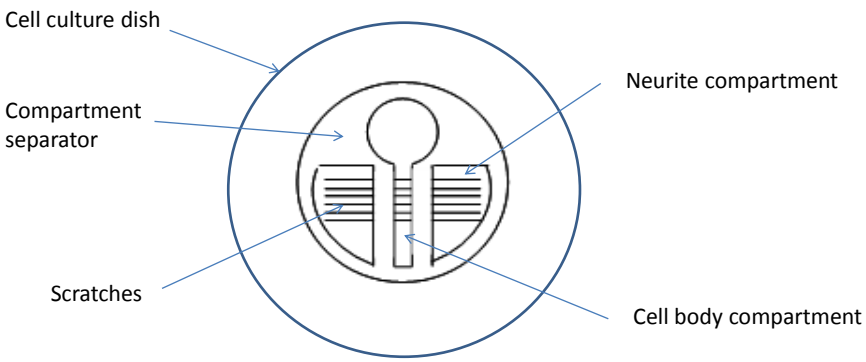

Figure 4-3 Diagram of compartmental culture setup. Culture dish is shown from above with compartment divider covering scratches made on the dish.

4.2.4 Detergent Resistant Membrane Separation

Lipid raft marker proteins are found in portions of the membrane resistant to solubilisation by non-ionic detergents, so they can be separated from other membrane proteins. Tissue samples were homogenised using a glass pestle and mortar in Solution B (150 mM NaCl, 5mM EDTA, 25 mM Tris-HCl pH 7.4) with 1:1000 mammalian protease inhibitor. Triton X-100 was added to a final concentration of 1%. For DRG culture membrane pellet, Solution D (Solution B with 1% Triton X-100) was used to resuspend. Solutions were incubated on ice for 30 minutes. Optiprep, 60% in water, and Solution D 10x stock solution were added to make the samples a final concentration of 40% optiprep in Solution D. 150ul was added to the bottom of a straight sided ultra centrifuge tube. The level of the solution was marked on the side of the tube. This was layered 3 times with 100ul 30% optiprep in Solution D with 1:1000 protease inhibitor, the level being marked each time. A final layer of 100ul of Solution D was added. The sample was centrifuged at 36000rpm in a TLA120.1 rotor for 4 hours 30 minutes. Following centrifugation 50ul from each of the 0% Optiprep layer, the

interface between 0% and 30% layers, the middle 30% layer, the bottom 30% layer and the 40 % layer was collected.

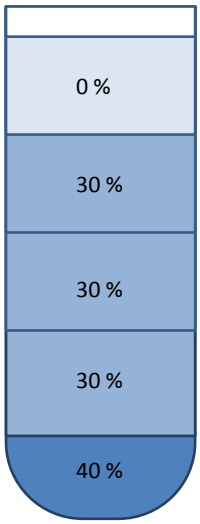

Figure 4-4 Discontinous layers for OptiPrep gradient ultracentrifugation, used for separating DRM fractions. Sample is loaded at the bottom in the 40 % OptiPrep layer and DRM concentrates around the interface of the 0 % and 30 % layers after ultracentrifugation, from where it can be collected.

4.2.5 Sciatic Nerve DRM sample Preparation

Sciatic nerve was dissected from an adult female rat weighing 150g. Tissue samples were homogenised using a glass pestle and mortar in Solution B (150 mM NaCl, 5mM EDTA, 25 mM Tris-HCl pH 7.4) with 1:1000 mammalian protease inhibitor. Triton X-100 was added to a final concentration of 1%. The homogenate was incubated for 30 minutes on ice. 60% OptiPrep in PBS was added to make a final concentration of 40% OptiPrep. The solution then formed the bottom layer of the OptiPrep gradient for the preparation of DRM by ultracentrifugation as previously described. Samples were taken from the interface between the 0% and 30% layers and from other layers for further analysis. Were repeated DRM separations were conducted in order to further purify the lipid raft fraction the interface was re-loaded in the 40% layer of a subsequent OptiPrep gradient for ultracentrifugation.

4.2.6 Gel Separation

Protein separation was carried out be SDS page electrophoresis, this was used for in gel staining, western blot and cleaning protein samples prior to mass spectrometer analysis. 10 % acrylamide mini-gels were prepared with 5ml HPLC water, 2.5 ml 4x photobuffer and 2.5 ml 40 % acrylamide for two gels. To polymerise the acrylamide 60 µl 1% APS and 6 µl temed were added. The solution was immediately poured into prepared glass plates held in frames. The solution was overlaid with 0.5 ml HPLC water for each gel, to prevent drying at the interface. Once the gel was set the water was drained out and the stacking layer was added, comprising: 4 ml HPLC water, 0.5 ml stacking buffer and 0.5 ml 40 % acrylamide, set with 60 µl 1% APS and 6ul Temed. The comb was immediately inserted. Once the gels were completely set they were removed from the frames and either used immediately or stored at 4 ^{O}C wrapped in moist tissue and cling film.

4.2.7 MS Sample Preparation

Polyacrylamide gels were constructed to comprise a 1 - 2 cm 4 % w/v polyacrylamide matrix on top of a 16 % w/v polyacrylamide matrix. Protein samples, either BSA (100 – 1000 ng per lane), rat brain membrane protein preparations (10 µg per lane) and pre-stained molecular weight markers were each prepared in Laemmli sample buffer also containing 10% Optiprep (these samples were used for method validation) and run into the gels in Tris-glycine running buffer (Invitrogen, Loughborough, UK) for 20 min at 150 V, or until the protein sample and molecular weight markers were observed to just pass around 0.5cm at the 4 – 16 % w/v gel interface. For lipid raft samples 100 µl was taken from the interface between the 30 % and 0 % optiprep layers resulting from DRM separation. This sample was made up to 2 % SDS, 10 % glycerol, 0.1 M DTT and 0.01 % bromophenol blue. The samples were heated to 60 ^{0}C for 30 min and then loaded on the gel with 20 µl per well.

The gels were briefly stained with colloidal Coomassie blue to visualise the proteins and to confirm their migration as a homogeneous population. The protein band visible at the 4 - 16 % w/v gel interface was excised from each lane and after washed extensively with 50% ACN, 0.1% formic acid in water, reduced with 5 mM Tris(2-

carboxyethyl)phosphine hydrochloride in 100 mM triethylammonium bicarbonate (TEAB) and free cysteine residues were protected with 10 mM methylmethanethiolsulfonate in 100 mM TEAB.

The proteins were digested with trypsin (Roche Diagnostics) overnight at 37^0C. Peptides were extracted from gel pieces by alternating washes of 100 mM TEAB and ACN and the pooled washes were lyophilised. The peptides from each lane were extracted and combined for injection on a nanoLC-MS/MS system. For method comparison, BSA and rat brain membrane preparations were also digested in solution. Briefly, BSA and rat brain membrane protein aliquots (10 µg) were solubilised in 500 µL denaturant solution (6 M guanidine hydrochloride, 0.1% w/v SDS, 0.1M Tris, pH 7.5, 0.1M sodium chloride) and reduced with 2 mM Tris(2-carboxyethyl)phosphine hydrochloride for 45 min at 50^0C. The solution was buffered to 50 mM TEAB, pH 8.0 and free cysteines were protected using 10 mM methylmethanethiolsulfonate for 20 min at ambient temperature. The solution was then diluted six-fold with 50 mM TEAB and the proteins digested with trypsin in a 40:1 protein:enzyme ratio overnight at 37 ^{0}C. In-solution digests were concentrated and desalted on Sep-Pak C18 cartridges (Waters, Elstree, UK) according to the manufacturer's protocols and recovered peptides were lyophilised. All method validation samples were analysed by an Applied Biosystem 4800 MALDI-TOF/TOF at Imperial College London. MS sample preparation was carried out in conjunction with Dr Kersti Karu, Imperial College London.

4.2.8 NanoLC-ES-MS/MS Analysis

The LC-MS/MS system consisted of a LTQ Orbitrap Velos (Thermo Fisher Scientific, UK) equipped with an ESI probe coupled to a Dionex Ultimate 3000 HPLC system (Dionex, UK) fitted with a nanospray ion source (Proxeon, UK). The samples were injected through a 10 µL loop in a pick-up injection mode, 3 µL per sample. The injected peptides were separated on a C18 analytical column, which was prepared by packing a Picotip spray emitter (150 mm length, 100 µm internal diameter, New Objective) with ProntoSIL C18 phase matrix (120 Å pore size, 3 µm bead size, Bischoff Chromatography). Peptides separated using gradient program with a mobile phase A of 0.1 % formic acid in water, and mobile phase B of 0.1 % formic acid in 80 %

acetonitrile. The LC gradient was as follows. After 3.1 minutes at 2 % B, the proportion of B was raised to 15 % B over the next 32 minutes using gradient curve 8 (Chromeleon software, Dionex). The proportion of B was then increased to 60 % over 75 minutes, before returning to 20 % B in 0.1 minutes. The column was re-equilibrated for 10 minutes giving a total run time of 120 minutes. The flow rate was 300 nL/minute, and the eluetent was directed to the ESI source of the LTQ-Orbitrap mass spectrometer.

MS data was acquired using a data-dependent acquisition mode, and operated at 60,000 resolution (full width at half maximum height, FWHM definition), and the top five 2+, 3+ and 4+ ions in the 300 - 1800 m/z were selected for MS/MS. Charge state 1+ ions were rejected. The automatic gain control for the Orbitrap was set to 500,000 ions, and the automatic gain control for the MS/MS in the ion trap was set at 10,000 ions. For MS/MS the isolation width was set at 2, the collision energy was 35%. Three MS/MS microscans for each precursor were accumulated. Maximum injection time into the ion trap in MS/MS was 200 ms, and maximum accumulation time in the Orbitrap was 500 ms. Dynamic exclusion was enabled, and selected ions were excluded for 180 s before they could be selected for another round of MS/MS. MS analysis was carried out by the Computational Biology Research Group and Central Proteomics Facility, Oxford University as part of a collaboration with Imperial College London.

4.2.9 Protein Matching

MS/MS peak lists were converted to mzXML format using ReAdW version 4.4.1 (LTQ XL Orbitrap data). Data was uploaded to the central proteomics facilities pipeline (https://mascot.molbiol.ox.ac.uk/cgi). Files were searched using Mascot version 2.3.01 (Matrix science), against a concatenated target and reversed decoy version of the UniProt_SwissProt database containing 537,505 sequences; 190,795,142 residues. Enzyme was set to trypsin allowing for up to 3 missed cleavages. Carbamidomethyl (C) was set as a fixed modification, and acetyl (N-term), deamidated (NQ), oxidation (M), and Glu->pyro-Glu (N-term E) were set as variable modifications. Mass tolerances for MS and MS/MS peak identifications were 20 ppm and 0.02 Da respectively.

4.2.10 Proteome Analysis

The protein population found was analysed for gene ontology (GO) term representation. The protein population was formed into a network using STRING. Highly represented pathways within the network of proteins were discovered, using STING and Gorilla.

Known proteins are annotated with gene ontology (GO) terms in databases. These record the known biological functions and in which cellular component the gene products are located. GO slim is a cut down subset of the GO terms, this gives a coarser categorisation of proteins for easier detection of trends and summarisation of protein sets.

4.2.11 Western Blot

Samples of DRM from DRG cultures were prepared as previously described and separated on 10% SDS gel. Separated proteins were transferred from the gel onto nitrocellulose membrane by dry blot using the iBlot system (Invitrogen) at 23 V for 6 minutes. Membranes were washed three times with PBST and incubated with the primary anti-body in PBST 10 % goat serum for 1 hour at room temperature. Membranes were washed three times in PBST and then incubated with secondary anti-body in PBST 10 % goat serum for 1 hour. Membranes were washed three time in PBST.

4.3 Results

4.3.1 Proteins from Sciatic Nerve

Rat sciatic nerve was homogenised and DRM was separated as previously described. As can be seen by dot blot using CTB lipid raft proteins concentrate at the interface between the 30 % and 0 % Optiprep layers. This fraction was removed and the DRM separation was repeated using with this adjusted to 40% Optiprep and loaded at the bottom of the density gradient. The second run of the DRM separation was used in order to further purify the proteins. The interface from the second DRM separation was run on a 10 % SDS gel such that the protein only ran 1 cm into the resolving gel.

This centimetre was then cut into 3 pieces and the top two were analysed by MS to identify the population of proteins contained. The 40 % fraction from the first run was also re-loaded for a second run of DRM separation. This shows that lipid raft proteins remaining in the 40 % portion after the first run, still remained in the 40 % and could not be floated in subsequent runs, as can be seen in Figure 4-5. In the second run of the DRM separation of CTB staining remains strong at the interface and decreases in all other fractions. This implies the lipid raft fraction has been further purified by repeat DRM separation.

Proteins identified by MS from both strips are listed in Figure 4-6, with their combined score from each strip (if found in both). In total 20 unique proteins were identified. The score is based on the sum of the scores of the individual peptides identified within that protein. It is a reflection of how likely the identification is a correct match. The cut off is calculated such that a protein identified with the cut off score has a 0.05 % chance of being a false positive match. The highest scoring protein was neurofilament light polypeptide, which is a neuron structural protein. As a structural protein, responsible for the morphology of nerve cells, it is unlikely to be an integral lipid raft protein, although it may bind to lipid raft proteins. Lipid raft proteins have been shown to bind to structural proteins to anchor lipid rafts. There are three neurofilament proteins that work together to form the structure of the neuron. The other two are neurofilament medium and neurofilament heavy polypeptide. Both of these were also found in the sample and they were ranked 4^{th} and 12^{th} respectively. Periaxin and Myelin Protein 0 were both found. These are both known to be Schwann cell proteins, where they are involved in the maintenance of the myelin sheath. Periaxin is found in the membrane of Schwann cells, which also contains abundant cholesterol, and therefore large portions of it are likely to be extracted with DRM separation. Other studies have also found myelin protein 0 located in the DRM of the rat sciatic nerve (Taguchi et al. 2007).

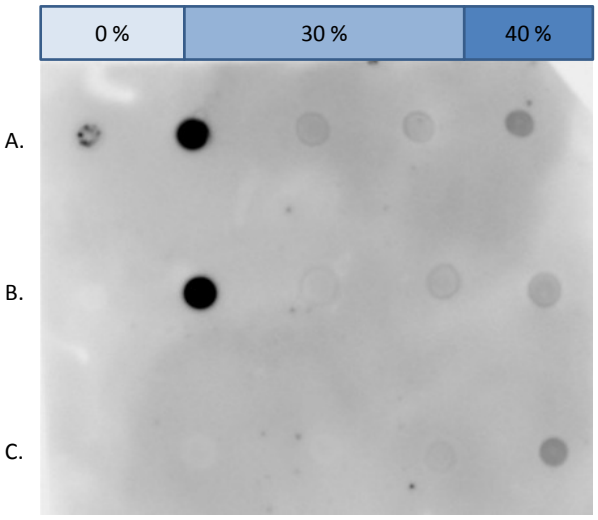

Figure 4-5. CTB staining of DRM preparation of sciatic nerve homogenate. Dot blot staining with CTB for GM1 ganglioside. There are five sample dots in each row taken from DRM separation using optiprep, from left to right they are the: 0 %, interface between the 0 % and 30 %, middle 30 %, bottom 30 %, and 40 % optiprep portions. The samples are A. Sciatic nerve homogenate, B. The interface portion of run A, and C. The 40 % portion of run A.

	Protein	Combined Score
1	Neurofilament light polypeptide	566
2	Periaxin	392
3	Histone H4	197
4	Neurofilament medium polypeptide	188
5	Keratin, type II cytoskeletal 6A	159
6	Histone H3.1	79
7	Myelin protein P0	68
8	Histone H2A type 1-C	58
9	Histone H2A.Z	53
10	Anionic trypsin-2	50
11	Anionic trypsin-1	49
12	Neurofilament heavy polypeptide	47
13	Keratin, type II cytoskeletal 1b	40
14	Tubulin beta-2B chain	36
15	Ornithine aminotransferase, mitochondrial	33
16	Protein disulfide-isomerase A4	32
17	SAP domain-containing ribonucleoprotein	26
18	Histone H2B type 1-A	23
19	Rho GTPase-activating protein 27	22
20	Ubiquitin thioesterase OTUB1	18

Figure 4-6 Double DRM separation of sciatic nerve homogenate MS analysis. Repeated DRM separation was used to isolate lipid raft proteins of the sciatic nerve. Many high ranking proteins, such as Periaxin, are known Schwann cell proteins. Other proteins, such as keratin, are likely to be contaminants.

The Trypsin used to cleave the proteins was detected in the sample. None of the lipid raft marker proteins were found and neither was $Na_V1.8$ or any of its associated proteins.

Other proteins found in the sample, primarily Keratin but also proteins, such as Histones, are likely to be present due to contamination during sample preparation. Keratin makes up a large part of human skin and if sample preparation isn't entirely isolated from the environment, it is likely to contaminate the sample. Sample preparation was conducted as far as possible using uncontaminated materials and in isolation. Later results appear less contaminated, mainly due to increased competency with the techniques involved. Contaminant proteins also feature more highly in the list when the sample is small.

This technique did not provide satisfactory results as proteins that were expected were not found and many contaminant and glial cell derived proteins were present.

4.3.2 Proteins from Compartmental Cultured Neurons

Compartmental cultures offered a number of challenges for proteomic MS sample preparation. The small surface areas inevitably lead to small yields for preparation. Also, culturing the neurites in a manner spatially separated from the cell bodies and glial cells meant they became very fragile and the media in which they were cultured was crucial for stability. Only cultures where the neurite side chambers were cultured with media containing serum produced healthy and stable neurites. When side chamber contained only serum free media with or with supplementation from B27 NeuroMix, the neurites were not healthy and prone to being washed away easily. The samples for MS analysis were taken from the side chambers only, such that rafts from the cell body would be excluded. Once collected the raft portion of the neurites was separated using DRM separation, from which the interface of 30 % and 0 % OptiPrep fractions was taken. This was run a very small distance on an SDS before digestion and MS analysis, Figure 4-7 .

Figure 4-7 Protein samples from serum free DRG culture run on a SDS gel. Proteins were run until they reached the boundary between the stacking and resolving gel, they were exised and then diegested.

Hit	Name	Score
1	Voltage-dependent anion-selective channel protein 1	468
2	ADP/ATP translocase 1	418
7	Periaxin	162
10	Actin, cytoplasmic 2	154
11	Tubulin alpha-1C chain	150
12	Anionic trypsin-1	146
13	Serum albumin	127
16	Annexin A5	105
18	Sodium/potassium-transporting ATPase subunit alpha-1	101
19	ATP synthase subunit d, mitochondrial	99
21	Electrogenic sodium bicarbonate cotransporter 1	92
22	Excitatory amino acid transporter 1	86
23	ATP synthase subunit b, mitochondrial	84
29	Annexin A1	69
75	Thy-1 membrane glycoprotein	23
76	Caveolin-1	22

Figure 4-8 Summary of results from DRM of neurites from compartmental culture MS analysis. Neurite compartments were cultured in media containing serum. Many contaminant proteins from preparation, such as Keratin, and from serum, such as serum albumin, were found.

Contaminants from the sample preparation, such as many forms of Keratin, were found in the sample. The list of proteins found in the compartmental culture DRM samples, Figure 4-8, contained the known serum protein serum albumin. This is derived from the serum added to the medium in the side compartments of the culture. It is not known which other proteins may derive from the serum as the exact constituents are unknown. Trypsin was present from which was added in order to cleave the proteins. Periaxin is present in the sample which is a well known Schwann cell protein. This would imply the presence of some Schwann cells in the sample despite the barrier between the plating and sampling compartments. It is possible for some Schwann cells to proliferate across if the seal between compartments is compromised. Schwann cell proliferation as describe was not observed immediately

prior to sample collection. It is also possible that periaxin is present in the cultured cells although there is no evidence for this in the literature.

The highest scoring protein found from compartmental culture was voltage dependant anion-selective channel 1 (VDAC1). The VDAC family of proteins are thought to be mainly mitochondrial proteins, but they do appear frequently when neuronal membrane DRM samples are analysed, (Herrera et al. 2011). Others believe that they are not present in the plasma membrane or lipid rafts, (Zheng et al. 2009).

The Annexins A5 and A1 were found in the sample. These are membrane associated proteins. Another Annexin, A2, may be associated with $Na_V1.8$ via their mutual binding partner p11. A variety of Annexins are associated with lipid rafts.

The Sodium potassium pump, NaKATPase, was found in the DRM samples from compartmental culture. This pump is responsible for creating, maintaining and rectifying the concentration gradient (and therefore resting voltage) across the membrane of neurons and other electrically active cells.

The lipid raft marker proteins Thy1 and Caveolin1 were found in the sample. This supports the validity of the sample as actually containing the lipid raft portion of the membrane. The lipid raft marker protein Flotillin was absent. This may indicate preferential extraction of subtypes of lipid rafts that exclude Flotillin, such as caveola type rafts. It may be due to low sample yield making the level of the protein undetectable. The low protein yield from compartmentally cultured neurites made this method unsuitable for obtaining a full proteome of the lipid rafts of DRG neurons. We moved on to methods with higher yields.

4.3.3 Proteins from Serum Free DRG Culture

Samples of cultured DRG neurons with extended neurites were prepared for HPLC MS/MS analysis by first separating the membrane portion of the sample and then preparing the DRM using an OptiPrep gradient. Samples were run in an SDS gel and Trypsin digested in gel.

Hit Number	Accesion Number	Name	Score	Matches
1	sp|P14668|ANXA5_RAT	Annexin A5	972	41
2	sp|P06685|AT1A1_RAT	Sodium/potassium-transporting ATPase subunit alpha-1	760	27
3	sp|Q07936-2|ANXA2_RAT	Isoform Long of Annexin A2	638	40
7	tr|D3ZSA3|D3ZSA3_RAT	Sodium/potassium-transporting ATPase subunit alpha-2	488	18
14	sp|P02770|ALBU_RAT	Serum albumin	277	16
20	sp|Q9Z2L0|VDAC1_RAT	Voltage-dependent anion-selective channel protein 1	242	13
53	sp|Q64541|AT1A4_RAT	Sodium/potassium-transporting ATPase subunit alpha-4	156	7
70	tr|B3Y9H3|B3Y9H3_RAT	S100 calcium binding protein A10 - p11	132	5
73	sp|P49134|ITB1_RAT	Integrin beta-1	127	9
91	sp|P21807|PERI_RAT	Peripherin	104	9
103	tr|D3ZJL3|D3ZJL3_RAT	Integrin alpha-7 heavy chain	92	9
125	sp|P06907|MYP0_RAT	Myelin protein P0	80	6
133	tr|F1LQJ3|F1LQJ3_RAT	Voltage-dependent anion-selective channel protein 2	80	4
207	sp|Q63425|PRAX_RAT	Periaxin	52	1
239	tr|F1LMA1|F1LMA1_RAT	Flotillin-2	43	6
243	tr|F1LNV8|F1LNV8_RAT	Scn7a -NaX	43	3
276	sp|Q9Z1E1|FLOT1_RAT	Flotillin-1	36	3
373	sp|P01830|THY1_RAT	Thy-1 membrane glycoprotein	27	2
390	sp|Q9JIP0-2|TRPV5_RAT	Isoform 2 of Trpv5	23	3

Figure 4-9 Serum free DRG culture 1st run summary of results. Some of the proteins found in the first sample, included are lipid raft marker proteins, NaK-ATPase subunits and a VGSC.

Serum contains many proteins, not all of which have been identified. In order to minimise the contamination of our sample from serum proteins we used a serum free supplement known as B27 Neuromix (PAA). This still contains additional proteins but as they are known they can be excluded from the resulting proteome. Serum free DRG samples were cultured for one week with NGF and Aphidicholine in order to obtain fully extended neurites and minimise Schwann cell proportion. Before DRM separation a simple plasma membrane separation was used to purify the sample. The interface portion of the OptiPrep density gradient from DRM separation was used for analysis following in gel trypsin digestion. Peptides identified by MS were used to identify the proteins in the sample using the MASCOT database.

Hit Number	Accesion Number	Name	Score	Matches
1	Q63425	Periaxin	1453	190
2	P06907	Myelin protein P0	1186	103
3	P21807	Peripherin	457	31
4	Q07936-2	Isoform Long of Annexin A2	715	53
6	P48037	Annexin A6	510	61
7	P06685	Sodium/potassium-transporting ATPase subunit alpha-1	537	41
7	P06686	Sodium/potassium-transporting ATPase subunit alpha-2	298	29
7	P06687	Sodium/potassium-transporting ATPase subunit alpha-3	295	24
7	Q64541	Sodium/potassium-transporting ATPase subunit alpha-4	122	10
15	P14668	Annexin A5	333	24
16	P02688-2	Isoform 2 of Myelin basic protein S	310	41
18	G3V8L3	Lamin A, isoform CRA_b	268	24
27	P55260	Annexin A4	188	8
28	P02770	Serum albumin	230	12
29	Q9Z2L0	Voltage-dependent anion-selective channel protein 1	230	11
32	D3ZFE1	Integrin beta	209	12
33	Q9Z1E1	Flotillin-1	205	17
40	F1M779	Clathrin heavy chain 1	180	15
41	P49134	Integrin beta-1	179	15
72	F1LMA1	Flotillin-2	123	13
73	P16409	Myosin light chain 3	34	1
115	P01830	Thy-1 membrane glycoprotein	93	11
131	Q63524	Transmembrane emp24 domain-containing protein 2	86	5
163	D3ZZR6	Potassium channel, subfamily V, member 2 (Predicted)	21	1
178	G3V6P7	Myosin, heavy polypeptide 9, non-muscle	69	11
185	P10252	CD48 antigen	68	3
211	P07340	Sodium/potassium-transporting ATPase subunit beta-1	62	10
268	Q63377	Sodium/potassium-transporting ATPase subunit beta-3	50	4
284	F1LYL3	Transmembrane emp24 domain-containing protein 10 (Fragment)	48	4
336	Q9Z2Z8	7-dehydrocholesterol reductase	42	1
375	D3ZWE4	Dynamin-1-like protein	38	1
410	D3ZH35	Sodium/potassium-transporting ATPase subunit beta-2	34	1
412	F1LLV8	CD44 antigen	34	4
440	P00762	Anionic trypsin-1	31	3
445	F1LR19	Phosphatidylinositol-binding clathrin assembly protein	30	3
446	P63004	Platelet-activating factor acetylhydrolase IB subunit alpha	30	2
461	Q04679	Sodium/potassium-transporting ATPase subunit gamma	29	2
621	P04631	Protein S100-B	18	1
628	D4A7B6	Protein Tmem87b	18	1
631	G3V6N2	Protein Tmed4	18	2
670	D3ZIR1	P2X4 purinoceptor	15	1
681	G3V7U4	Lamin-B1	14	1
702	Q64663	P2X purinoceptor 7	13	4

Figure 4-10 Serum free DRG culture 2nd run summary of results. In addition to many of the proteins found in the first sample, other known lipid raft proteins and $Na_V1.8$ associated proteins were found.

Two replicate samples were analysed and protein matches with above the significance threshold of 0.05 were returned. The first sample returned 710 protein hits and the second sample returned 1108 protein hits. 300 of the proteins hits were the same in both samples.

As with previous samples multiple Keratin proteins were found. There were many hits for Keratin, so they are not shown in the summary tables. The presence of keratin shows that despite precautions taken contamination from the lab environment still occurred. Other proteins in the samples may be contaminants, but it is not possible to differentiate which ones.

Many different subunits of the sodium potassium pump NaKATPase were found. An alpha subunit was also found in the previous compartmental culture sample. There are 4 known alpha subunits, 4 beta subunits and 1 gamma subunit. Peptides matching for each of the 4 alpha subunits were found. Due to substantial sequence overlap it cannot be conclusively stated that all were present in the sample. It is an important protein for maintaining the homeostatic transmembrane concentrations of sodium and potassium. There is little existing evidence for its inclusion in lipid rafts. Functional NaKATPase is a heterodimer of one alpha and one beta subunit. It is known to reside in the plasma membrane along the length axons in the sciatic nerve, which originate from DRG neurons, (Gerbi et al. 2002). Reduced action of NaKATPase plays a key role in neuropathy of peripheral nerves due to diabetes, which often leads to neuropathic pain in the patients affected.

The lipid raft marker proteins Flotillin 1 and 2 and Thy1 were found in both samples. This is consistent with and expected considering the DRM sample preparation. It supports the assertion that DRM isolated using the methods described is analogous to the lipid raft portion of the membrane. $Na_V1.8$ was not found in the sample, although it's known interaction partner p11, also known as S100 A10, was identified. The absence of $Na_V1.8$ undermines the hypothesis of its inclusion within lipid rafts. It is possible that it was lost during sample preparation, not cleaved by trypsin adequately to or in too small concentration to allow detection.

Although $Na_V1.8$ wasn't identified in the samples, the voltage gated sodium channel Na_X was found. Na_X is the least well characterised VGSC, and its sequence and function differ considerably to the other VGSC. Although it is structurally related to other VGSC, it has not been found to play a role in the transmission of AP. Its main role is

influencing the resting the membrane potential and it is sensitive to sodium concentrations as well as voltage. As a sodium sensor it is postulated to have a role in sodium homeostasis (Hiyama et al. 2002). Na_X is also expressed in non-myelinating Schwann cells of the peripheral nervous system, which could possibly be included in our sample (Watanabe et al. 2002).

The protein potassium channel, subfamily V, member 2 was found in the second sample. This is a voltage gated potassium channels also known as $K_V11.1$ and also $K_V8.2$. This channel has been found to reside in lipid rafts in other cell types, specifically myocytes and HEK cells, (Balijepalli et al. 2007). It has also been found that depletion of cholesterol from the membrane by MBCD alters the functioning of the channel. Its voltage dependence of activation was shifted positively and the rate of deactivation was increased. This raises the interest possibility that it is the effect of cholesterol depletion on potassium channels rather than sodium channels which influences its effects on axonal conduction.

Annexins are a family of membrane associated proteins. A number of members of this family were found in the samples analysed. In both samples the Annexins A1, A2, A4, A5, A6, A7 were found and in sample 2 Annexin A11 was also present. Annexin A2 has been shown to interact with lipid rafts along with its binding partner p11 and link smaller rafts into larger aggregates. Annexin A6 has also been shown to interact with lipid rafts (Domon et al. 2011; Cuschieri et al. 2005). Annexin A5 co-localises with the lipid raft marker GM1 (Dillon et al. 2000), which supports our identification of it within the DRM fraction of DRG neurons. These Annexins, A2, A6 and A5, were all found to be associated with lipid raft domains in a calcium dependant manner in a study on muscle cells (Babiychuk & Draeger 2000). Annexin A1 has been shown to be protective against inflammatory pain (Pei et al. 2011).

Four different Integrins were found in both samples, they were; beta 1, beta 4, alpha 7 heavy chain and alpha 6 isoform CRA. In sample 2 Integrin alpha 1 was also found.

Clathrin Heavy chain 1 was found, which is known to interact with $Na_V1.8$. However, the protein sodium and Clathrin linker 1, also known as CAP-1A or Sclt1, which links

$Na_V1.8$ and Clathrin was not found in the samples. Clathrin has been shown to be colocalised with the caveola type lipid raft marker caveolin, which further supports an association with lipid rafts, (Ares & Ortiz 2012; Rollason et al. 2007).

In sample 2 the purinoreceptors P2X4 and P2X7 were found. Both have been implicated in neuropathic pain, although only when expressed in microglia. They have also been found to interact with each other (Antonio et al. 2011). Other purinoreceptors have also been implicated in pain, P2X3 in particular, which is expressed in c-type nociceptors.

4.3.3.1 GO Slim analysis

The gene ontology (GO) is a database of annotated genes. For each gene it contains information about biological processes they are involved in, cellular components to which they belong and molecular function. Genes can be annotated with more than one term from each type, such as if they are found in multiple cell compartments or involved in multiple processes. GO slim is a version of the GO terms with fewer options, such that it is more generalised and can provide an overview of the terms in a large sample. The proteins discovered from the proteomic analysis of the second sample from serum free DRG cultured were analysed to give the respective representation of GO terms within this population.

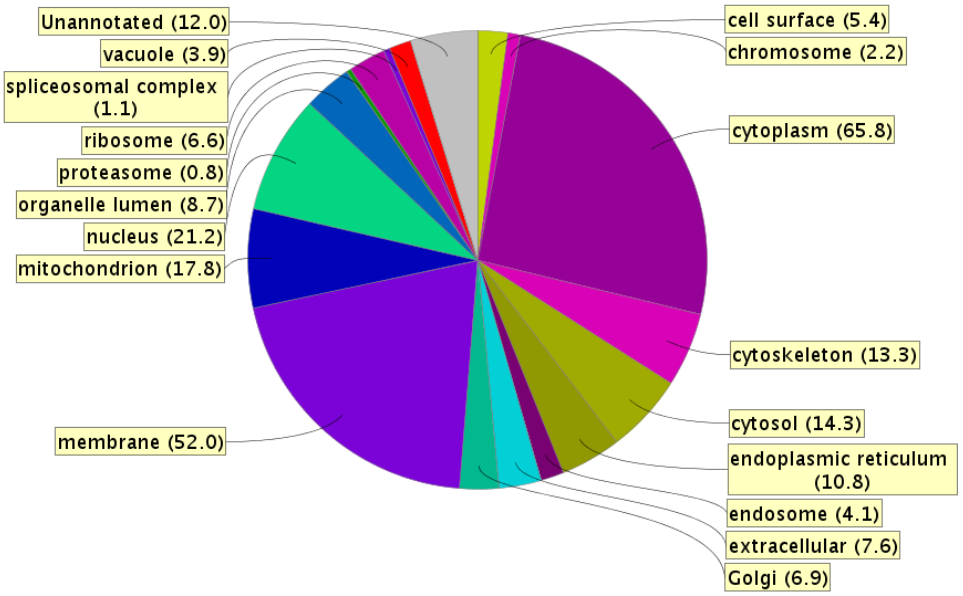

Figure 4-11 GO slim cellular compartment term representation in DRG culture DRM sample 2. Proteins from the membrane (52 %) and cytoplasm (65.8 %) were both highly represented in the sample. Many proteins have more than one cellular compartment annotated to them, and therefore the total percentage is greater than 100 %.

The representation of GO terms for cellular component was found from the population of proteins. Proteins maybe annotated within more than one term for cellular component in the GO database, and therefore percentages shown add up to more than 100 percent. In the second sample 52 % of the proteins were annotated with the GO term membrane for cellular component, Figure 4-11. Although the highest represented GO term for cellular compartment was cytoplasm, with 65.8 % of proteins annotated with this term. The high proportion of proteins annotated with membrane for cellular compartment confirms membrane proteins have been extracted as the membrane preparation protocol prior to DRM separation intended. The GO slim terms do not included one specifically for proteins found in lipid raft membrane

microdomains. So it is not clear whether these are enriched in the sample from this analysis.

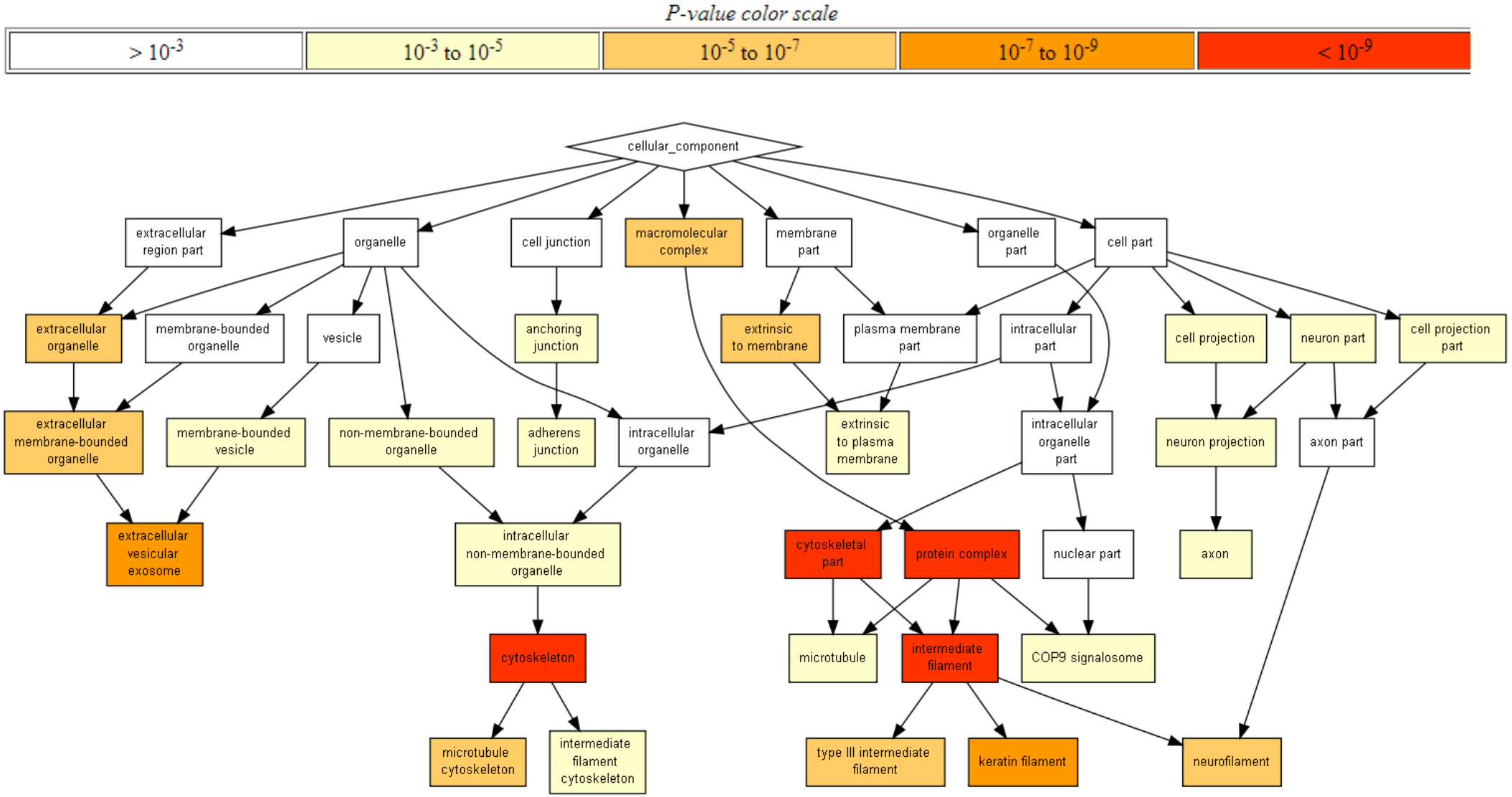

Figure 4-12 Gorilla Network of enriched GO terms for cellular component from serum free DRG culture DRM sample 2. The most highly enriched terms are cytoskeleton, cytoskeletal part, protein complex and intermediate filament.

A similar analysis was also carried out using the GOrilla tool, (Eden et al. 2009). The list of proteins found in serum free DRG culture DRM was the input and a network of the GO terms enriched within the sample was created, which is shown in Figure 4-12. Terms related to the cyctoskeleton are enriched in the network. This seems to be due to the presence of contaminating keratins in the sample, as well as neurofilaments being present. From the GO slim analysis 13.3% of proteins appear to be associated with the cytoskeleton, however, this does not give whether or not this is a high proportion. As the sample should be membrane only, this does appear large. Many lipid raft proteins have been shown to form complexes which interact with the cytoskeleton. Proteins associated with extracellular exosomes and ones extrinsic to the membrane (membranes associated proteins) were also enriched significantly. Lipid rafts have previously been associated with endocytosis and exosome transport, (de Gassart et al. 2003; Valapala & Vishwanatha 2011).

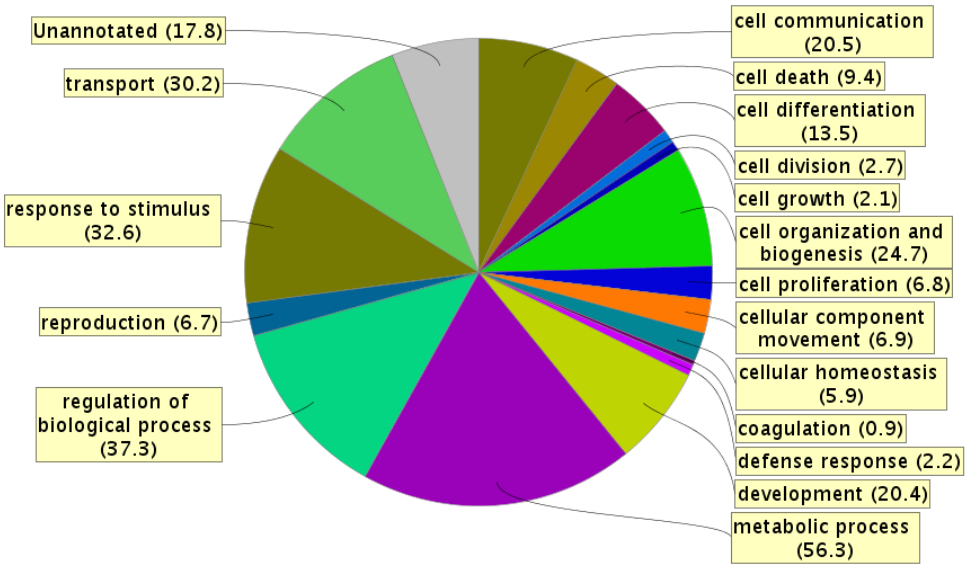

Figure 4-13 GO slim biological process term representation in DRG culture DRM sample 2. Proteins involved in metabolic processes (56.3 %) were highly represented in the sample.

Metabolic process was by far the highest represented biological process in the sample, with 56.3 % of proteins annotated to be involved in it, Figure 4-13. Three other processes were highly represented; these were transport, response to stimulus, and regulation of biological process. In the Gorilla analysis for protein function, terms related to transmembrane ion movement and ATPase activity were enriched (data not shown). These terms would be covered by the umbrella to metabolic process by the GO slim analysis.

4.3.3.2 STRING analysis

STRING is a tool used to look at networks of proteins and their interactions. It can be used to predict the interactions of proteins as was shown in the introduction to this

chapter. It can also be used to arrange proteins from high throughput assays into networks based on known and predicted interactions. These networks can then be analysed further to find clustering and pathways within them and to suggest which other proteins intact with the ones in the group. The latest version of STRING supplies 29 putative interaction partners for $Na_V1.8$ with interaction scores greater than 0.4 (the cut off they suggest using). Of these 4 proteins were found in the samples analysed. They were p11, Annexin A2, Actin and Clathrin Heavy Chain 1.

The unique proteins from the second sample were used as input for STRING, with only the top protein from each family used. Along with these $Na_V1.8$ was entered. The accession numbers from mascot were used to identify the proteins in STRING. Of the 701 proteins entered, 349 were identified by STRING and formed into a network.

4.4 Discussion

A variety of sample preparation techniques was used in order to try to purify the lipid raft portion of the axonal membrane of DRG neurons. It was hoped that this would identify $Na_V1.8$ as being present in this part of the membrane. It was also carried out to identify other proteins present in these microdomains which might functional partners for $Na_V1.8$ or important for signal transduction in these axons. Samples directly from the sciatic nerve contained a large amount of Schwann cell proteins due to the tissue including alot of myelin. In order to reduce the contribution of proteins from Schwann cells, cultured DRG neurons were used instead. Ideally the sample would contain no Schwann cells and also exclude the proteins from the cell bodies of DRG neurons, as axonal lipid raft proteins are the target population. In order to achieve this, compartmental cultures, where the axons are physically separated from the cell bodies and any glial cells in the culture, were used as a samples for proteomic analysis. This sample yielded lipid raft proteins, but not $Na_V1.8$. Due to the constraints of culturing the cells in this manner a very low yield of protein was extracted by this method, which resulted in low protein identification for the sample. In order to increase the amount of protein in the sample to be analysed large scale DRG cultures were used for the sample. DRG's from 5 rats were pooled for each sample. The cells

were cultured for a week in serum free media which reduced contamination from serum and Schwann cells and allowed neurites to be extended, increasing the proportion of axonal type membrane. The large yield from these samples allowed extra purification of the membranes from the sample prior to DRM, leading to more accurate results.

Over 1500 proteins were identified between the 2 samples analysed from serum free DRG culture. It was not possible to look at the possible interesting associations for each protein discovered. Proteins with known associations to $Na_V1.8$ were taken from the STRING database to be compared to the proteome. Two known interaction proteins with $Na_V1.8$ were found in the samples, which were p11 (as was its other binding partner Annexin A2) and Clathrin heavy chain. Although these findings lend support to the hypothesis that $Na_V1.8$ is present in lipid rafts, it was not itself found in the samples. This suggests $Na_V1.8$ may not in fact be present in lipid rafts in the sample from which we extracted the DRM. Other interesting putative and known lipid raft proteins were discovered, which lends credence to the sample consisting of lipid raft membrane proteins.

4.4.1 Contamination and Sample Preparation

Keratin was found in all the samples. This is most likely derived from contamination during sample preparation. In the samples from sciatic nerve and compartmental DRG culture keratin and other contaminant proteins featured highly in the lists of proteins with scores which were high relative to the other proteins identified. This is in part due to the low yield of true sample proteins. It is also due to the level of skill with which the sample were prepared and the level of isolation during preparation improving with subsequent samples. The highest score for Keratin in the first serum free DRM sample was 217 making it the 30^{th} ranked protein found. The highest score for Keratin found in the second sample was 530, making it the 8^{th} ranked protein on the list. These are quite high scores which suggest there is still substantial contamination of the sample occurring during preparation.

The protocol used for sample preparation was designed to reduce contamination as much as possible following best practise guidelines for proteomic sample preparation, http://www.proteomics.ox.ac.uk/protocols.html. Contamination from Polyethyleneglycol (PEG), which is found in the detergent used, Triton-X100, was removed from the sample. To avoid keratin contamination samples were prepared in a laminar flow hood and precautions were taken to avoid samples being exposed to the environment in the lab.

4.4.2 Sodium Regulation

The sodium potassium pump NaK-ATPase is found in the DRM samples from cultured DRG neurons. Previous studies have been contradictory as to whether it is included or excluded from lipid rafts. One study has found it collocated with GABA receptors in lipid raft clusters of rat cerebella granule cells (Dalskov et al. 2005). It has also been implicated that lipid rafts are important for it's delivery to the membrane (Welker et al. 2007) It is found in the plasma membrane of many cells and is involved in a variety of biological processes including regulating cell volume and signal transduction. Of most interest to us is its crucial role in establishing and maintaining ionic gradients and therefore the resting membrane potential in neurons and other electronically active cells. The maintenance of the resting membrane potential and ionic gradients is important to the functioning of $Na_V1.8$ in neurons (Faber et al. 2012). NaK-ATPase helps regulation by transporting sodium ions out of and potassium ions into the cell, thereby creating a concentration gradient of ions across the membrane. When action potentials are transmitted through a cell this gradient is partially eroded and so NaK-ATPase is essential for re-establishing the ionic gradient.

The atypical Sodium channel Na_X was also found in a sample from the DRM of cultured DRG neurons. Although it is in the same class with the other voltage gated sodium channels it has a distinct sequence from the other sub types, there being only 50 % sequence homology between them. It is also thought to have a distinct function compared to other voltage gated sodium channels. Its primary role appears to be sodium concentration sensing. It is the main channel involved in sodium homeostasis (Hiyama et al. 2002). It is located in glial cells in the brain in order to control sodium

intake on an organism level. It is known to be located in peripheral neurons, but its role in this case is less clear. It is thought to have a role in the setting of resting membrane potential.

Na_X acts cooperatively with NaK-ATPase pumps in order to maintain sodium homeostasis (Berret et al. 2013). This action is achieved by NaK-ATPase regulating the permeability of the Na_X channel. Increased expression of Na_X in DRG neurons contributes to pain states by increasing neuronal excitability (Ke et al. 2012). The same study has mainly found Na_X expressed in larger diameter DRG neurons. However, only the soma was stained and therefore Na_X maybe still be expressed along the axons of small diameter c-type DRG neurons.

It is possible both NaK-ATPase and Na_X are working to re-establish the sodium concentration following the passage of an AP, thereby allowing repeated firing.

4.4.3 Lipid Raft Proteins

The lipid raft marker proteins Flotillin and Thy1 were both found in the samples from cultured DRG neurons. This confirms that the sample contains DRM proteins and should contain further proteins which preferentially partition into lipid rafts. As well as integral lipid raft membrane proteins, proteins which are membrane associated, and in particular with lipid rafts, were found in the sample.

A variety of Annexins and Integrins were found, which are both families of membrane associated proteins. Some members of these families have been previously associated with lipid rafts (Rescher et al. 2004; Mayran et al. 2003) (Leitinger & Hogg 2002; Bodin et al. 2005). Annexins generally interact with lipid raft membrane in a calcium dependant manner, although Annexin A2 can interact with the lipid raft membrane in a calcium independent manner when link to p11. This formation also allows lateral binding between the heterodimers leading to the formation of arrogations of lipid rafts. Annexin A1 has shown to have an anti-inflamatory role and an inhibitory effect on the associated pain, (Girol et al. 2013). There is a lack of evidence in the literature for an association between Annexin A1 and lipid rafts or with $Na_V1.8$ or its known associations. CD44 has been shown to be located in lipid rafts that also associate with

Annexin A2. Lipid rafts contain CD44 also recruit actin bundles to anchor themselves to the cytoskeleton (Oliferenko et al. 1999).

Painful hyperalgesia mediated by prostegladin E2 (PGE2) requires integrin alpha 1 and 3, and beta 1. Additionally alpha 1 has been previously found located in the DRM fraction (Dina et al. 2005). PGE2 promotes the cell surface expression of $Na_V1.8$ (Liu et al. 2010).

4.4.4 $Na_V1.8$ and Interaction Partners

The protein which is the main subject of this research, $Na_V1.8$, was not found within any of the samples. From previous work supporting an association with lipid raft, we would expect to identify it in the DRM proteome of DRG axons. It is a large protein which might reduce the likely hood of retaining it in the sample throughout the preparation protocol. However, other similarly sized proteins, such as Na_X, and larger ones, such as myosin heavy chain, were identified in the samples. Membrane bound proteins in general present problems when it comes to extracting them for mass spectrometry analysis, (Mirza et al. 2007). $Na_V1.8$ had been difficult to identify in other MS experiments. In one experiment, specifically fishing for $Na_V1.8$, it was only found in 1 out of 12 recovery samples, (Ohman et al. 2008). They still concluded a positive interaction with the bait used. The reason given for lack of detection is the difficulty of cleaving the hydrophobic regions of $Na_V1.8$ with trypsin.

Although $Na_V1.8$ was not found in the sample, proteins that are known to interact with it were. Some of these proteins have also been previously found to associate with lipid rafts. In particular Annexin A2 and p11 have a role in the aggregation of lipid rafts. Clathrin Heavy chain 1 is known to interact with $Na_V1.8$ through the linker protein sodium channel clathrin linker 1. Clathrin has sometimes been used as a marker of non-lipid raft membrane (Welker et al. 2007) due to its known co-localisation with transferrin which is consistently found in the bottom fraction following DRM separation by gradient ultracentrifugation. Conversely it has also been implicated in endocytosis of integral lipid raft proteins (Rollason et al. 2007; Ares & Ortiz 2012). The lipid raft marker Caveolin was found, which has been associated with $Na_V1.8$. This

marker would be expected in the sample of DRM, but the known interaction lends support for an association of $Na_V1.8$ with lipid rafts.

5 Discussion and Conclusions

5.1 Summary

Previous work in our lab supported an association between the voltage gate sodium channels $Na_V1.8$ and lipid rafts. Based on this the hypothesis, that this association plays a function role in the $Na_V1.8$ mediated conduction of signals, was formulated. Investigation of the association and its putative function was carried out along three different lines. Firstly, the effect of the distribution of $Na_V1.8$ along axons was investigated with computational modelling. This did not test directly the effect of rafts, but rather the resulting distribution which was previously observed via confocal microscopy. Secondly, confirmation of the clustered distribution formed by $Na_V1.8$ and lipid raft marker proteins, and there integrity when disrupted, was sought using sub light resolution microscopy techniques. Thirdly, many lipid raft proteins form part of signalling assemblies which rely upon lipid rafts to function by bringing them into close proximity. To understand better if $Na_V1.8$ is forming part of a functional assembly, it was undertaken to try to identify the whole population of proteins resident in the lipid rafts of DRG neurons.

Further direct evidence for an association between $Na_V1.8$ and lipid rafts was not found in the current study. The clustered distribution of $Na_V1.8$ consistently observed gives rise to advantageous conduction properties in small diameter unmyelinated axons.

Investigating the distribution of $Na_V1.8$ at the nanoscale was unable to further characterise the distribution or how it relates to that of lipid rafts. Viewing the distribution using SEM was unsuccessful due to poor labelling of $Na_V1.8$. This may be due to intracellular epitiope for the anti-body for $Na_V1.8$ combined with gold particles to large to pass the membrane. FRET studies were reliant on expressing two forms of $Na_V1.8$ with an attached fluorophore within a single cell. This expression was a technical barrier to the experiment as methods conventionally used to express $Na_V1.8$ have limited expression efficiency in DRG neurons. $Na_V1.8$ is a long gene which is

difficult to express and DRG cells are a not an easy cell type in which to express vectors.

SEM studies did elucidate the distribution of lipid raft markers on the axons of DRG. Surprisingly when the distributions were analysed they were found to be more regular than would be expected by a random distribution. This would suggest a mechanism controlling their spacing, although it may be due to the combination labelling and image analysis not being able to detect particles in close proximity to one another. Cultures treated with MBCD, which is an established method of raft disruption, did not show a significantly different distribution of lipid raft marker proteins. The distribution of both markers has been previously observed using transmission electron microscopy, (Wilson et al. 2004). They found that clusters of Thy1 do not colocalise with GM1, which suggests separate populations of rafts. Using the distribution analysis from the current study on their images, confirmed that it was clustered as they concluded. Their study was in isolated membranes, smaller gold particles or only 5 nm and 10 nm were used for labelling and magnification achieved was higher than in our study. Clustering may be more marked in the membranes they used from the cell line RBL than in DRG cells. It is likely that the smaller particles and higher resolution make it possible to resolve proteins in close proximity to one another as separate individuals. The method used may be possible to use for identifying Thy1 and GM1 on DRG membranes.

We investigated the possibility that the disruption of lipid rafts may lead to a change in FRET signal from fluorescently tagged lipid raft marker protein Flotillin. No change in FRET signal was observed. It is possible that Flotillin and other lipid raft proteins are linked together by raft associated proteins such that they remain grouped despite disruption of lipid rafts. They may otherwise or as well be link to the cytoskeleton. Integrin proteins have been known to associate preferentially with lipid rafts and have been shown to have a role in interaction between the cytoskeleton and lipid rafts (Bodin et al. 2005). Cholesterol may be preferentially sequestered from non-lipid raft membrane due to being more available for MBCD uptake.

5.2 $Na_V1.8$ association with lipid rafts

Previous research within our group has supported an association between $Na_V1.8$ and lipid rafts, (Pristerà et al. 2012). The evidence for this association was from immunocytochemistry, western blotting and live cell recording with voltage sensitive dyes. The current study has not found further evidence of an association.

$Na_V1.8$ appears to be colocalised with lipid raft marker proteins when both were labelled using antibodies as well as when fluorescently tagged $Na_V1.8$ was over-expressed in cells. Along the axons of DRG neurons this colocalisation appears as patches of fluorescence every few µm. All patches of $Na_V1.8$ appeared to have lipid raft markers colocalised, but not all patches of lipid raft markers were positive for $Na_V1.8$. The colocalisation observed may be an artefact of the limited resolution available with conventional light microscopy, when in fact the $Na_V1.8$ is located near but not in lipid rafts. This would still, however, prompt the question of why it was concentrated in the vicinity of lipid rafts rather than evenly distributed along axons. Most of the work was conducted in cultured DRG neurons, and only some in ex-vivo teased nerve preparations. This raises the possibility that the clustering is due the cultured condition rather than a representation of $Na_V1.8$ distribution in vivo. Other studies have found that in free nerve ending $Na_V1.8$ does not display an evenly distributed pattern of labelling, but this is in common with other VGSC in these fibres (except for $Na_V1.9$ which is evenly distributed) (Persson et al. 2010).

$Na_V1.8$ was also detected in the DRM fraction from both the sciatic nerve and cultured DRG neurons. This is compelling evidence of their inclusion within lipid rafts. There are different types of lipid rafts and subpopulations exist contain unique compositions of proteins. It could be that $Na_V1.8$ exists only in certain lipid rafts. It may only be associated with them in the processes of trafficking to the membrane. Caveola type rafts are known to form endosomes for transport to the membrane. The association between Caveolin and $Na_V1.8$ may promote its trafficking to the membrane in such endosomes, but it may no longer require a lipid raft environment in the plasma

membrane. These may be excluded from the DRM sample collected in the current study. $Na_V1.8$ is known to bind to lipid raft associated proteins, such as p11 and cavaeolin. This binding may cause $Na_V1.8$ to be pulled into the DRM fraction during the separation protocol, where as in native membrane the areas are distinct. These interactions with proteins associated with lipid rafts support the theory that it is also associated with rafts, even if it is not resident within them.

Live cell imaging of culture neurons can be used to view the propagation of signals along their length using calcium and voltage sensitive dyes. This technique showed that signals could be blocked by pan sodium channel blockers but not TTX, consistent with the view that AP conduction in small fibre DRG neurons is dependent on $Na_V1.8$ function. These signals were almost abolished following treatment to disrupt lipid rafts with MBCD. This supports the theory that conduction mediated by $Na_V1.8$ is functionally dependant on lipid rafts.

$Na_V1.8$ clustering at sub light miscopy resolution scales has not been confirmed by this study. Although some groups of label $Na_V1.8$, at the scale at which lipid rafts are thought to exist, was observed there was not enough evidence to confirm whether this was generally the case.

In our proteomic samples of the DRM from DRG neurons, proteins which are known to interact with $Na_V1.8$ were found. Some of these proteins are established lipid raft associated proteins. Many other proteins were found which could be putative targets for interaction with or complementary function to $Na_V1.8$. One possible interaction partner is Periaxin. This was the highest scoring protein found in the second serum free DRG sample. It has been previous identified as possibly interacting with $Na_V1.8$ via a yeast to hybrid screen, (Malik-Hall et al. 2003). It is primarily thought to be a glial cell protein, so it may in this case be derived purely from Schwann cells in the sample. Even if this is the case, it is still possible that it may interact with external portions of $Na_V1.8$ where neurons come into contact with glial cells. The original binding from yeast two hybrid was found using an intracellular bait from $Na_V1.8$.

5.3 Sodium Regulation

One raft of $Na_V1.8$ can pass roughly 1500 sodium ions across the membrane during one AP, thereby roughly doubling the internal concentration of sodium ions. This change in concentration could lead to inhibition of the conduction of further AP. Therefore to maintain the ability to conduct spike trains the concentration gradient must be established using pumps. The pump NaK-ATPase is found in the lipid raft fraction of the membrane. Therefore it is likely it coexists with $Na_V1.8$ in lipid rafts. This proximity could reduce the impact of the high input of sodium ions during AP by pumping them out close to the site of highest concentration change.

One NaK-ATPase protein can cycle up to 48 times per second (although some estimates put this at up to 200 cycles) and each cycle moves 3 Na ions across the membrane, (Lüpfert et al. 2001). One cluster of $Na_V1.8$ channels can transmit roughly 1500 Na ions per AP conducted across the membrane. C-fibre neurons have been measured to conduct spike trains with frequencies up to 50 Hz (AP per second). In order to re-establish equilibrium with a firing rate of 50 Hz you would need 500 NaK-ATPase pumps. However the firing frequency of 50 Hz is not sustainable for long periods of time and the diameter of axons from which this was measured is unknown. This frequency may only be possible in larger diameter c-fibres whereas our models looked at the lowest known diameter of 0.1 µm. At larger diameters the internal Sodium ion concentration would not change so dramatically and therefore repeated firing would be more sustainable. The estimate of 500 channels in a small segment of thin diameter axon does not seem feasible and unfortunately our proteomics data does not give a direct indication of the quantities of the proteins present in the sample.

Sodium will also diffuse along the length of the axon if there is a concentration gradient. In other neurons it has been shown that diffusion of ions along the axon plays a greater role in the maintenance of ion gradient than pumps do (Fleidervish et al. 2010). If Sodium was only entering the axon at rafts then the concentration would be much greater there than the adjacent sections of axon. At the point of AP initiation

in a patch of membrane there is also a significant potential drop between the site and membrane further ahead of the AP. This is what causes the current to flow axially along the axon. As the internal potassium concentration is generally far greater than the sodium concentration, potassium is the dominant charge carrier for the axial current. However, as the sodium concentration increases internally more of the axial current will be carried by sodium ions, and therefore they will be transported away from the site of entry to areas of lower concentration.

Although the internal concentration of Sodium can change dramatically, as the external concentration is many times higher the difference still remains large. This means there is little change in the resting membrane potential. There is a more substantial change in the Sodium reversal potential, which would affect the peak AP voltage and current. These together imply that the axon may well be able to conduct multiple AP before conduction failure even if NaK-ATPase pumps were unable to match the rate of Sodium influx. Although we have found NaK-ATPase in lipid rafts this does not exclude the possibility that it also resides in the bulk membrane. The reliable detection of NaK-ATPase in all our samples with a high degree of certainty of identification and sequence coverage does suggest that it is an abundant protein in lipid rafts of DRG neuron fibres.

5.4 Future work

The function of $Na_V1.8$ may depend directly on the surrounding lipids rather than on other proteins or the spatial distribution of channels. Hydrophobic coupling between the trans-membrane regions of the protein and the lipid bilayer can affect conformation and consequently protein function. Lipid rafts contain a distinct mix of lipids which change their properties compared to the bulk membrane. They are stiffer and thicker than the rest of the membrane. Cholesterol, which partitions preferentially in to lipid rafts, is known to cause negative curvature of the membrane, making rafts more rigid. Cholesterol levels in the membrane have been shown to regulate protein function, in particular the function of $Na_V1.4$ (Lundbaek et al. 2004). Detergents, such as Triton-X-100, have the opposite effect, increasing membrane flexibility and

therefore can also regulate membrane bound protein function. Cholesterol in the membrane inhibits the inactivation of $Na_V1.4$, making it more available for repeated firing. Cholesterol also increased the voltage of activation and reduced the peak current in the same experiments. There may be similar effects on the function of $Na_V1.8$ by membrane cholesterol which cause the previously observed reduction in signal transduction when lipid rafts are disrupted in $Na_V1.8$ expressing DRG neurons (Pristerà et al. 2012). A similar experiment could be conducted with $Na_V1.8$. Unfortunately it is hard to record from $Na_V1.8$ in small diameter DRG neurons, except from the soma. This is due to the small and fragile nature of the neurites. Clustering of $Na_V1.8$ has not been observed in the soma of these cells and removing cholesterol does not prevent channel activity in the soma (unpublished observation). If the changes to the electrophysiological properties by cholesterol are subtle they may only make a difference to conduction in the axon and not the larger area of the soma as has been observed. Detailed observation of the changes to electrophysiological properties by the removal and addition of cholesterol should be made to ascertain the extent of effects. Specifically the gating properties of $Na_V1.8$ should be recorded and any changes due to cholesterol depletion observed.

5.5 Conclusions

$Na_V1.8$ clustering has electrophysical advantags for signal conduction. This may be the evolutionary driver for $Na_V1.8$ to be clustered in lipid rafts along the axons of unmyelinated c-type neurons. However, the lack of signal transduction previously observed following raft disruption is unlikely to be accounted for by small differences in the spacing of the channels following treatment. Sequestering cholesterol from the membrane may also lead to a change in gating of $Na_V1.8$ and therefore its failure to function. Some of the proteins which associate with $Na_V1.8$ are also associated with lipid rafts. In which case disrupting lipid rafts may lead to the removal of $Na_V1.8$, or its associated proteins, from the plasma membrane, leading to a loss of function. $Na_V1.8$ may be working with NaK-ATPase, as has been found with other VGSC (Black & Waxman 2013), to regulate sodium and membrane potential. As both have been found to be located in lipid rafts, this functional relationship may depend on the integrity of

lipid rafts. It is not clear if there is a direct interaction between $Na_V1.8$ and NaK-ATPase, but just being co-located in rafts maybe helpful in maintaining Sodium concentrations within the axon. Our computational models showed that with clustered Sodium channels and small diameter axons the current passing the membrane from even a single AP can have a large effect on the internal Sodium ion concentration. Having NaK-ATPase at these sites may compensate in order to enable the neuron to sustain rapid firing.

6 References

Abriel, H. et al., 2000. Regulation of the cardiac voltage-gated Na+ channel (H1) by the ubiquitin-protein ligase Nedd4. *FEBS Letters*, 466(2), pp.377–380. Available at: http://www.sciencedirect.com/science/article/pii/S001457930001098X [Accessed November 3, 2013].

Andrey, P. et al., 2010. Statistical analysis of 3D images detects regular spatial distributions of centromeres and chromocenters in animal and plant nuclei. C. Zimmer, ed. *PLoS computational biology*, 6(7), p.e1000853. Available at: http://dx.plos.org/10.1371/journal.pcbi.1000853 [Accessed June 18, 2014].

Anon, Fluorescence SpectraViewer. Available at: http://www.lifetechnologies.com/uk/en/home/life-science/cell-analysis/labeling-chemistry/fluorescence-spectraviewer.html# [Accessed January 9, 2014].

Antonio, L.S. et al., 2011. P2X4 receptors interact with both P2X2 and P2X7 receptors in the form of homotrimers. *British journal of pharmacology*, 163(5), pp.1069–77. Available at: http://www.pubmedcentral.nih.gov/articlerender.fcgi?artid=3130952&tool=pmcentrez&rendertype=abstract [Accessed September 28, 2013].

Ares, G.R. & Ortiz, P.A., 2012. Dynamin2, clathrin, and lipid rafts mediate endocytosis of the apical Na/K/2Cl cotransporter NKCC2 in thick ascending limbs. *The Journal of biological chemistry*, 287(45), pp.37824–34. Available at: http://www.ncbi.nlm.nih.gov/pubmed/22977238 [Accessed October 20, 2013].

Babiychuk, E.B. & Draeger, a, 2000. Annexins in cell membrane dynamics. Ca(2+)-regulated association of lipid microdomains. *The Journal of cell biology*, 150(5), pp.1113–24. Available at: http://www.pubmedcentral.nih.gov/articlerender.fcgi?artid=2175252&tool=pmcentrez&rendertype=abstract.

Baker, M.D., 2005a. Protein kinase C mediates up-regulation of tetrodotoxin-resistant, persistent Na+ current in rat and mouse sensory neurones. *The Journal of physiology*, 567(Pt 3), pp.851–67. Available at: http://www.pubmedcentral.nih.gov/articlerender.fcgi?artid=1474230&tool=pmcentrez&rendertype=abstract [Accessed May 1, 2013].

Baker, M.D., 2005b. Protein kinase C mediates up-regulation of tetrodotoxin-resistant, persistent Na+ current in rat and mouse sensory neurones. *The Journal of physiology*, 567(Pt 3), pp.851–67. Available at: http://www.pubmedcentral.nih.gov/articlerender.fcgi?artid=1474230&tool=pmcentrez&rendertype=abstract [Accessed May 1, 2013].

Balijepalli, R. et al., 2007. Kv11.1 (ERG1) K+ Channels Localize in Cholesterol and Sphingolipid Enriched Membranes and Are Modulated by Membrane Cholesterol. *Channels*, 1(4), pp.263–272. Available at: https://www.landesbioscience.com/journals/channels/article/4946/?nocache=556804241 [Accessed July 14, 2014].

Benn, S.C. et al., 2001. Developmental expression of the TTX-resistant voltage-gated sodium channels Nav1.8 (SNS) and Nav1.9 (SNS2) in primary sensory neurons. *The Journal of neuroscience : the official journal of the Society for Neuroscience*, 21(16), pp.6077–85. Available at: http://www.ncbi.nlm.nih.gov/pubmed/11487631.

Berret, E. et al., 2013. Regulation of central Na+ detection requires the cooperative action of the NaX channel and α1 Isoform of Na+/K+-ATPase in the Na+-sensor neuronal population. *The Journal of neuroscience : the official journal of the Society for Neuroscience*, 33(7), pp.3067–78. Available at: http://www.jneurosci.org/content/33/7/3067.long [Accessed October 10, 2013].

Black, J.A. et al., 2012. Expression of Nav1.7 in DRG neurons extends from peripheral terminals in the skin to central preterminal branches and terminals in the dorsal horn. *Molecular pain*, 8(1), p.82. Available at: http://www.molecularpain.com/content/8/1/82 [Accessed July 14, 2014].

Black, J.A. & Waxman, S.G., 2013. Noncanonical roles of voltage-gated sodium channels. *Neuron*, 80(2), pp.280–91. Available at: http://www.ncbi.nlm.nih.gov/pubmed/24139034 [Accessed January 22, 2014].

Bodin, S. et al., 2005. Integrin-dependent interaction of lipid rafts with the actin cytoskeleton in activated human platelets. *Journal of cell science*, 118(Pt 4), pp.759–69. Available at: http://jcs.biologists.org/content/118/4/759.long [Accessed September 20, 2013].

Breivik, H. et al., 2006. Survey of chronic pain in Europe: prevalence, impact on daily life, and treatment. *European journal of pain (London, England)*, 10(4), pp.287–333. Available at: http://www.ncbi.nlm.nih.gov/pubmed/16095934 [Accessed October 22, 2013].

Brown, D.A. & London, E., 1998. FUNCTIONS OF LIPID RAFTS.

Choi, J.-S. et al., 2004. Functional role of the C-terminus of voltage-gated sodium channel Na(v)1.8. *FEBS letters*, 572(1-3), pp.256–60. Available at: http://www.ncbi.nlm.nih.gov/pubmed/15304358 [Accessed May 1, 2013].

Cox, J.J. et al., 2010. Congenital insensitivity to pain: novel SCN9A missense and in-frame deletion mutations. *Human mutation*, 31(9), pp.E1670–86. Available at:

http://www.pubmedcentral.nih.gov/articlerender.fcgi?artid=2966863&tool=pmcentrez&rendertype=abstract [Accessed January 20, 2014].

Crombez, G. et al., 1999. Pain-related fear is more disabling than pain itself: evidence on the role of pain-related fear in chronic back pain disability. *Pain*, 80(1), pp.329–339. Available at: http://www.sciencedirect.com/science/article/pii/S0304395998002292 [Accessed January 27, 2014].

Cummins, T.R. & Waxman, S.G., 1997. Downregulation of tetrodotoxin-resistant sodium currents and upregulation of a rapidly repriming tetrodotoxin-sensitive sodium current in small spinal sensory neurons after nerve injury. *The Journal of neuroscience : the official journal of the Society for Neuroscience*, 17(10), pp.3503–14. Available at: http://www.ncbi.nlm.nih.gov/pubmed/9133375 [Accessed January 31, 2014].

Cuschieri, J. et al., 2005. Oxidative-induced calcium mobilization is dependent on annexin VI release from lipid rafts. *Surgery*, 138(2), pp.158–64. Available at: http://www.surgjournal.com/article/S0039-6060(05)00199-6/abstract [Accessed October 1, 2013].

Dalskov, S.-M. et al., 2005. Lipid raft localization of GABA A receptor and Na+, K+-ATPase in discrete microdomain clusters in rat cerebellar granule cells. *Neurochemistry international*, 46(6), pp.489–99. Available at: http://www.ncbi.nlm.nih.gov/pubmed/15769551 [Accessed March 12, 2013].

Dillon, S.R. et al., 2000. Annexin V binds to viable B cells and colocalizes with a marker of lipid rafts upon B cell receptor activation. *Journal of immunology (Baltimore, Md. : 1950)*, 164(3), pp.1322–32. Available at: http://www.jimmunol.org/content/164/3/1322.full [Accessed October 1, 2013].

Dina, O. a et al., 2005. Primary afferent second messenger cascades interact with specific integrin subunits in producing inflammatory hyperalgesia. *Pain*, 115(1-2), pp.191–203. Available at: http://www.ncbi.nlm.nih.gov/pubmed/15836982 [Accessed May 1, 2013].

Dixon, P.M., 2001. Nearest Neighbor Methods Nearest neighbor methods for spatial point processes. , (December), pp.1–26.

Djouhri, L. et al., 2006. Spontaneous pain, both neuropathic and inflammatory, is related to frequency of spontaneous firing in intact C-fiber nociceptors. *The Journal of neuroscience : the official journal of the Society for Neuroscience*, 26(4), pp.1281–92. Available at: http://www.ncbi.nlm.nih.gov/pubmed/16436616 [Accessed May 24, 2013].

Domon, M.M. et al., 2011. *Annexin A6 is recruited into lipid rafts of Niemann–Pick type C disease fibroblasts in a Ca2+-dependent manner*, Available at: http://www.sciencedirect.com/science/article/pii/S0006291X11000131 [Accessed October 1, 2013].

Eden, E. et al., 2009. GOrilla: a tool for discovery and visualization of enriched GO terms in ranked gene lists. *BMC bioinformatics*, 10(1), p.48. Available at: http://www.biomedcentral.com/1471-2105/10/48 [Accessed July 15, 2014].

Elliott, B.Y.A.A. & Elliott, J.R., 1993. GANGLIA BY A. A. ELLIOTT AND J. R. ELLIOTT From the Department of Anatomy and Physiology, The University, Dundee DD1 4HN (Received 8 May 1992). , 1350(1993), pp.39–56.

Erik Fransen, J.T., 2011. Computational modeling of activity dependent velocity changes in peripheral C-fibers.

Faber, C.G. et al., 2012. Gain-of-function Nav1.8 mutations in painful neuropathy. *Proceedings of the National Academy of Sciences of the United States of America*, 109(47), pp.19444–9. Available at: http://www.pubmedcentral.nih.gov/articlerender.fcgi?artid=3511073&tool=pmcentrez&rendertype=abstract [Accessed October 22, 2013].

Faisal, a A. & Laughlin, S.B., 2007. Stochastic simulations on the reliability of action potential propagation in thin axons. *PLoS computational biology*, 3(5), p.e79. Available at: http://www.pubmedcentral.nih.gov/articlerender.fcgi?artid=1864994&tool=pmcentrez&rendertype=abstract [Accessed March 17, 2013].

Fink, M. & Noble, D., 2009. Markov models for ion channels: versatility versus identifiability and speed. *Philosophical transactions. Series A, Mathematical, physical, and engineering sciences*, 367(1896), pp.2161–79. Available at: http://rsta.royalsocietypublishing.org/content/367/1896/2161.long [Accessed January 30, 2014].

Fischer, T.Z. & Waxman, S.G., 2010. Familial pain syndromes from mutations of the NaV1.7 sodium channel. *Annals of the New York Academy of Sciences*, 1184, pp.196–207. Available at: http://www.ncbi.nlm.nih.gov/pubmed/20146699.

Fleidervish, I.A. et al., 2010. Na+ imaging reveals little difference in action potential-evoked Na+ influx between axon and soma. *Nature neuroscience*, 13(7), pp.852–60. Available at: http://dx.doi.org/10.1038/nn.2574 [Accessed January 26, 2014].

Foulkes, T. et al., 2006. Deletion of annexin 2 light chain p11 in nociceptors causes deficits in somatosensory coding and pain behavior. *The Journal of neuroscience : the official journal of the Society for Neuroscience*, 26(41), pp.10499–507.

Available at: http://www.ncbi.nlm.nih.gov/pubmed/17035534 [Accessed April 11, 2013].

Fozzard, H. a & Lipkind, G.M., 2010. The tetrodotoxin binding site is within the outer vestibule of the sodium channel. *Marine drugs*, 8(2), pp.219–34. Available at: http://www.pubmedcentral.nih.gov/articlerender.fcgi?artid=2852835&tool=pmcentrez&rendertype=abstract [Accessed May 29, 2013].

Gaida, W. et al., 2005. Ambroxol, a Nav1.8-preferring Na(+) channel blocker, effectively suppresses pain symptoms in animal models of chronic, neuropathic and inflammatory pain. *Neuropharmacology*, 49(8), pp.1220–7. Available at: http://www.ncbi.nlm.nih.gov/pubmed/16182323 [Accessed January 29, 2014].

De Gassart, A. et al., 2003. Lipid raft-associated protein sorting in exosomes. *Blood*, 102(13), pp.4336–44. Available at: http://www.ncbi.nlm.nih.gov/pubmed/12881314 [Accessed July 15, 2014].

Gerbi, A. et al., 2002. Localization of Na,K-ATPase α/β Isoforms in Rat Sciatic Nerves : Effect of Diabetes and Fish Oil Treatment. *Journal of Neurochemistry*, 73(2), pp.719–726. Available at: http://doi.wiley.com/10.1046/j.1471-4159.1999.0730719.x [Accessed July 15, 2014].

Girol, A.P. et al., 2013. Anti-inflammatory mechanisms of the annexin A1 protein and its mimetic peptide Ac2-26 in models of ocular inflammation in vivo and in vitro. *Journal of immunology (Baltimore, Md. : 1950)*, 190(11), pp.5689–701. Available at: http://www.ncbi.nlm.nih.gov/pubmed/23645879 [Accessed July 14, 2014].

Gold, M.S. et al., 2003. Redistribution of Na(V)1.8 in uninjured axons enables neuropathic pain. *The Journal of neuroscience : the official journal of the Society for Neuroscience*, 23(1), pp.158–66. Available at: http://www.ncbi.nlm.nih.gov/pubmed/12514212.

Goldin, A., 2000. Letter to the editor. *Biostatistics (Oxford, England)*, 28, pp.365–368. Available at: http://www.ncbi.nlm.nih.gov/pubmed/23630035.

Hermann, R., Walther, P. & Müller, M., 1996. Immunogold labeling in scanning electron microscopy. *Histochemistry and cell biology*, 106(1), pp.31–9. Available at: http://www.ncbi.nlm.nih.gov/pubmed/22100878.

Herrera, J.L. et al., 2011. Voltage-dependent anion channel as a resident protein of lipid rafts: post-transductional regulation by estrogens and involvement in neuronal preservation against Alzheimer's disease. *Journal of neurochemistry*, 116(5), pp.820–7. Available at: http://www.ncbi.nlm.nih.gov/pubmed/21214547 [Accessed July 14, 2014].

Hines, M.L. & Carnevale, N.T., 2001. Neuron: A Tool for Neuroscientists. *The Neuroscientist*, 7(2), pp.123–135. Available at: http://nro.sagepub.com/cgi/doi/10.1177/107385840100700207 [Accessed March 4, 2013].

Hiyama, T.Y. et al., 2002. Nax channel involved in CNS sodium-level sensing. *Nature Neuroscience*, 5(6), pp.511–512. Available at: http://dx.doi.org/10.1038/nn0602-856 [Accessed October 10, 2013].

Hogue, I.B. et al., 2011. Gag induces the coalescence of clustered lipid rafts and tetraspanin-enriched microdomains at HIV-1 assembly sites on the plasma membrane. *Journal of virology*, 85(19), pp.9749–66. Available at: http://jvi.asm.org/content/85/19/9749.full [Accessed July 13, 2014].

Horisberger, M. & Rosset, J., 1977. Colloidal gold, a useful marker for transmission and scanning electron microscopy. *Journal of Histochemistry & Cytochemistry*, 25(4), pp.295–305. Available at: http://jhc.sagepub.com/cgi/content/long/25/4/295 [Accessed January 11, 2014].

Huang, M., Volgushev, M. & Wolf, F., 2012. A small fraction of strongly cooperative sodium channels boosts neuronal encoding of high frequencies. S. E. Dryer, ed. *PloS one*, 7(5), p.e37629. Available at: http://dx.plos.org/10.1371/journal.pone.0037629 [Accessed June 7, 2014].

Hudmon, A. et al., 2008. Phosphorylation of sodium channel Na(v)1.8 by p38 mitogen-activated protein kinase increases current density in dorsal root ganglion neurons. *The Journal of neuroscience : the official journal of the Society for Neuroscience*, 28(12), pp.3190–201. Available at: http://www.ncbi.nlm.nih.gov/pubmed/18354022 [Accessed May 1, 2013].

IASP, International Association for the Study of Pain | Classification of Chronic Pain, 2nd edition. Available at: http://www.iasp-pain.org/AM/Template.cfm?Section=Publications&Template=/CM/HTMLDisplay.cfm&ContentID=2687 [Accessed May 28, 2013].

IASP, 2011. International Association for the Study of Pain | IASP Taxonomy. Available at: http://www.iasp-pain.org/AM/Template.cfm?Section=Pain_Definitions [Accessed May 3, 2013].

Ilangumaran, S. & Hoessli, D.C., 1998. Effects of cholesterol depletion by cyclodextrin on the sphingolipid microdomains of the plasma membrane. *The Biochemical journal*, 335 (Pt 2, pp.433–40. Available at: http://www.pubmedcentral.nih.gov/articlerender.fcgi?artid=1219799&tool=pmcentrez&rendertype=abstract [Accessed September 16, 2013].

Jack, J., Noble, D. & Tsien, R., 1975. Electric Current Flow In Excitable Cells.

Jensen, M.Ø. & Mouritsen, O.G., 2004. Lipids do influence protein function-the hydrophobic matching hypothesis revisited. *Biochimica et biophysica acta*, 1666(1-2), pp.205–26. Available at: http://www.ncbi.nlm.nih.gov/pubmed/15519316 [Accessed January 9, 2014].

Johannes, C.B. et al., 2010. The prevalence of chronic pain in United States adults: results of an Internet-based survey. *The journal of pain : official journal of the American Pain Society*, 11(11), pp.1230–9. Available at: http://www.ncbi.nlm.nih.gov/pubmed/20797916 [Accessed October 22, 2013].

Kaplan, M.R. et al., 2001. Differential Control of Clustering of the Sodium Channels Nav1.2 and Nav1.6 at Developing CNS Nodes of Ranvier. *Neuron*, 30(1), pp.105–119. Available at: http://www.cell.com/neuron/fulltext/S0896-6273(01)00266-5 [Accessed November 8, 2013].

Ke, C.B. et al., 2012. Enhanced SCN7A/Nax expression contributes to bone cancer pain by increasing excitability of neurons in dorsal root ganglion. *Neuroscience*, 227, pp.80–89. Available at: http://www.sciencedirect.com/science/article/pii/S0306452212009669 [Accessed November 1, 2013].

Kole, M.H.P. et al., 2008. Action potential generation requires a high sodium channel density in the axon initial segment. *Nature neuroscience*, 11(2), pp.178–86. Available at: http://dx.doi.org/10.1038/nn2040 [Accessed November 8, 2013].

Kube, E., Weber, K. & Gerkes, V., 1992. Protein-Protein Interaction Studied by Site-directed Mutagenesis.

Langford, D.J. et al., 2010. Coding of facial expressions of pain in the laboratory mouse. *Nature methods*, 7(6), pp.447–9. Available at: http://www.ncbi.nlm.nih.gov/pubmed/20453868 [Accessed May 22, 2013].

Lawson, S.N., 2002. Nociceptors as Homeostatic Afferents : Central Processing Phenotype and function of somatic primary afferent nociceptive neurones with C-, Ad- or Aa / b-fibres. , (September 2001).

Leitinger, B. & Hogg, N., 2002. The involvement of lipid rafts in the regulation of integrin function. *Journal of cell science*, 115(Pt 5), pp.963–72. Available at: http://www.ncbi.nlm.nih.gov/pubmed/11870215.

Limpert, A.S., Karlo, J.C. & Landreth, G.E., 2007. Nerve growth factor stimulates the concentration of TrkA within lipid rafts and extracellular signal-regulated kinase activation through c-Cbl-associated protein. *Molecular and cellular biology*, 27(16), pp.5686–98. Available at: http://mcb.asm.org/content/27/16/5686.full [Accessed September 22, 2013].

Liu, C. et al., 2005. CAP-1A is a novel linker that binds clathrin and the voltage-gated sodium channel Na(v)1.8. *Molecular and cellular neurosciences*, 28(4), pp.636–49. Available at: http://www.ncbi.nlm.nih.gov/pubmed/15797711 [Accessed September 25, 2013].

Liu, C. et al., 2010. Prostaglandin E2 promotes Na1.8 trafficking via its intracellular RRR motif through the protein kinase A pathway. *Traffic (Copenhagen, Denmark)*, 11(3), pp.405–17. Available at: http://www.ncbi.nlm.nih.gov/pubmed/20028484 [Accessed September 30, 2013].

Liu, C.J. et al., 2006. A High-Capacity Membrane Potential FRET-Based Assay for NaV1.8. *ASSAY and Drug Development Technologies*, 4(1).

Locke, D., Liu, J. & Harris, A.L., 2005. Lipid rafts prepared by different methods contain different connexin channels, but gap junctions are not lipid rafts. *Biochemistry*, 44(39), pp.13027–42. Available at: http://www.ncbi.nlm.nih.gov/pubmed/16185071.

Loura, L.M.S., 2012. Simple Estimation of Förster Resonance Energy Transfer (FRET) Orientation Factor Distribution in Membranes. *International journal of molecular sciences*, 13(11), pp.15252–70. Available at: http://www.pubmedcentral.nih.gov/articlerender.fcgi?artid=3509639&tool=pmcentrez&rendertype=abstract [Accessed September 19, 2013].

Lundbaek, J. a et al., 2004. Regulation of sodium channel function by bilayer elasticity: the importance of hydrophobic coupling. Effects of Micelle-forming amphiphiles and cholesterol. *The Journal of general physiology*, 123(5), pp.599–621. Available at: http://www.pubmedcentral.nih.gov/articlerender.fcgi?artid=2234500&tool=pmcentrez&rendertype=abstract [Accessed March 3, 2013].

Lüpfert, C. et al., 2001. Rate limitation of the Na(+),K(+)-ATPase pump cycle. *Biophysical journal*, 81(4), pp.2069–81. Available at: http://www.pubmedcentral.nih.gov/articlerender.fcgi?artid=1301680&tool=pmcentrez&rendertype=abstract.

Malik-Hall, M. et al., 2003. Sensory neuron proteins interact with the intracellular domains of sodium channel NaV1.8. *Brain research. Molecular brain research*, 110(2), pp.298–304. Available at: http://www.ncbi.nlm.nih.gov/pubmed/12591166.

Mann, M., Hendrickson, R.C. & Pandey, a, 2001. Analysis of proteins and proteomes by mass spectrometry. *Annual review of biochemistry*, 70, pp.437–73. Available at: http://www.ncbi.nlm.nih.gov/pubmed/11395414.

Matthews, E.A., Wood, J.N. & Dickenson, A.H., 2006. Na(v) 1.8-null mice show stimulus-dependent deficits in spinal neuronal activity. *Molecular pain*, 2(1), p.5. Available at: http://www.molecularpain.com/content/2/1/5 [Accessed January 21, 2014].

Mayran, N., Parton, R.G. & Gruenberg, J., 2003. Annexin II regulates multivesicular endosome biogenesis in the degradation pathway of animal cells. *The EMBO journal*, 22(13), pp.3242–53. Available at: http://www.pubmedcentral.nih.gov/articlerender.fcgi?artid=165635&tool=pmcentrez&rendertype=abstract.

Mazo, I., Rivera-Arconada, I. & Roza, C., 2013. Axotomy-induced changes in activity-dependent slowing in peripheral nerve fibres: role of hyperpolarization-activated/HCN channel current. *European journal of pain (London, England)*, 17(9), pp.1281–90. Available at: http://www.ncbi.nlm.nih.gov/pubmed/23494886 [Accessed July 24, 2014].

McIntosh, T.J., Vidal, A. & Simon, S.A., 2003. Sorting of lipids and transmembrane peptides between detergent-soluble bilayers and detergent-resistant rafts. *Biophysical journal*, 85(3), pp.1656–66. Available at: http://www.pubmedcentral.nih.gov/articlerender.fcgi?artid=1303339&tool=pmcentrez&rendertype=abstract [Accessed January 21, 2014].

Mirza, S.P. et al., 2007. Improved method for the analysis of membrane proteins by mass spectrometry. *Physiological genomics*, 30(1), pp.89–94. Available at: http://physiolgenomics.physiology.org/content/30/1/89 [Accessed July 15, 2014].

Müller, T. et al., 2011. Sense and nonsense of pathway analysis software in proteomics. *Journal of proteome research*, 10(12), pp.5398–408. Available at: http://www.ncbi.nlm.nih.gov/pubmed/21978018.

Nassar, M.A. et al., 2005. Neuropathic pain develops normally in mice lacking both Na(v)1.7 and Na(v)1.8. *Molecular pain*, 1(1), p.24. Available at: http://www.molecularpain.com/content/1/1/24 [Accessed January 21, 2014].

Ohman, E. et al., 2008. Use of surface plasmon resonance coupled with mass spectrometry reveals an interaction between the voltage-gated sodium channel type X alpha-subunit and caveolin-1. *Journal of proteome research*, 7(12), pp.5333–8. Available at: http://dx.doi.org/10.1021/pr800498t [Accessed October 10, 2013].

Okuse, K. et al., 2002. Annexin II light chain regulates sensory neuron-specific sodium channel expression. *Nature*, 417(6889), pp.653–6. Available at: http://www.ncbi.nlm.nih.gov/pubmed/12050667.

Olausson, B., 1998. Recordings of polymodal single c-fiber nociceptive afferents following mechanical and argon-laser heat stimulation of human skin. *Experimental brain research. Experimentelle Hirnforschung. Expérimentation cérébrale*, 122(1), pp.44–54. Available at: http://www.ncbi.nlm.nih.gov/pubmed/9772110.

Oldfield, S. et al., 2009. Receptor-mediated suppression of potassium currents requires colocalization within lipid rafts. *Molecular pharmacology*, 76(6), pp.1279–89. Available at: http://molpharm.aspetjournals.org/content/76/6/1279.long [Accessed September 22, 2013].

Oliferenko, S. et al., 1999. Analysis of CD44-containing lipid rafts: Recruitment of annexin II and stabilization by the actin cytoskeleton. *The Journal of cell biology*, 146(4), pp.843–54. Available at: http://www.pubmedcentral.nih.gov/articlerender.fcgi?artid=2156143&tool=pmcentrez&rendertype=abstract [Accessed September 22, 2013].

Orstavik, K., 2003. Pathological C-fibres in patients with a chronic painful condition. *Brain*, 126(3), pp.567–578. Available at: http://www.brain.oupjournals.org/cgi/doi/10.1093/brain/awg060 [Accessed July 24, 2014].

Owen, D.M. et al., 2012. The lipid raft hypothesis revisited--new insights on raft composition and function from super-resolution fluorescence microscopy. *BioEssays : news and reviews in molecular, cellular and developmental biology*, 34(9), pp.739–47. Available at: http://www.ncbi.nlm.nih.gov/pubmed/22696155 [Accessed July 13, 2014].

Pei, L. et al., 2011. Annexin 1 exerts anti-nociceptive effects after peripheral inflammatory pain through formyl-peptide-receptor-like 1 in rat dorsal root ganglion. *British journal of anaesthesia*, 107(6), pp.948–58. Available at: http://bja.oxfordjournals.org/content/107/6/948.long [Accessed October 1, 2013].

Persson, A.-K. et al., 2010. Sodium-calcium exchanger and multiple sodium channel isoforms in intra-epidermal nerve terminals. *Molecular pain*, 6, p.84. Available at: http://www.pubmedcentral.nih.gov/articlerender.fcgi?artid=3002896&tool=pmcentrez&rendertype=abstract [Accessed July 15, 2014].

Pike, L.J., 2003. Lipid rafts: bringing order to chaos. *Journal of lipid research*, 44(4), pp.655–67. Available at: http://www.ncbi.nlm.nih.gov/pubmed/12562849 [Accessed March 11, 2013].

Poon, W.-Y.L. et al., 2004. Identification of binding domains in the sodium channel Na(V)1.8 intracellular N-terminal region and annexin II light chain p11. *FEBS*

letters, 558(1-3), pp.114–8. Available at: http://www.ncbi.nlm.nih.gov/pubmed/14759526 [Accessed May 1, 2013].

Praveen, B.B. et al., 2011. Enhancement and optimization of plasmid expression in femtosecond optical transfection. *Journal of biophotonics*, 4(4), pp.229–35. Available at: http://www.ncbi.nlm.nih.gov/pubmed/21446012 [Accessed January 26, 2014].

Pristerà, A., Baker, M.D. & Okuse, K., 2012. Association between tetrodotoxin resistant channels and lipid rafts regulates sensory neuron excitability. J. D. Spafford, ed. *PloS one*, 7(8), p.e40079. Available at: http://dx.plos.org/10.1371/journal.pone.0040079 [Accessed September 20, 2013].

Prkachin, K.M., 2009. Assessing pain by facial expression: facial expression as nexus. *Pain research & management : the journal of the Canadian Pain Society = journal de la société canadienne pour le traitement de la douleur*, 14(1), pp.53–8. Available at: http://www.pubmedcentral.nih.gov/articlerender.fcgi?artid=2706565&tool=pmcentrez&rendertype=abstract.

Qian, N. & Sejnowski, T.J., 1989. Biological Cybernetics. , 15, pp.1–15.

Renganathan, M., Cummins, T.R. & Waxman, S.G., 2001. Contribution of Na(v)1.8 sodium channels to action potential electrogenesis in DRG neurons. *Journal of neurophysiology*, 86(2), pp.629–40. Available at: http://www.ncbi.nlm.nih.gov/pubmed/11495938.

Rescher, U. et al., 2004. Annexin 2 is a phosphatidylinositol (4,5)-bisphosphate binding protein recruited to actin assembly sites at cellular membranes. *Journal of cell science*, 117(Pt 16), pp.3473–80. Available at: http://www.ncbi.nlm.nih.gov/pubmed/15226372 [Accessed April 11, 2013].

Rescher, U. & Gerke, V., 2004. Annexins--unique membrane binding proteins with diverse functions. *Journal of cell science*, 117(Pt 13), pp.2631–9. Available at: http://www.ncbi.nlm.nih.gov/pubmed/15169834 [Accessed April 4, 2013].

Rollason, R. et al., 2007. Clathrin-mediated endocytosis of a lipid-raft-associated protein is mediated through a dual tyrosine motif. *Journal of cell science*, 120(Pt 21), pp.3850–8. Available at: http://jcs.biologists.org/content/120/21/3850.long [Accessed October 20, 2013].

Rothman, S.M., Guarino, B.B. & Winkelstein, B.A., 2009. Spinal microglial proliferation is evident in a rat model of painful disc herniation both in the presence of behavioral hypersensitivity and following minocycline treatment sufficient to attenuate allodynia. *Journal of neuroscience research*, 87(12), pp.2709–17.

Available at: http://www.ncbi.nlm.nih.gov/pubmed/19382225 [Accessed July 25, 2014].

Rowe, A.H. et al., 2013. Voltage-gated sodium channel in grasshopper mice defends against bark scorpion toxin. *Science (New York, N.Y.)*, 342(6157), pp.441–6. Available at: http://www.ncbi.nlm.nih.gov/pubmed/24159039 [Accessed January 24, 2014].

Seal, R.P. et al., 2009. Injury-induced mechanical hypersensitivity requires C-low threshold mechanoreceptors. *Nature*, 462(7273), pp.651–655. Available at: http://dx.doi.org/10.1038/nature08505.

Shimizu, H. et al., 2007. Glial Nax channels control lactate signaling to neurons for brain [Na+] sensing. *Neuron*, 54(1), pp.59–72. Available at: http://www.cell.com/neuron/fulltext/S0896-6273(07)00210-3 [Accessed November 1, 2013].

Silvius, J.R. & Nabi, I.R., 2006. Fluorescence-quenching and resonance energy transfer studies of lipid microdomains in model and biological membranes. *Molecular membrane biology*, 23(1), pp.5–16. Available at: http://www.ncbi.nlm.nih.gov/pubmed/16611577 [Accessed March 7, 2013].

Simons, K. & Ikonen, E., 1997. Functional rafts in cell membranes. *Nature*, 387(6633), pp.569–72. Available at: http://www.ncbi.nlm.nih.gov/pubmed/9177342 [Accessed November 6, 2013].

Simons, K. & Van Meer, G., 1988. Lipid sorting in epithelial cells. *Biochemistry*, 27(17), pp.6197–6202. Available at: http://dx.doi.org/10.1021/bi00417a001 [Accessed November 6, 2013].

Simons, K. & Toomre, D., 2000. Lipid rafts and signal transduction. *Nature reviews. Molecular cell biology*, 1(1), pp.31–9. Available at: http://www.ncbi.nlm.nih.gov/pubmed/11413487.

Sindrup, S.H. et al., 2005. Antidepressants in the Treatment of Neuropathic Pain. *Basic <html_ent glyph="@amp;" ascii="&"/> Clinical Pharmacology <html_ent glyph="@amp;" ascii="&"/> Toxicology*, 96(6), pp.399–409. Available at: http://doi.wiley.com/10.1111/j.1742-7843.2005.pto_96696601.x [Accessed January 27, 2014].

Singer, S.J. & Nicolson, G.L., 1972. The Fluid Mosaic Model of the Structure of Cell Membranes. *Science* , 175 (4023), pp.720–731. Available at: http://www.sciencemag.org/content/175/4023/720.abstract.

Taguchi, K. et al., 2007. Myelin protein zero is one of the components of the detergent-resistant membrane microdomain fraction prepared from rat pituitary. *Journal of*

molecular histology, 38(1), pp.79–85. Available at: http://www.ncbi.nlm.nih.gov/pubmed/17318342 [Accessed October 8, 2013].

Taraboulos, A. et al., 1995. Cholesterol depletion and modification of COOH-terminal targeting sequence of the prion protein inhibit formation of the scrapie isoform. *The Journal of cell biology*, 129(1), pp.121–32. Available at: http://www.pubmedcentral.nih.gov/articlerender.fcgi?artid=2120366&tool=pmcentrez&rendertype=abstract [Accessed October 19, 2013].

Thorn, H. et al., 2003. Cell surface orifices of caveolae and localization of caveolin to the necks of caveolae in adipocytes. *Molecular biology of the cell*, 14(10), pp.3967–76. Available at: http://www.pubmedcentral.nih.gov/articlerender.fcgi?artid=206992&tool=pmcentrez&rendertype=abstract [Accessed September 16, 2013].

Tracey, I., 2008. Imaging pain. *British journal of anaesthesia*, 101(1), pp.32–9. Available at: http://bja.oxfordjournals.org/content/101/1/32.long [Accessed January 21, 2014].

Tracey, I. & Bushnell, M.C., 2009. How neuroimaging studies have challenged us to rethink: is chronic pain a disease? *The journal of pain : official journal of the American Pain Society*, 10(11), pp.1113–20. Available at: http://www.ncbi.nlm.nih.gov/pubmed/19878862 [Accessed May 1, 2013].

Vabnick, I. et al., 1996. The clustering of axonal sodium channels during development of the peripheral nervous system. *The Journal of neuroscience : the official journal of the Society for Neuroscience*, 16(16), pp.4914–22. Available at: http://www.ncbi.nlm.nih.gov/pubmed/8756423.

Valapala, M. & Vishwanatha, J.K., 2011. Lipid raft endocytosis and exosomal transport facilitate extracellular trafficking of annexin A2. *The Journal of biological chemistry*, 286(35), pp.30911–25. Available at: http://www.pubmedcentral.nih.gov/articlerender.fcgi?artid=3162451&tool=pmcentrez&rendertype=abstract [Accessed July 15, 2014].

Vijayaragavan, K., O'Leary, M.E. & Chahine, M., 2001. Gating properties of Na(v)1.7 and Na(v)1.8 peripheral nerve sodium channels. *The Journal of neuroscience : the official journal of the Society for Neuroscience*, 21(20), pp.7909–18. Available at: http://www.ncbi.nlm.nih.gov/pubmed/11588164.

Watanabe, E. et al., 2002. *Nax sodium channel is expressed in non-myelinating Schwann cells and alveolar type II cells in mice*, Available at: http://www.sciencedirect.com/science/article/pii/S0304394002007085 [Accessed October 10, 2013].

Waxman, S., 1995. *The Axon : structure, function and pathophysiology*, New York [etc.]: Oxford University Press.

Weidner, C. et al., 1999. Functional attributes discriminating mechano-insensitive and mechano-responsive C nociceptors in human skin. *The Journal of neuroscience : the official journal of the Society for Neuroscience*, 19(22), pp.10184–90. Available at: http://www.ncbi.nlm.nih.gov/pubmed/10559426.

Welker, P. et al., 2007. Role of lipid rafts in membrane delivery of renal epithelial Na+-K+-ATPase, thick ascending limb. *American journal of physiology. Regulatory, integrative and comparative physiology*, 292(3), pp.R1328–37. Available at: http://www.ncbi.nlm.nih.gov/pubmed/17082358 [Accessed March 12, 2013].

Wilson, B.S. et al., 2004. Markers for detergent-resistant lipid rafts occupy distinct and dynamic domains in native membranes. *Molecular biology of the cell*, 15(6), pp.2580–92. Available at: http://www.pubmedcentral.nih.gov/articlerender.fcgi?artid=420084&tool=pmcentrez&rendertype=abstract [Accessed July 14, 2014].

Wright, S.H., 2004. Generation of resting membrane potential. , pp.139–142.

Yawn, B.P. et al., 2009. The prevalence of neuropathic pain: clinical evaluation compared with screening tools in a community population. *Pain medicine (Malden, Mass.)*, 10(3), pp.586–93. Available at: http://www.pubmedcentral.nih.gov/articlerender.fcgi?artid=2964880&tool=pmcentrez&rendertype=abstract [Accessed October 22, 2013].

Yuan, C. et al., 2002. The size of lipid rafts: an atomic force microscopy study of ganglioside GM1 domains in sphingomyelin/DOPC/cholesterol membranes. *Biophysical journal*, 82(5), pp.2526–35. Available at: http://www.pubmedcentral.nih.gov/articlerender.fcgi?artid=1302043&tool=pmcentrez&rendertype=abstract.

Zeng, S. & Tang, Y., 2009. Effect of clustered ion channels along an unmyelinated axon. *Physical Review E*, 80(2), p.021917. Available at: http://link.aps.org/doi/10.1103/PhysRevE.80.021917 [Accessed April 26, 2013].

Zhang, H. & Verkman, a S., 2010. Aquaporin-1 tunes pain perception by interaction with Na(v)1.8 Na+ channels in dorsal root ganglion neurons. *The Journal of biological chemistry*, 285(8), pp.5896–906. Available at: http://www.pubmedcentral.nih.gov/articlerender.fcgi?artid=2820815&tool=pmcentrez&rendertype=abstract [Accessed March 17, 2013].

Zhang, Z.-N. et al., 2008. The voltage-gated Na+ channel Nav1.8 contains an ER-retention/retrieval signal antagonized by the beta3 subunit. *Journal of cell*

science, 121(Pt 19), pp.3243–52. Available at: http://www.ncbi.nlm.nih.gov/pubmed/18782866 [Accessed March 5, 2013].

Zhao, J. et al., 2007. Lidocaine promotes the trafficking and functional expression of Na(v)1.8 sodium channels in mammalian cells. *Journal of neurophysiology*, 98(1), pp.467–77. Available at: http://www.ncbi.nlm.nih.gov/pubmed/17507497 [Accessed May 1, 2013].

Zheng, Y.Z., Berg, K.B. & Foster, L.J., 2009. Mitochondria do not contain lipid rafts, and lipid rafts do not contain mitochondrial proteins. *Journal of lipid research*, 50(5), pp.988–98. Available at: http://www.jlr.org/content/50/5/988.full [Accessed July 15, 2014].

Zimet, D.B. et al., 1995. CALCULATION OF RESONANCE ENERGY-TRANSFER IN CROWDED BIOLOGICAL-MEMBRANES. *Biophysical Journal*, 68, pp.1592–1603. Available at: <Go to ISI>://WOS:A1995RD16300037.

7 Appendix A – Example of NEURON hoc code

```
//Raft
load_file("nrngui.hoc") //brings up NEURON interface
load_file("NaV18Stoch.ses") //brings up definition of NaV1.8 channels in channel builder
load_file("KFast.ses") //brings up definition of KFast channels in channel builder


laxon = 10002 //axon length
dsoma = 0.1 //soma diameter
lsoma = 1 //length of soma section, part of initial segment for generating AP
daxon = 0.1 //axon diameter
lraft = 0.2 //raft cluster length
draft = 3 //distance frequency of raft clusters
naxon = laxon/(draft) //number of compartments, 10 segments per um
nacond = 0.12 //maximum sodium channel conductance (0.12 S/cm2)
nan = 27 // number of channels per cluster
CondProp = 1 //Proportion of default sodium conductance in rafts
cellcap = 0.81 //membrane capacitance in uF/cm2
intRes = 70 //internal resistance in ohmcm
pos = 0.01 //postion of first channel in cluster
Runs = 2 //number of multiple runs required

//define objects for recording variables into and outputting to file
objref tRun, voltageHalf, voltageEnd, iHalf, resHalf

tRun = new Vector()
voltageHalf = new Vector()
voltageEnd = new Vector()

objref iHalf
```

```
iHalf = new Matrix()

objref tempmatrix
tempmatrix = new Matrix()

objref sData
sData = new File()

//define the different types of compartment the model will use
create soma, intialSegments[10], axonRaft[naxon], axon[naxon]

access soma

soma {
        nseg = 1 //number of segments in this compartment
        diam = dsoma
        L = dsoma
        cm = cellcap
        Ra = intRes
        insert hh
        gnabar_hh = nacond
        insert pas
        g_pas = 0.00014
}

//intial 10 sections at full conductance to establish AP
for i = 0, 9 intialSegments[i] {
        nseg = 100      //number of segments in this compartment 10 per um
        diam = daxon
        L = 10
```

```
        cm = cellcap
        Ra = intRes
        insert hh       //use hodgkin-huxley channels
        gnabar_hh = nacond //set the conductance
        insert pas      // insert passive mechanism which includes leak current
        g_pas = 0.00014     // set the conductance as the inverse of the membrane
                            resistance
}

//raft clusters
for i = 0, naxon-1 axonRaft[i] {
        nseg = lraft * 10       //number of segments in this compartment 10 per um
        diam = daxon
        L = lraft               //length of compartment is length of raft
        cm = cellcap
        Ra = intRes
        //insert KFast //use fast potassium channels (Baker) //leave out of clusters
        insert pas
        g_pas = 0.00014
}

//sections between raft clusters
for i = 0, naxon-1 axon[i] {
        nseg = (draft - lraft)*10 //number of segments in this compartment 10 per um
        diam = daxon
        L = draft - lraft //length of compartment is frequency of rafts minus the length
of a raft
        cm = cellcap
        Ra = intRes
        insert KFast //use fast potassium channels (Baker)
```

```
        insert pas
        g_pas = 0.00014
}

//connect the segments together, starting at the soma
connect intialSegments[0](0), soma(1)

for i = 1, 9 {
        connect intialSegments[i](0), intialSegments[i-1](1)
}

connect axonRaft[0](0), intialSegments[9](1)
connect axon[0](0), axonRaft[0](1)

for i = 1, naxon-1 {
        connect axonRaft[i](0), axon[i-1](1)
        connect axon[i](0), axonRaft[i](1)
}

objref smlist // will be a List that contains all instances of the stochastic NaV1.8 mechanism
smlist = new List()


for i = 0, naxon-1 axonRaft[i] {                    //access each cluster
        for j = 0, nan-1 {                          //for each channel in the cluster
                pos = (1/(nan*2))+(j*(1/(nan)))     //starting at pos define the place where the channel will be placed
                smlist.append(new Nastoch(pos))     //insert the channel
```

```
                smlist.o(((i*nan)+j)).Nsingle = 1        //set the number of channels at this point (1)
        }
}

load_file("24992011stoch.ses")        // load a file to show a graph in the user interface

//Record variables into vectors

tRun.record(&t)                //record the time step
voltageHalf.record(&axon[(naxon/2)].v(0.5))//record the voltage at the midway point along the axon
voltageEnd.record(&axon[(naxon-1)].v(0.5)) //record the voltage at the end of the axon

//definea list of vectors
objref tmpvec, iveclist
iveclist = new List()
for j = 0, (nan)-1 {                    //for each channel
        tmpvec = new Vector()                //create a new vector
        tmpvec.record(&Nastoch[((naxon/2)*nan)+j].i)      //record the current from that channel
        iveclist.append(tmpvec)                    //add the record vector to the list
}


tstop = 200     //the length of time (ms) each simluation will run for (ie steps not compution time)

//for each run add the record variable into a matrix
```

```
for j = 0, Runs-1 {

        run()

        tempmatrix.resize(voltageHalf.size(), (1+((2+nan)*Runs)))
        tempmatrix.setcol((1+(j*(2+nan))), voltageHalf)
        tempmatrix.setcol((2+(j*(2+nan))), voltageEnd)
        for i = 0, nan-1 {
                tempmatrix.setcol(((3+i)+(j*(2+nan))), iveclist.o(i))
        }
        //tempmatrix.setcol((4+(j*4)), resHalf)

}
tempmatrix.setcol(0, tRun)

//output the matrix of recorded variables into an excel file
sData.wopen("RecordedVariables.xls")
tempmatrix.fprint(sData, "\t%g")
sData.close()
```